R77AEG475

NASA CR-135325

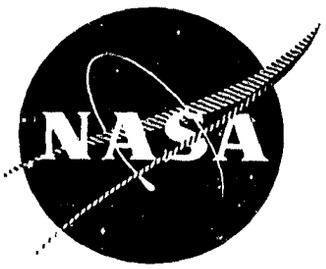

Quiet Clean Short-Haul Experimental Engine (QCSEE)

Over-The-Wing (OTW) Propulsion System Test Report

Volume III - Mechanical Performance

(NASA-CR-135325) QUIET CLEAN SHORT-HAUL EXPERIMENTAL ENGINE (QCSEE) OVER-THE WING (OTW) PROPULSION SYSTEM TEST REPORT. VOLUME 3: MECHANICAL PERFORMANCE (General Electric Co.) 121 p HC A06/MF A01 CSCL 21E G3/07

N80-15126

Unclas 33511

Advanced Engineering and Technology Programs Department

GENERAL ELECTRIC COMPANY

Prepared For

National Aeronautics and Space Administration

NASA Lewis Research Center

NAS3-18021

1. Report No. NASA CR-135325	2. Government Accession No.	3. Recipient's Catalog No.

4. Title and Subtitle	5. Report Date
QUIET CLEAN SHORT HAUL EXPERIMENTAL ENGINE (QCSEE) OVER-THE-WING (OTW) PROPULSION SYSTEM TEST REPORT Volume III - Mechanical Performance	February 1978
	6. Performing Organization Code
7. Author(s) Advanced Engineering and Technology Programs Department Group Advanced Engineering Division	8. Performing Organization Report No. R77AEG475
	10. Work Unit No.
9. Performing Organization Name and Address General Electric Company 1 Jimson Road Cincinnati, Ohio 45215	11. Contract or Grant No. NAS3-18021
	13. Type of Report and Period Covered Contractor Report
12. Sponsoring Agency Name and Address National Aeronautics and Space Administration Washington, D.C. 20546	14. Sponsoring Agency Code

15. Supplementary Notes

Test Report; Project Manager: C.C. Ciepluch, QCSEE Project Office; Technical Adviser: H.G. Yacobucci, NASA-Lewis Research Center, Cleveland, Ohio 44135

16. Abstract

The Quiet, Clean, Short-Haul, Experimental Engine (QCSEE) Program includes the design and testing of high-bypass, geared-turbofan engines, with nacelles, forming the propulsion systems for short-haul, passenger aircraft. These systems contain the technology required for externally blown-flap-type aircraft for introduction into passenger service in the 1980's.

This report covers sea level static ground testing of the Over-the-Wing (OTW) engine and boilerplate nacelle components. The report consists of four volumes and two appendices as follows:

Volume I	Summary Report NASA CR-135323	
Volume II	Aerodynamics and Performance NASA CR-135324	
Volume III	Mechanical Performance NASA CR-135325	
Volume IV	Acoustic Performance NASA CR-135326	
Appendix A	Detailed Engine Performance	For Government Use Only
Appendix B	Acoustic Data	For Government Use Only

17. Key Words (Suggested by Author(s))

Aircraft Propulsion and Power
Integrated Engine/Nacelle Structures
Propulsion System Testing

19. Security Classif. (of this report)	20. Security Classif. (of this page)	21. No. of Pages	22. Price*
Unclassified	Unclassified	113	

* For sale by the National Technical Information Service, Springfield, Virginia 22151

TABLE OF CONTENTS

LIST OF ILLUSTRATIONS

LIST OF ILLUSTRATIONS (Continued)

LIST OF ILLUSTRATIONS (Concluded)

LIST OF TABLES

1.0 SUMMARY

Mechanical operation of the OTW engine was very satisfactory, allowing the planned test program to be completed approximately six weeks ahead of schedule. Overall dynamic response of the engine was excellent. Rotor synchronous vibration and fan blade stress levels were low throughout the normal operating range. Because of minor deviations in core airflow and turbine efficiency, turbine inlet temperatures ran 38 K (68° F) higher than predicted at high speeds. Consequently, the engine would be T_{41} limited on a 306 K (90° F) day.

The main reduction gear was not disassembled or inspected following the test, but all test data indicated satisfactory operation. Heat-rejection data indicated slightly lower than predicted gear efficiencies.

Accessory gearbox flooding problems encountered on the first UTW test were corrected by improved internal baffling and by elimination of the shop-air-powered eductor.

The composite frame indicated low stresses at all times and encountered no structural problems. Some oil leakage occurred from the accessory drive shaft housing, but this was corrected by potting the area with Furane 9210 adhesive. No further evidence of oil leakage was noted, but some oil loss continued during high speed operation.

The full authority digital control provided smooth starting (without overtemperature) and stable, accurate, fan speed control. The engine met the required acceleration from 62% to 95% thrust in one second with 25° core stator reset.

2.0 INTRODUCTION

The General Electric Company is currently engaged in the Quiet, Clean, Short-haul, Experimental Engine Program (QCSEE) under Contract NAS3-18021 to the NASA Lewis Research Center. The Over-the-Wing (OTW) experimental engine was designed and built under the program to develop and demonstrate technology applicable to engines for future commercial, short-haul, turbofan aircraft. The initial buildup of the OTW engine and boilerplate nacelle was tested at General Electric's Peebles, Ohio Outdoor Test Site 4D during the period from March 31, 1977 through June 9, 1977.

The "D" shaped OTW exhaust nozzle contained a moveable roof that could be positioned to form a thrust-reverser blocker. The exhaust nozzle was run in the inverted position so that, during reverse-thrust testing, the exhaust gases would be directed downward rather than into the test facility and instrumentation lines.

Initial testing included a mechanical and systems checkout with hard-wall acoustic panels and a bellmouth inlet. Performance data were taken over a range of fan speeds and at three exhaust nozzle areas (side door angles). This phase of testing provided data in the range of takeoff and approach operating conditions to explore "uninstalled" performance with minimum loss of ram recovery. Fan performance characteristics were mapped over a range of fan speeds and operating lines. An acoustic baseline was also run in the unsuppressed, forward-thrust configuration.

The inlet was then changed to the boilerplate high Mach number design to investigate installed performance with real ram-recovery losses. Points were repeated at takeoff and approach operating conditions. Reverse-thrust testing included 105° and 115° blocker angles with a 0.6 lip-length ratio. A reingestion shield, 3.66 m (12 ft) in diameter and 9.14 m (30 ft) long, was used to reduce reingestion of hot exhaust gases during reverse-thrust testing, and the effect of this shield on thrust measurements was calibrated in the forward-thrust mode.

Following reverse-thrust performance testing, all hard-wall panels were changed to acoustically treated panels, and an acoustic splitter was added in the fan duct. Fully suppressed acoustic data was taken in the reverse and forward-thrust modes. Additional acoustic tests were then conducted to evaluate the contribution of inlet treatment and the combined effect of the splitter and core exhaust nozzle treatment.

Following the completion of acoustic testing, additional tests were conducted to evaluate control characteristics and engine throttle response in the forward-thrust mode.

The engine was inspected, refurbished, and delivered to NASA Lewis Research Laboratory on June 30, 1977 for further planned testing adjacent to a wing section.

This volume of the propulsion system test report includes a detailed discussion of the engine mechanical performance with emphasis on the advanced technology components.

3.0 SYSTEM DYNAMICS

The overall vibratory response of the OTW propulsion system was found to be within acceptable limits for normal engine operation. The low pressure and high pressure rotor synchronous response was very low throughout the operating range of the engine. The fan response was higher than predicted but did not exceed safety monitoring limits.

The overall vibration characteristics of the QCSEE OTW engine were found to be within acceptable limits for normal engine operation. Twenty vibration sensors were used to measure the engine response. The maximum vibration levels observed for each sensor are presented in Table I.

The synchronous vibration levels for the high pressure (HP) rotor activity were very low, less than 0.025 mm (1 mil) double amplitude (DA), for all vibration sensors; this is consistent with predicted behavior over the core operating range.

For the low pressure (LP) rotor activity, the synchronous vibration levels were less than 0.051 mm (2 mils) DA.

The low response for both the LP and HP rotor systems indicates that they were very well balanced.

The fan synchronous vibration levels were also low for most of the fan operating range. The most significant vibration, 0.188 mm (7.4 mils) DA, was noted on the horizontal pickup for the No. 2 bearing housing (front bearing for the LP shaft) at about 2200 rpm. The slipring experienced some high localized vibration. The fan-excited-vibration response was less than 0.109 mm (4.3 mils) DA for the remaining pickups over the normal operating range.

It should be emphasized tht Table I is a compilation of the maximum levels experienced for all the testing. It includes peak values as well as steady-state levels. A list of some typical 1/rev fan synchronous vibration readings, which indicate lower levels at certain steady-state conditions, is presented in Table II.

Table I. Maximum Synchronous Vibration Response for QCSEE OTW Engine Accelerometers.

Vibration Sensor		Fan			LP System			HP System		
		Max. Response		Speed	Max. Response		Speed	Max. Response		Speed
		mm	(mils-DA)	rpm	mm	(mils-DA)	rpm	mm	(mils-DA)	rpm
Core Cowl		0.051	(2.0)	3351	0.046	(1.8)	6491	0.008	(0.3)	11054
Slip Ring		0.381	(15.0)	3095	0.015	(0.6)	3510	0.010	(0.4)	11054
Fan Frame	V	0.066	(2.6)	3095	0.015	(0.6)	5196	0.003	(0.1)	12350
Fan Frame	H	0.076	(3.0)	3095	0.025	(1.0)	3510	0.008	(0.3)	11800
No. 1 Brg	V	0.109	(4.3)	2706	0.015	(0.6)	5196	0.003	(0.1)	12630
No. 1 Brg	H	0.041	(1.6)	3708	0.018	(0.7)	3510	0.003	(0.1)	12630
No. 2 Brg	V	0.033	(1.3)	2484	0.013	(0.5)	5196	0.003	(0.1)	12150
No. 2 Brg	H	0.188	(7.4)	2184	0.033	(1.3)	3510	0.003	(0.1)	12350
No. 3 Brg	V	0.051	(2.0)	3095	0.025	(1.0)	3510	0.015	(0.6)	13550
No. 3 Brg	H	0.051	(2.0)	3095	0.010	(0.4)	6124	0.015	(0.6)	13360
Red. Gear	V	0.102	(4.0)	2463	----	---	----	0.003	(0.1)	12350
Red. Gear	H	0.102	(4.0)	3095	0.041	(1.6)	3510	0.015	(0.6)	13360
Comp Stator Aft Flange	V	0.033	(1.3)	3488	0.025	(1.0)	6394	0.023	(0.9)	13550
Comp Stator Aft Flange	H	0.046	(1.8)	3095	0.043	(1.7)	3510	0.015	(0.6)	13550
No. 5 Brg	V	0.041	(1.6)	3488	0.046	(1.8)	3510	0.020	(0.8)	13550
No. 5 Brg	H	0.020	(0.8)	3351	0.025	(1.0)	3437	0.005	(0.2)	12260
Exhaust Cone		0.041	(1.6)	3148	0.020	(0.8)	6095	0.003	(0.1)	12070
Accessory Gearbox	A	0.071	(2.8)	1729	0.036	(1.4)	5196	0.008	(0.3)	13550
Accessory Gearbox	H	0.051	(2.0)	3095	0.020	(0.8)	3510	0.008	(0.3)	13550
Digital Control		0.114	(4.5)	3095	0.033	(1.3)	6124	0.005	(0.2)	12150

Table II. Typical Steady-State Fan Synchronous Vibration Response for QCSEE OTW Engine Accelerometers.

Vibration Pickup		Steady-State Fan Speed, rpm					
		1667	1887	2484	2955	3351	3675
		mm (mils-DA)	mm (mils-DA)	mm (mils-DA)	mm (mils-DA)	mm (mils-DA)	mm (mils-DA)
Fan Cowl		0.003 (0.1)	0.010 (0.4)	0.008 (0.3)	0.051 (2.0)	0.051 (2.0)	-- --
Slipring		0.267 (10.5)	0.152 (6.0)	0.185 (7.3)	0.234 (9.2)	0.302 (11.9)	0.170 (6.7)
Fan Frame	V	0.018 (0.7)	0.033 (1.3)	0.010 (0.4)	0.023 (0.9)	0.036 (1.4)	0.023 (0.9)
Fan Frame	H	0.018 (0.7)	0.023 (0.9)	0.005 (0.2)	0.036 (1.4)	0.033 (1.3)	0.023 (0.9)
No. 1 Brg	V	0.025 (1.0)	0.041 (1.6)	0.015 (0.6)	0.028 (1.1)	0.028 (1.1)	0.015 (0.6)
No. 1 Brg	H	0.018 (0.7)	0.015 (0.6)	0.015 (0.6)	0.033 (1.3)	0.008 (0.3)	0.025 (1.0)
No. 2 Brg	V	0.020 (0.8)	--- --	0.033 (1.3)	0.018 (0.7)	0.023 (0.9)	-- --
No. 2 Brg	H	0.051 (2.0)	0.036 (1.4)	0.066 (2.6)	0.023 (0.9)	0.033 (1.3)	0.041 (1.6)
No. 3 Brg	V	0.010 (0.4)	0.020 (0.8)	0.008 (0.3)	0.023 (0.9)	0.028 (1.1)	0.025 (1.0)
No. 3 Brg	H	0.010 (0.4)	0.008 (0.3)	0.005 (0.2)	0.022 (0.9)	0.023 (0.9)	0.018 (0.7)
Red. Gear	V	--- —	0.028 (1.1)	--- --	--- —	--- --	
Red. Gear	H	0.036 (1.4)	0.033 (1.3)	0.013 (0.5)	0.099 (3.9)	0.028 (1.1)	0.051 (2.0)
Comp. Stator Aft Flange	V	0.003 (0.1)	0.015 (0.6)	0.008 (0.3)	0.018 (0.7)	0.025 (1.0)	0.015 (0.6)
Comp. Stator Aft Flange	H	0.008 (0.3)	0.010 (0.4)	0.003 (0.1)	0.013 (0.5)	0.025 (1.0)	0.036 (1.4)
No. 5 Brg	V	0.005 (0.2)	0.010 (0.4)	0.003 (0.1)	0.013 (0.5)	0.028 (1.1)	0.041 (1.6)
No. 5 Brg	H	0.005 (0.2)	0.003 (0.1)	0.008 (0.3)	0.013 (0.5)	0.020 (0.8)	0.013 (0.5)
Exhaust Cone		0.036 (1.4)	0.003 (0.1)	0.028 (1.1)	0.041 (1.6)	0.025 (1.0)	0.010 (0.4)
Acc. G/B	A	0.008 (0.3)	0.056 (2.2)	0.010 (0.4)	0.023 (0.9)	0.028 (1.1)	0.048 (1.9)
Acc. G/B	H	0.013 (0.5)	0.018 (0.7)	0.010 (0.4)	0.013 (0.5)	0.041 (1.6)	0.020 (0.8)
Digital Control		0.018 (0.7)	0.041 (1.6)	0.020 (0.8)	0.041 (1.6)	0.056 (2.2)	0.066 (2.6)

4.0 FAN ROTOR

The OTW fan rotor, consisting of the titanium disk, blades, and blade retainers; aluminum flow-path adapter; and spinner functioned satisfactorily throughout the test. The only instrumented parts were the blades, which are covered in detail in this section.

4.1 BLADE DECRIPTION

The Over-the-Wing experimental fan is a single-stage fan having 28 fixed-pitch, titanium 6-4 blades. The rotor is shown in Figure 1. The conceptual design of the OTW fan was based on using composite fan blades, but metal blades were substituted for reasons of economy and low risk. The conceptual composite blade design dictates the absence of blade shrouds, determines the number of fan blades, and affects the sizing of such parameters as the blade solidity, reduced velocity, and leading edge thickness. In the flight engine, composite blades would be substituted for the metal blades without aerodynamic change or compromise in the composite blade mechanical design.

Radial variation in chord, maximum-thickness-to-chord ratio, and camber and stagger angles for the OTW blade are shown in Figures 2, 3, and 4. Figure 5 is a picture of the blade. Table III lists some of the more significant aerodynamic and mechanical features of the fan.

4.2 BLADE STRESS ANALYSIS AND PRETEST PREDICTIONS

The fan blades are a "low flexed" design; i.e., the first-flexural frequency of the blades crosses the two-per-rev line in the fan operating speed range. The crossover occurs at about 61% speed (slightly above idle) and, based on experience with the UTW simulator, would not be expected to produce excessive stresses during transient operation in this speed range. The Campbell diagram (Figure 6) shows that the low-mode, low-per-rev crossings occur at relatively low speeds, thus, minimizing blade vibratory response at these points. Calculations show that the lower modes have adequate frequency margin from engine per revs at 100% fan speed.

Fan blade steady-state, spanwise stresses were obtained by combining calculated beam analysis results from the Twisted Blade program and laboratory end-effects data. These showed the steady-state stresses in the airfoil to be highest at the blade midchord, approximately 248 MN/m^2 (36 ksi), with the leading and trailing edges in compression except at the root (Figure 7). Maximum steady-state stresses in the blade are at the junction of the airfoil root and the platform. These are: 511 MN/m^2 (74 ksi) at the concave midchord and 531 MN/m^2 (77 ksi) near the trailing edge convex (Figure 8).

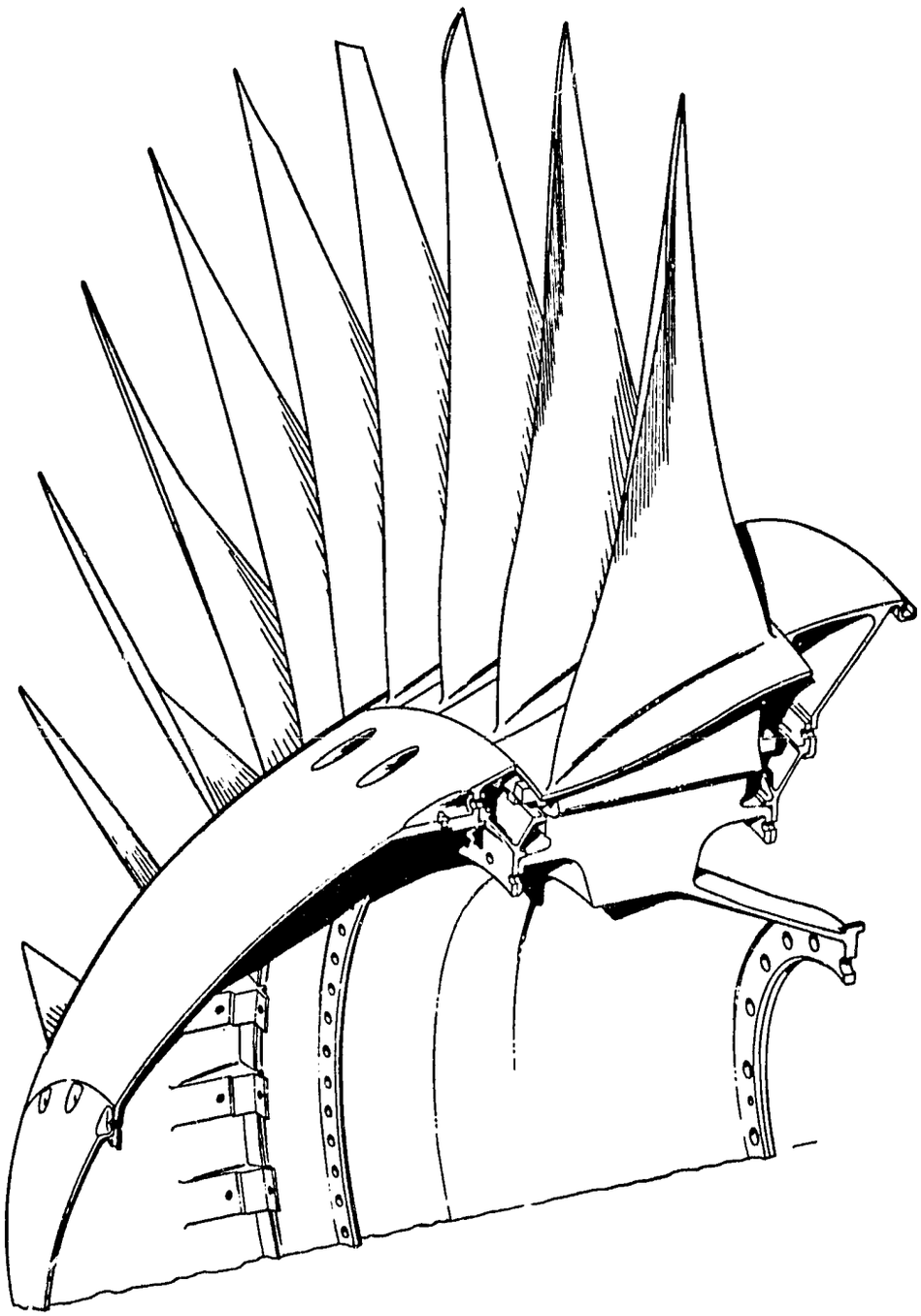

Figure 1. OTW Fan Rotor.

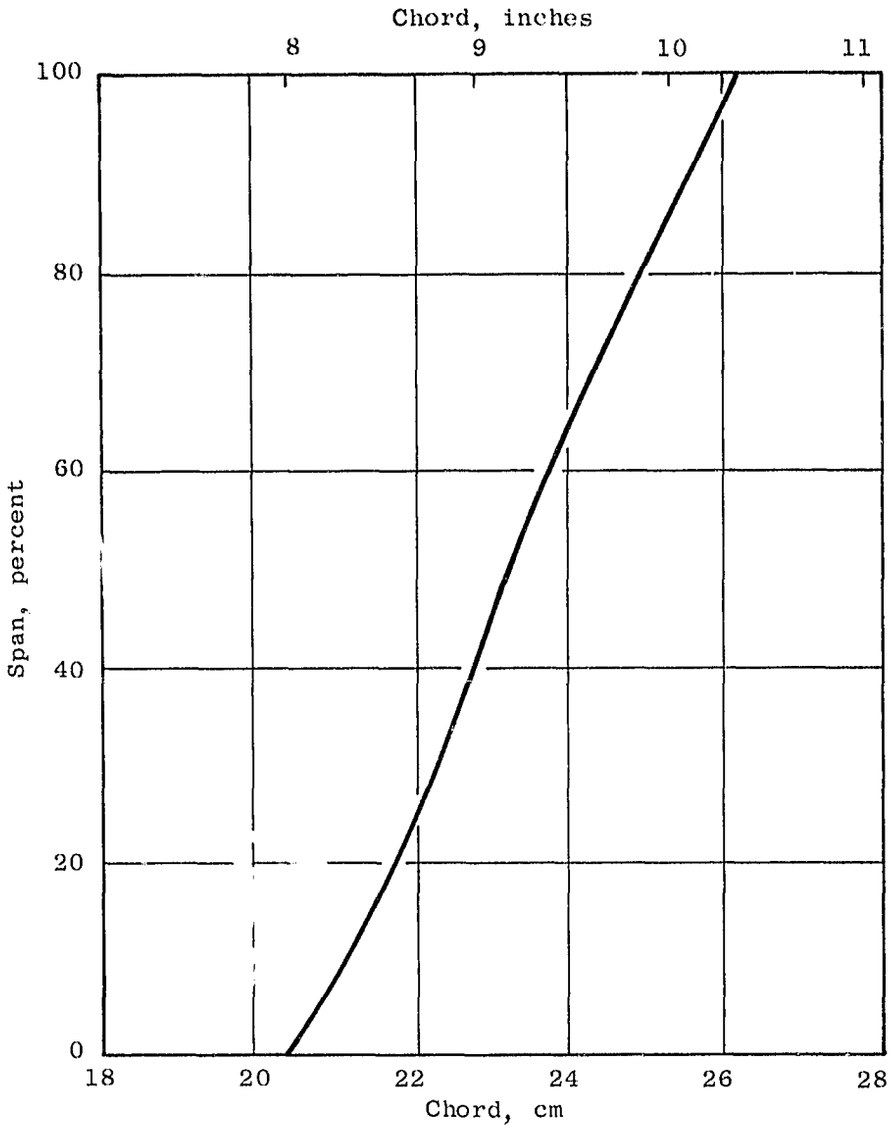

Figure 2. OTW Fan Blade Chord Vs. Span.

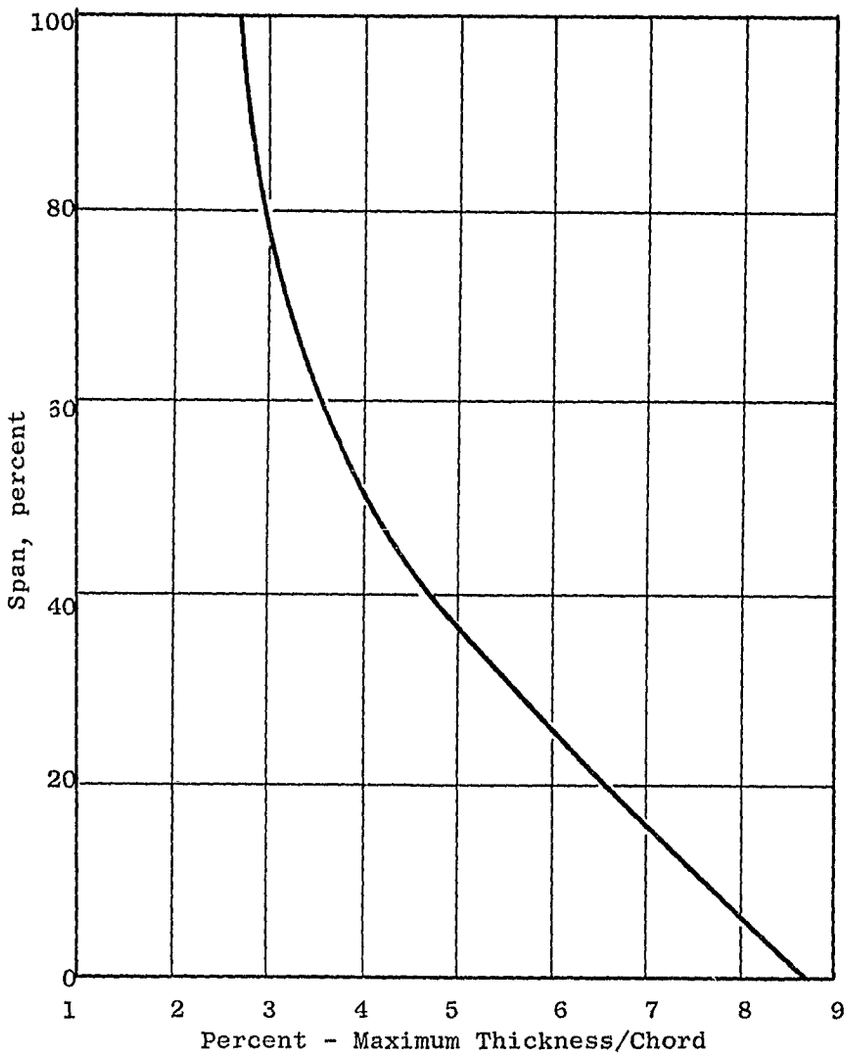

Figure 3. OTW Fan Blade Maximum Thickness Chord Vs. Span.

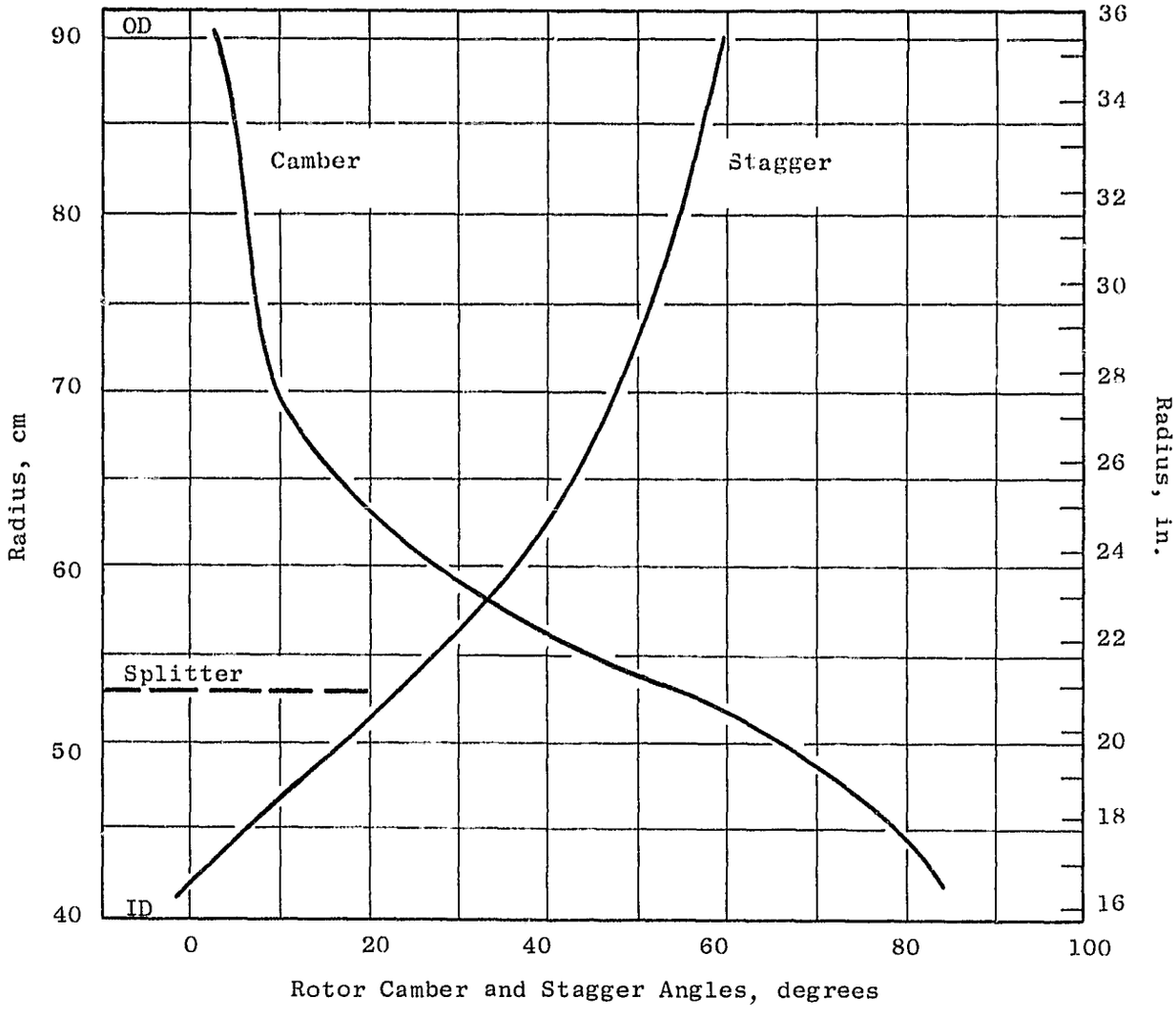

Figure 4. OTW Camber and Stagger Radial Distribution.

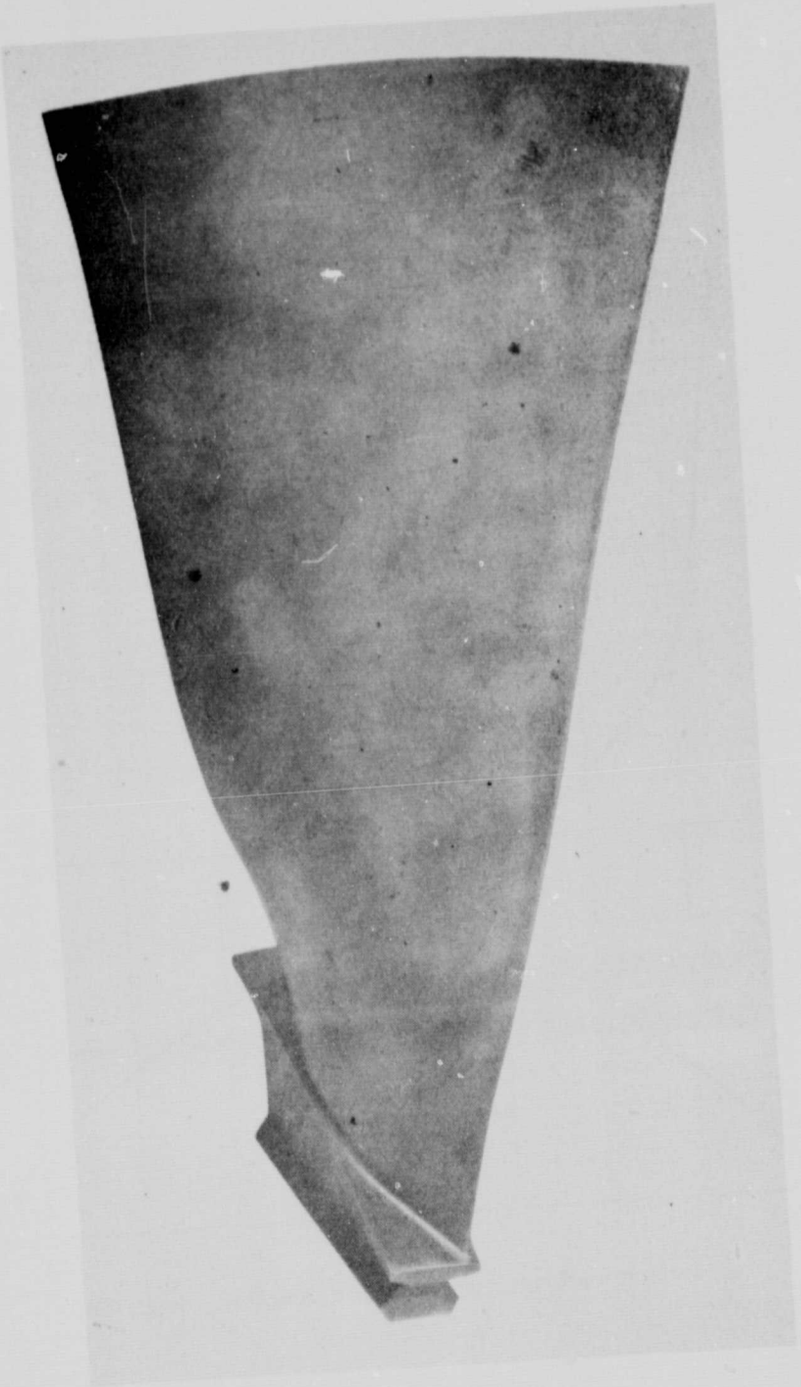

Figure 5. OTW Fan Blade.

Table III. QCSEE OTW Fan Design Features.

Total Fan Flow (Design Point)	408 kg/sec	(900 lb/sec)
Pressure Ratio - Bypass Flow	1.36	
Pressure Ratio - Core Flow	1.43	
Bypass Ratio	9.9	
Corrected Tip Speed - Design Point	358 m/sec	(1175 ft/sec)
Inlet Radius Ratio	0.42	
Flow Per Annulus Area	145 kg/sec-m^2	(29.8 lb/sec-ft^2)
Blade Tip Solidity	1.3	
Blade Hub Solidity	2.2	
Blade Tip Diameter	(180.3 cm)	71 in.
Fan Speed (100%)	3792 rpm	
Number of Blades	28	
Blade Chord - Tip	(26.26 cm)	10.34 in.
Root	(20.68 cm)	8.14 in.
Maximum Thickness/Chord - Tip	2.65%	
Root	8.6%	

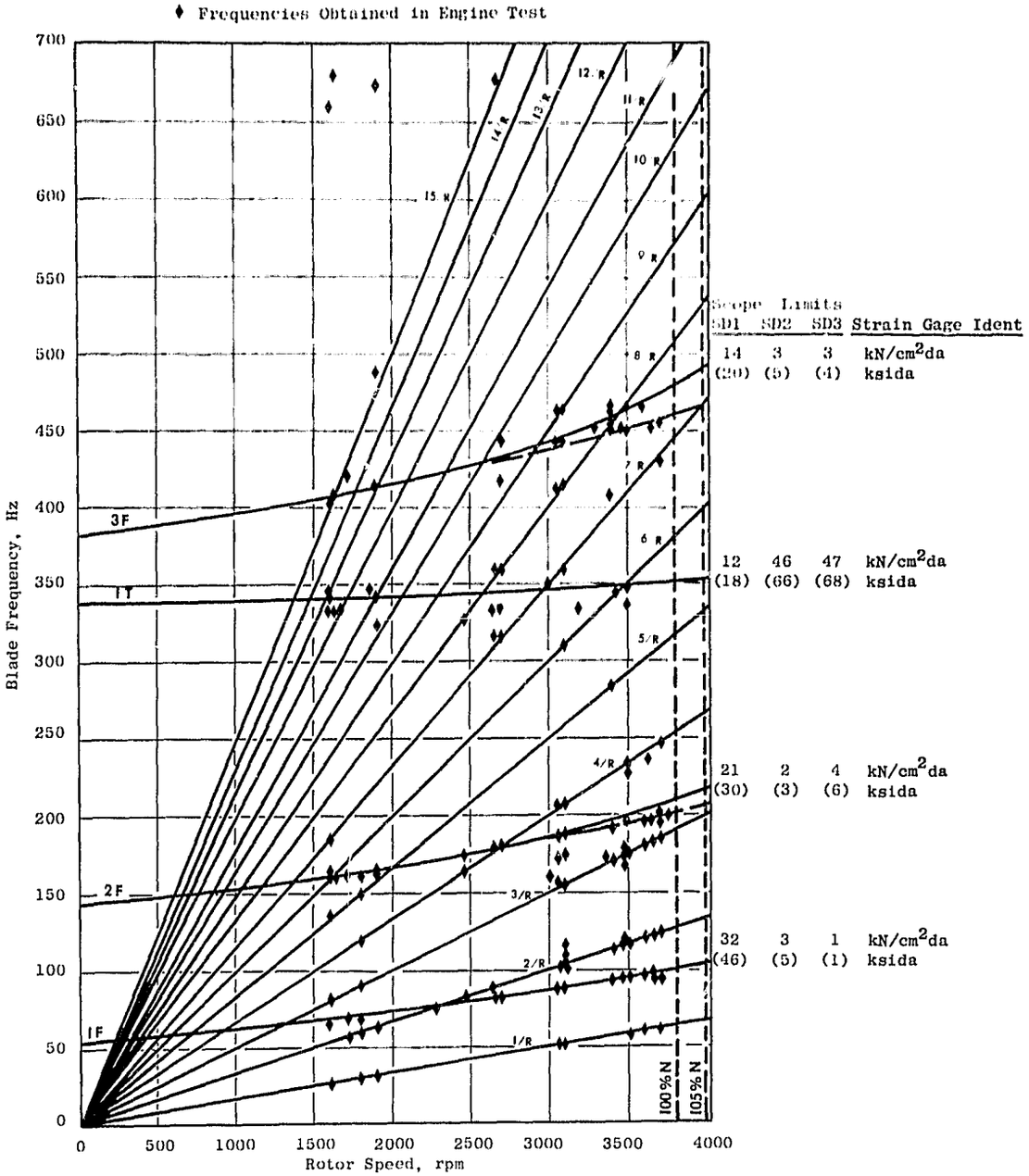

Figure 6. QCSEE OTW Fan Blade Campbell Diagram.

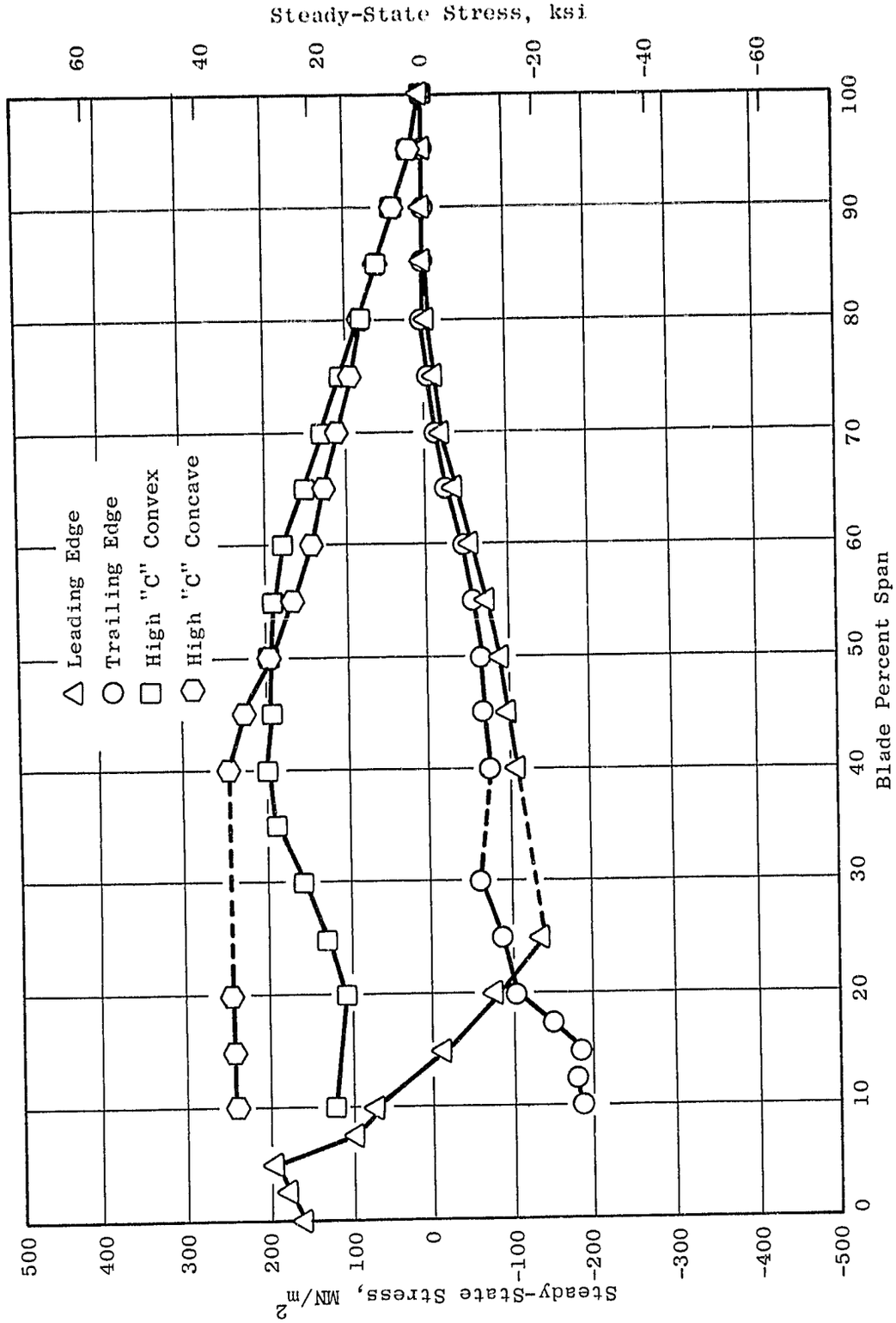

Figure 7. Steady-State, Spanwise Stress at 3792 RPM.

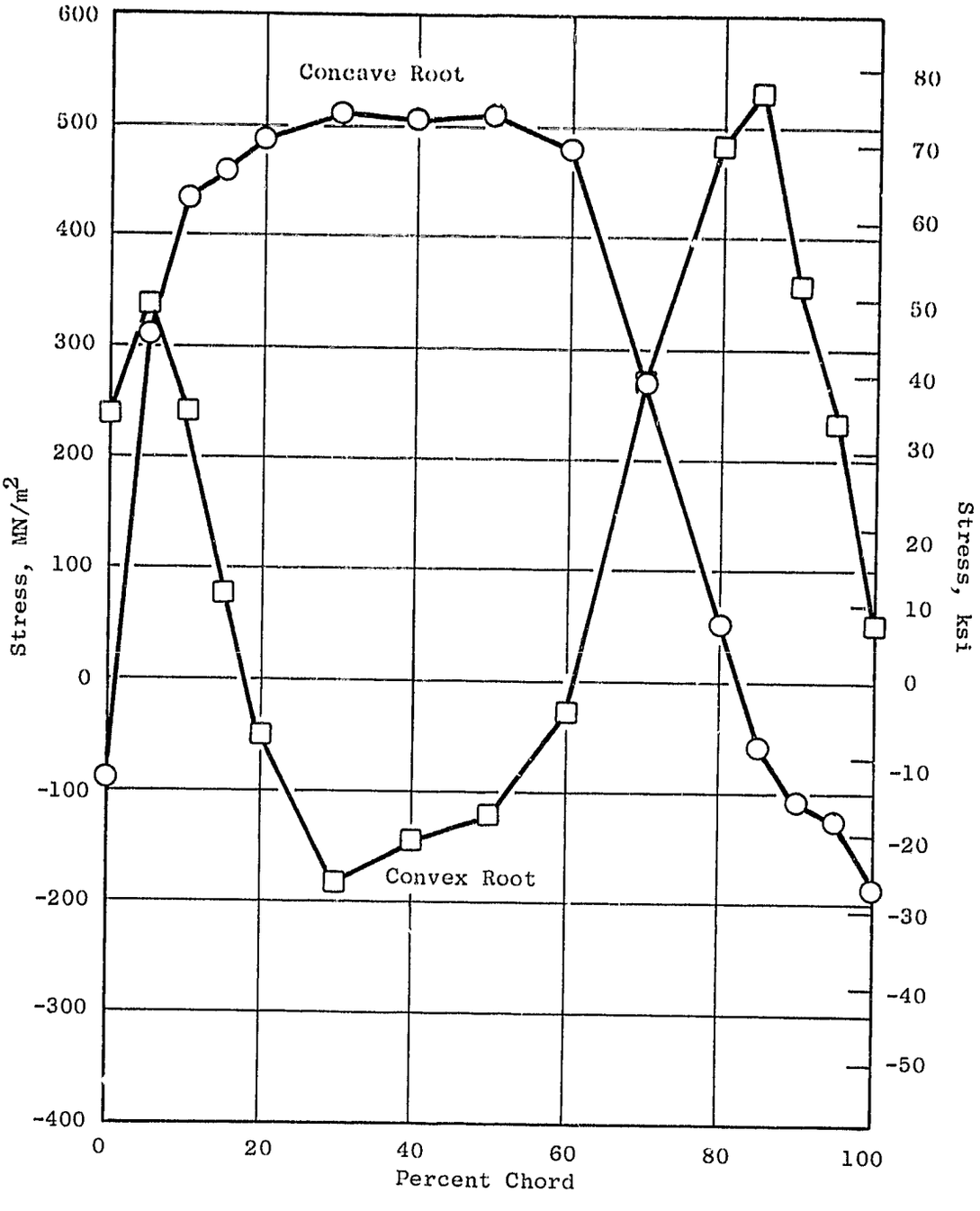

Figure 8. Airfoil Root Steady-State Stress (3792 rpm).

Predictions of blade instability or limit cycle vibration, by correlating the calculated reduced velocity parameter/incidence with past experience, indicated that the fan would be free of torsional instability. A similar correlation indicated that flexural instability could occur prior to stall at exit areas less than 1.58 m^2 (2444 $in.^2$) as shown in Figure 9.

4.3 BLADE INSTRUMENTATION AND SCOPE LIMITS

Engine gage locations were chosen in blade areas of relatively high vibratory stress response and low stress gradient based on data from bench test. Each instrumented blade had three gages to maximize the sensitivity of readout in the flexural, torsional, stripe, and plate modes. Gage positions are illustrated in Figure 10.

Scope limits or vibratory stress limits for the subject engine gages were calculated for the first four modes using calculated vibratory stress distributions while the higher modes scope limits, up through fan OGV passing frequency, were determined from laboratory stress distributions. These limits normally represent the maximum vibratory stress at which the blade may be allowed to continuously vibrate without initiating a fatigue failure at some location on the blade. The location where a fatigue crack would be initiated is referred to as the "critical location" and can be different for each vibratory mode.

The critical location depends upon both the steady-state stresses, including end effects, and the vibratory stresses. Since the blade steady-state stress level increases roughly with the speed squared, the scope limits are calculated as a function of fan speed. Scope limits are based on Goodman Diagram (Figure 11) allowable vibratory stresses including the three-sigma, endurance-limit reduction and steady-state stresses.

The first four fan modes scope limits were calculated by the Scope Limits Generator Program utilizing vibratory stress distributions from the Twisted Blade Program in conjunction with blade-root, end-effects data for zero and design speeds. The higher modes scope limits are based on bench test vibratory stress distribution data at zero speed. The effect of the centrifugal field on mode shape and vibratory stress distribution is minimal for the higher modes of vibration and, therefore, is normally not used to adjust the higher mode scope limits. Double-amplitude scope limits for a particular airfoil strain gage are calculated using the following equation.

$$\text{Scope Limit} = \frac{2 \times (\sigma e)\ \text{C.P.} \times \dfrac{\sigma g}{(\sigma_{vib})\ \text{C.P.}}}{K_v \times K_e \times K_c}$$

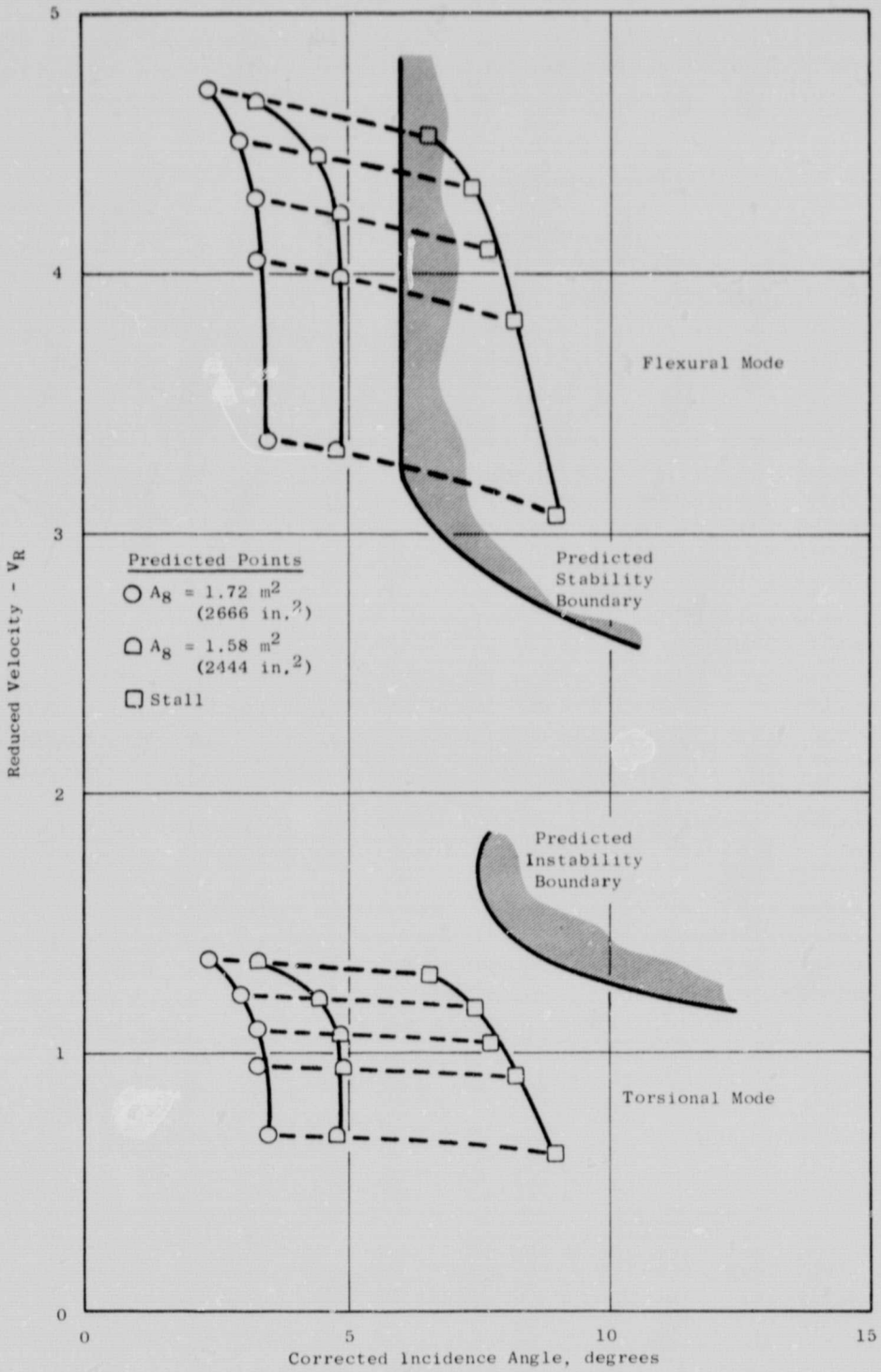

Figure 9. Reduced Velocity Parameter Vs. Corrected Incidence Angle.

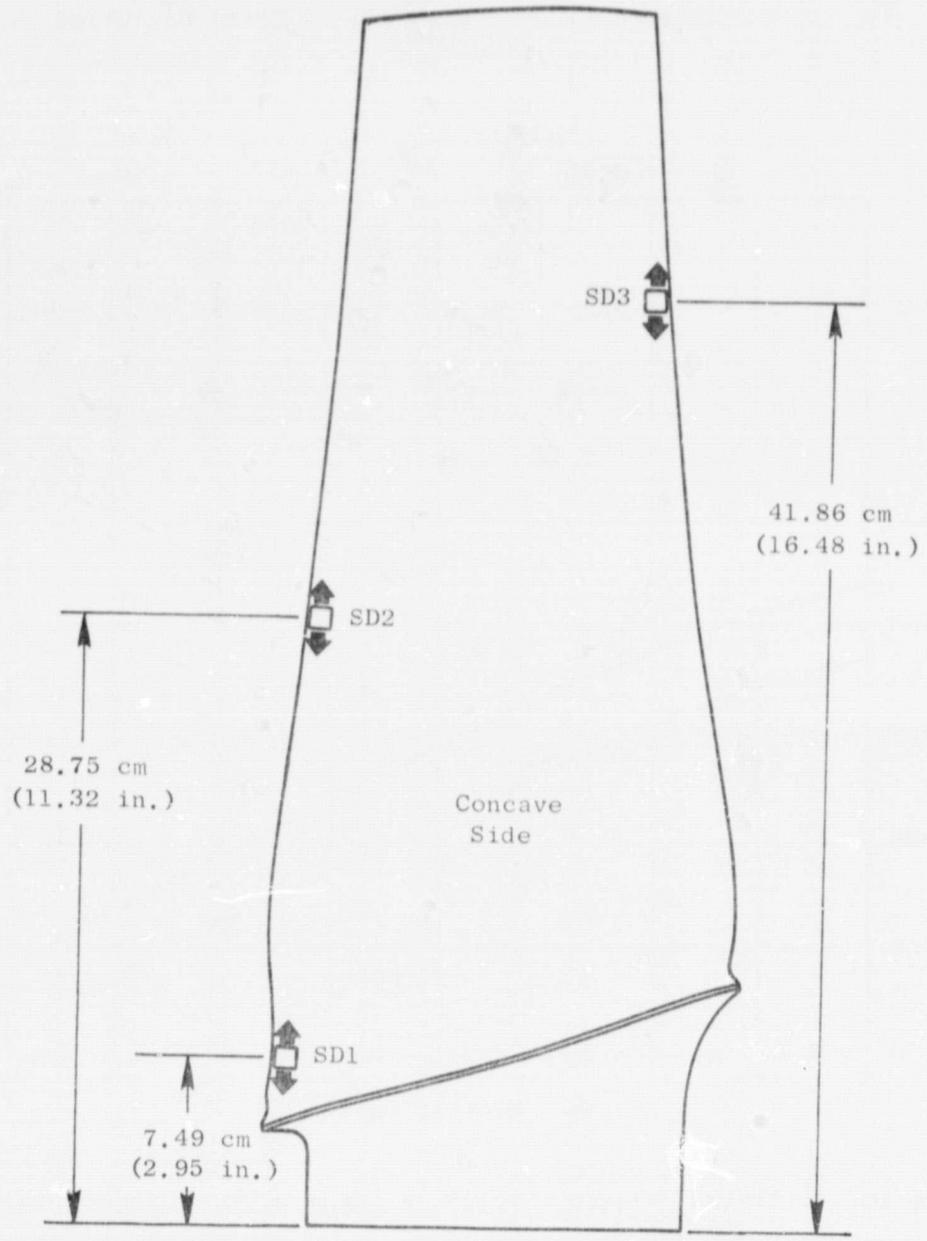

Figure 10. Fan Blade Strain Gage Map.

Solid Line: Average

Dashed Line: Average minus Three Deviation Units

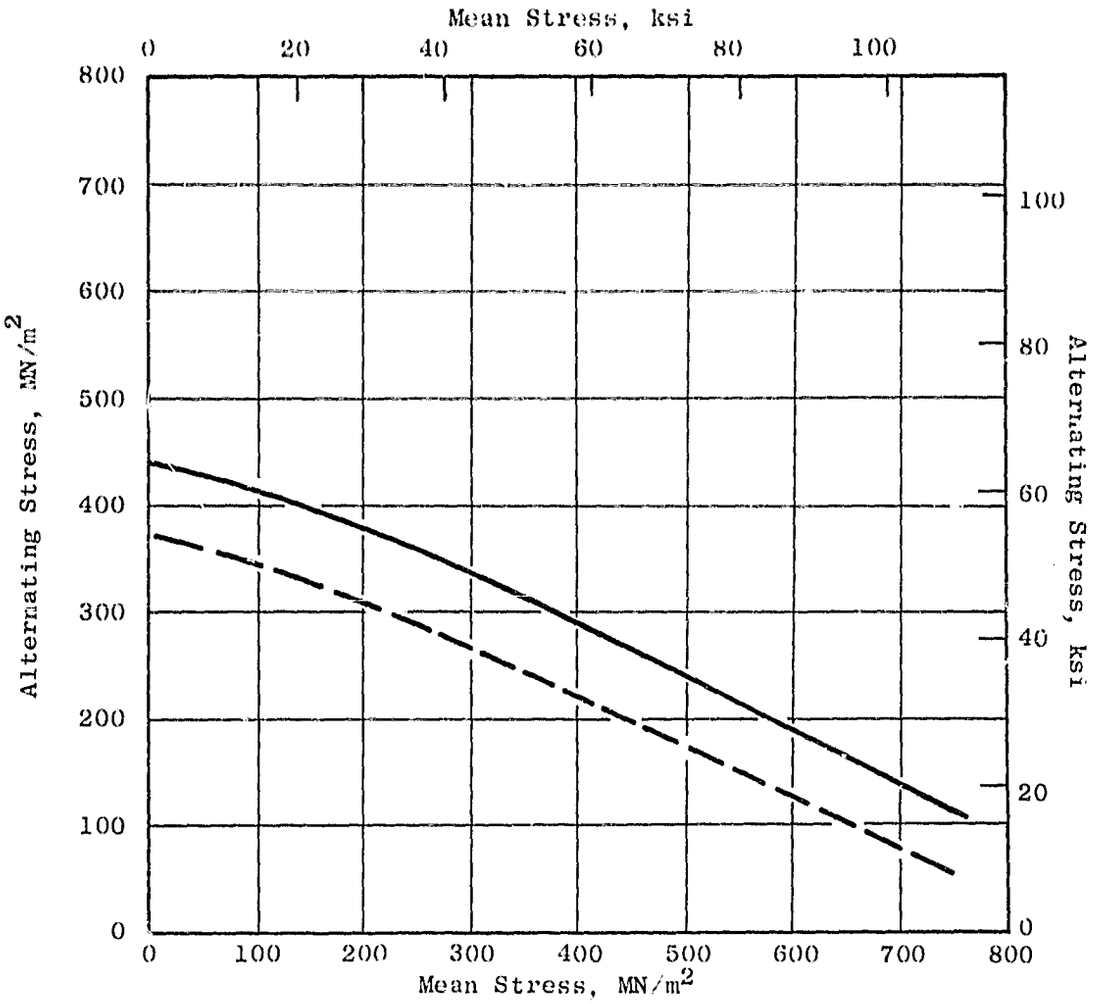

Figure 11. Titanium 6Al-4Va Forging; Fatigue Limit (Goodman) Diagram.

σ_e = The single-amplitude endurance limits at the location of maximum vibratory stress, based on the steady-state stress at the location (critical point), from the Goodman diagram for the operating temperature of the blade material (including three-sigma reductions of average endurance limit for minimum properties).

$\frac{\sigma_g}{(\sigma_{vib})_{C.P.}}$ = The ratio of vibratory stress at the gage location to the vibratory stress at the critical point on the blade for the mode of vibration being considered.

K_v = A blade-to-blade vibratory response variation factor (usually 1.30).

K_e = A factor for tolerance in the strain gage circuit (usually 1.05).

K_c = A geometric concentration factor normally applied to engine gages when the critical point for a particular mode is located at or near high stress concentration areas such as fillet radii (usually 1.15).

A list of the scope limits is shown in Table IV for all modes up to 2400 Hz. The variation of scope limit with speed is shown in Figure 12 for the first four modes for the three engine gages.

4.4 ENGINE TEST RESULTS

Four engine inlet configurations were tested from which fan blade vibratory response data were taken:

1. Bellmouth Inlet
2. Accelerating Inlet
3. Reverse Thrust with Reingestion Shield
4. Forward Thrust with Reingestion Shield

In these configurations several operating lines were traversed from idle to maximum speed (limited by T_{41}) to expand coverage of the fan map.

Fan blade strain gage data obtained from testing were analyzed to determine overall level of vibratory response and were reduced on the Fast Fourier Transform analyzer system (FFT) to provide a breakdown of the stress amplitude of each frequency through the operating range. Blade data were further condensed by expressing the FFT vibratory stress amplitude as a percentage of allowable vibratory stress (percent scope limits); this value has more meaning than absolute stress without reference to limits. The resulting diagrams (Figures 13 through 18) show percent scope limits attained by the instrumented blades during a fan-speed transient from idle to approximately 100% speed. Each peak is the maximum response of any one of several instrumented blades; thus, the curve does not represent a continuous trace of one blade but the maxima of all instrumented blades for a particular test condition.

Table IV. Scope Limits at 100% Speed.

Mode	Frequency, hertz	Scope Limit MN/m^2 double-amplitude (ksida)		
		SD1	SD2	SD3
1F	101	317(46)	35(5)	7(1)
2F	208	207(30)	21(3)	41(6)
1T	362	124(18)	455(66)	469(68)
3F	499	138(20)	35(5)	28(4)
5	676	28(4)	331(48)	214(31)
6	718	55(8)	21(3)	159(23)
7	778	7(1)	235(34)	490(71)
8	822	41(6)	159(23)	110(16)
9	950	104(15)	110(16)	7(1)
10	1078	0(0)	179(26)	104(15)
11	1208	62(9)	166(24)	35(5)
12	1302	97(14)	28(4)	366(53)
13	1494	21(3)	497(72)	62(9)
14	1602	41(6)	28(4)	193(28)
15	1726	76(11)	97(14)	255(37)
16	1790	145(21)	186(27)	55(8)
17	1830	14(2)	62(9)	21(3)
18	1962	35(5)	76(11)	28(4)
19	2232	41(6)	462(67)	373(37)
20	2318	228(33)	14(2)	117(12)

* Frequencies of the first four modes are at 100% speed. Other modes are zero-speed bench frequencies.

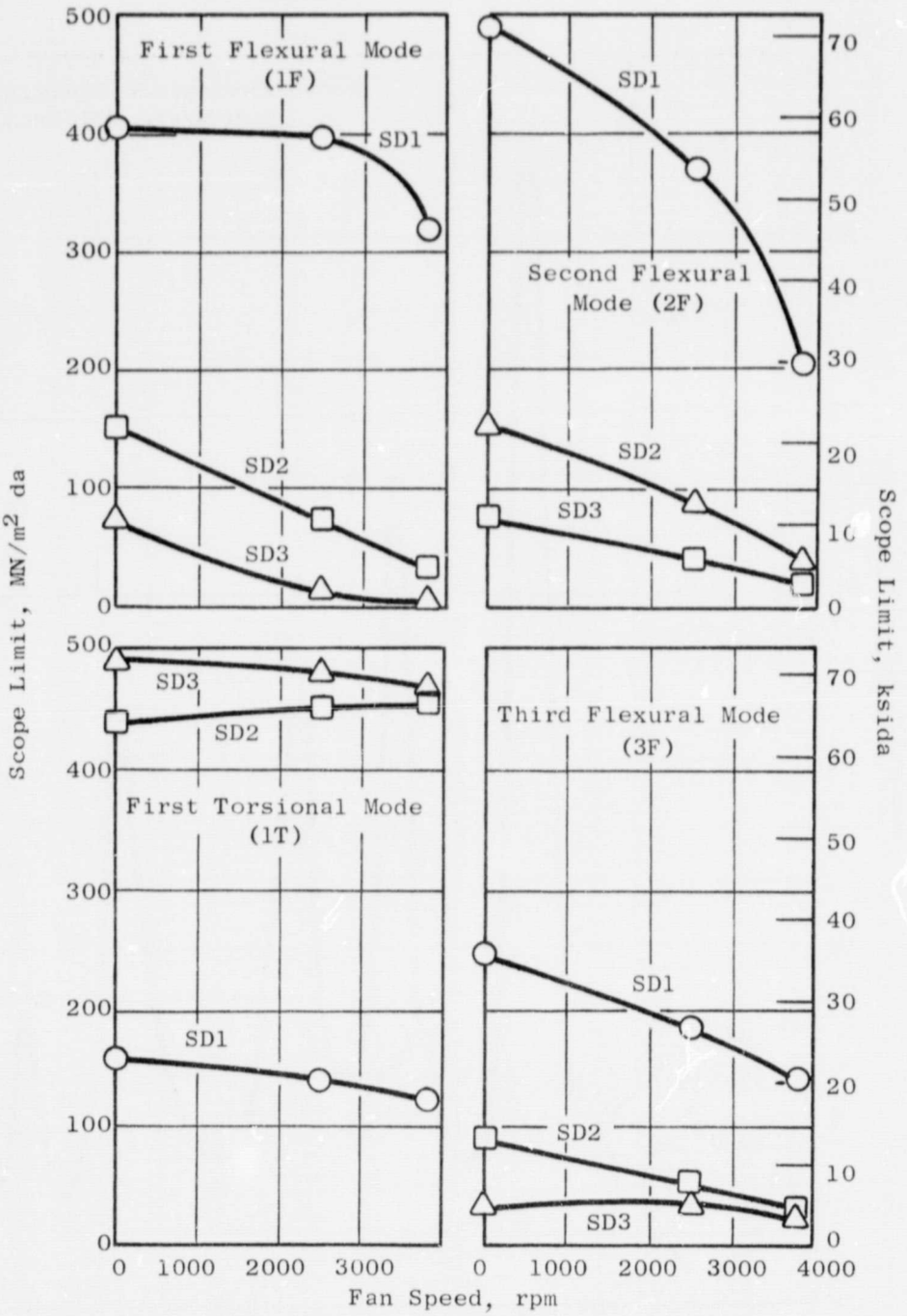

Figure 12. OTW Fan Blade Scope Limits.

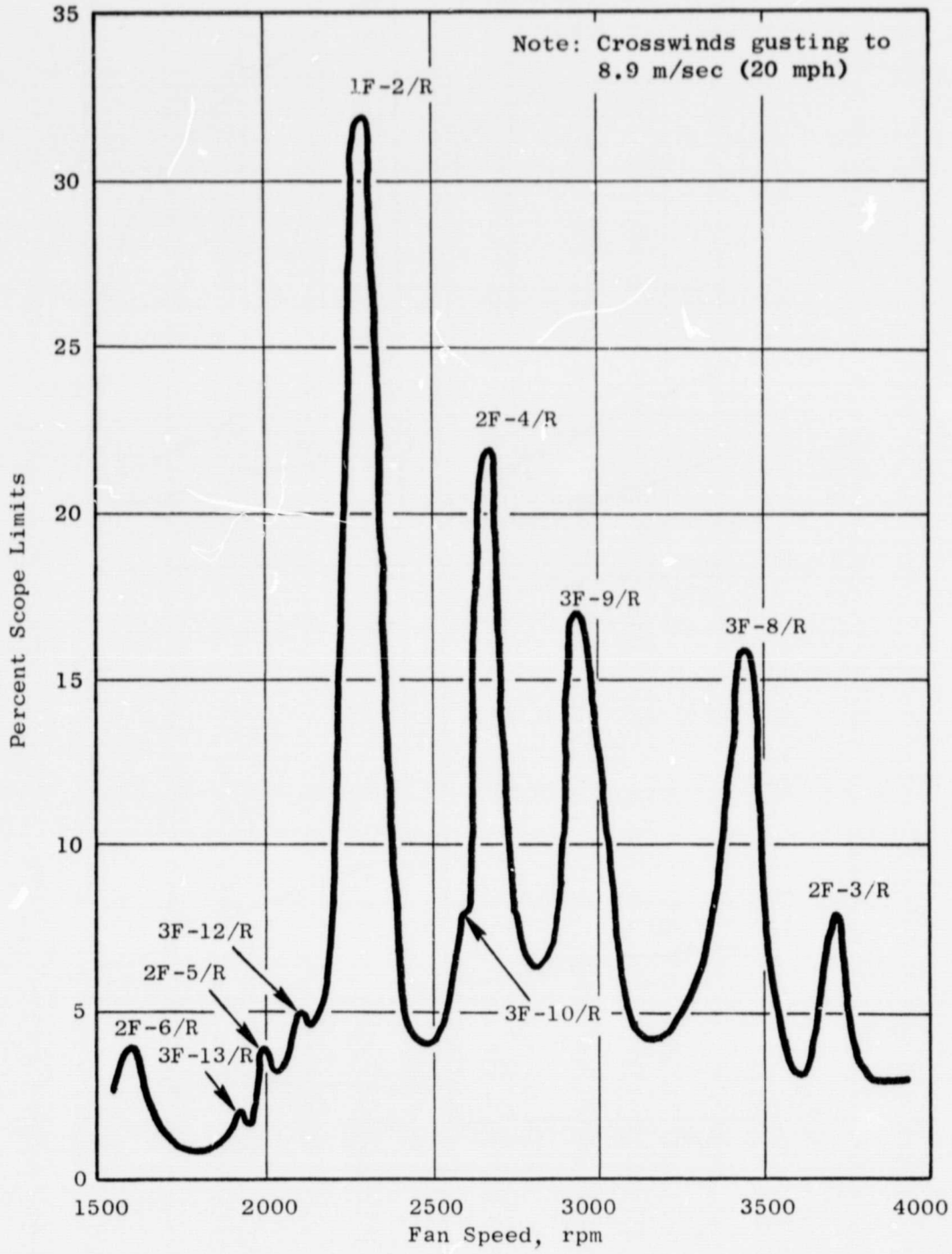

Figure 13. QCSEE OTW Fan Blade Checkout; Bellmouth Inlet, A_8 = 1.72 m^2 (2666 $in.^2$).

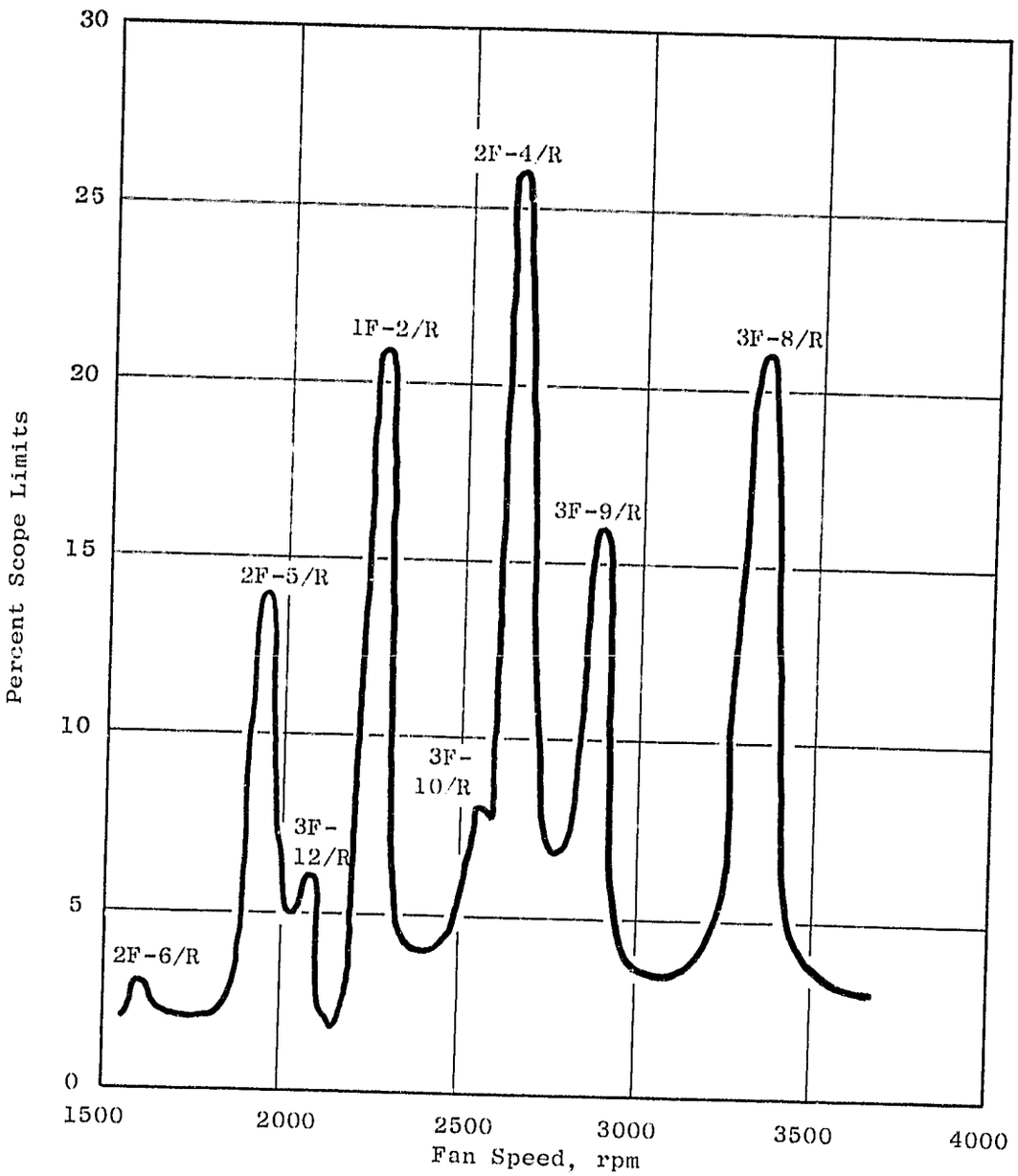

Figure 14. QCSEE OTW Fan Blade Checkout; Bellmouth Inlet, A_8 = 1.58 m^2 (2444 $in.^2$).

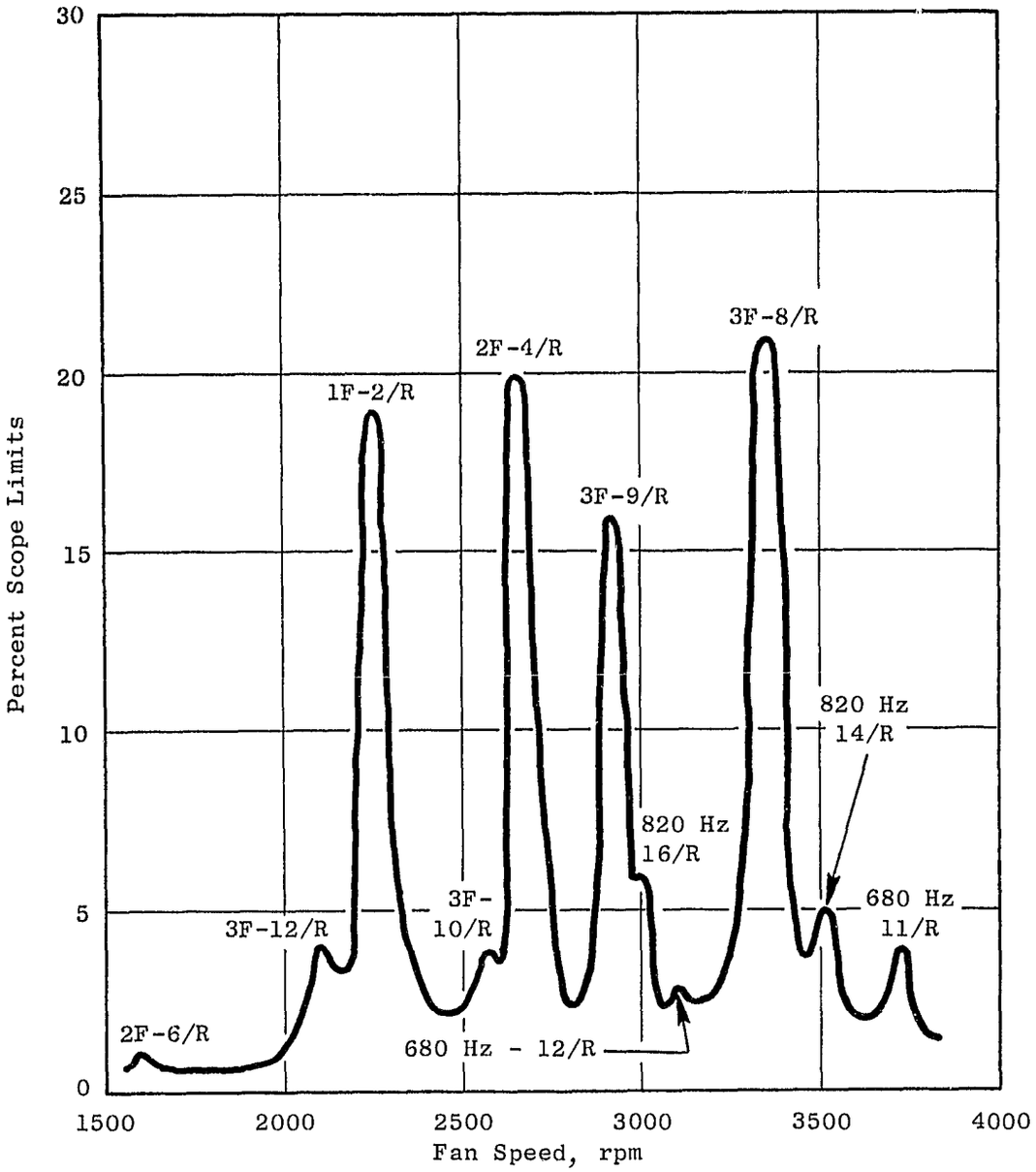

Figure 15. QCSEE OTW Fan Blade Checkout; Bellmouth Inlet, A_8 = 1.90 m^2 (2947 $in.^2$).

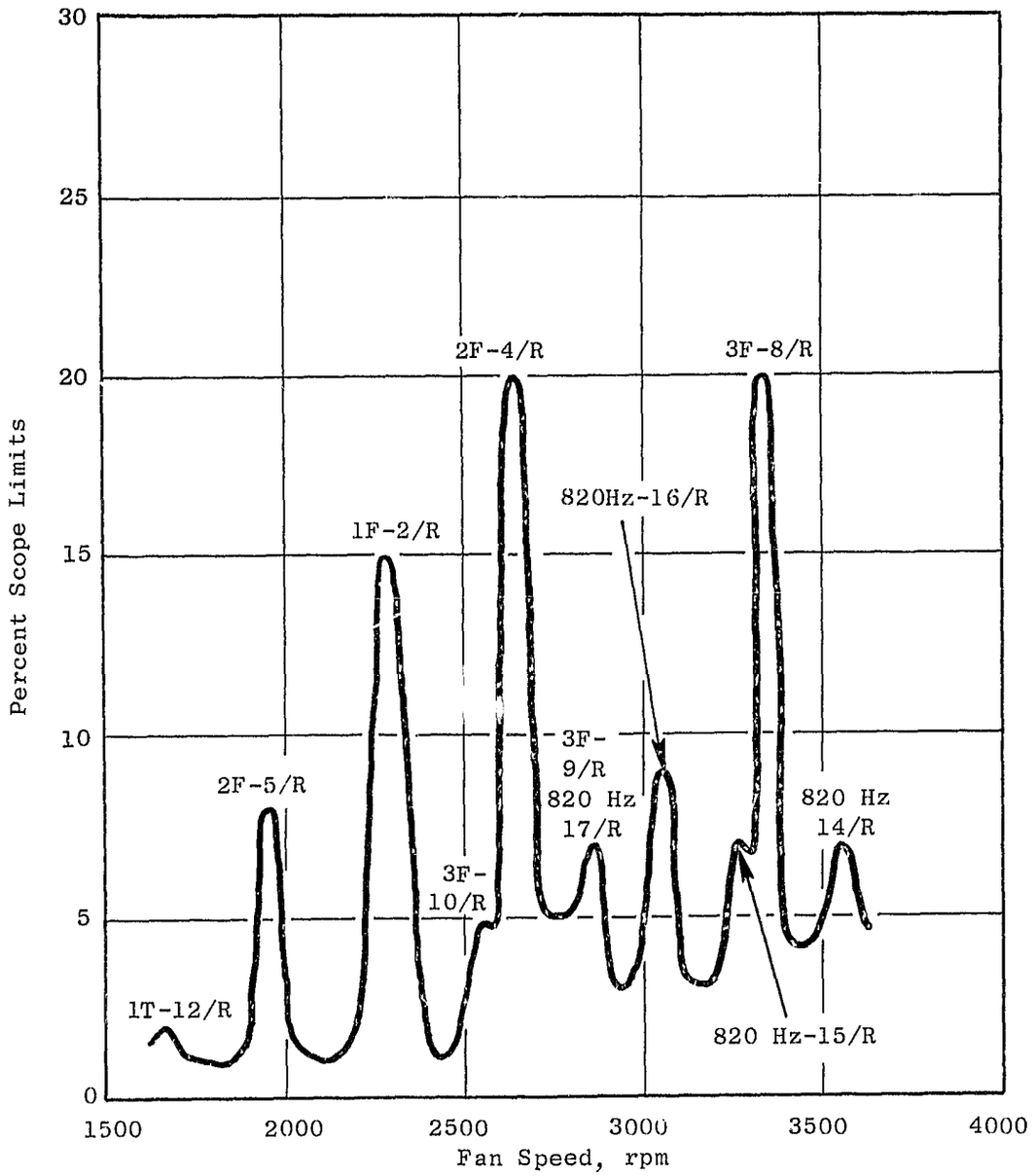

Figure 16. QCSEE OTW Fan Blade Checkout; Accelerating Inlet, A_g = 1.72 m^2 (2666 $in.^2$).

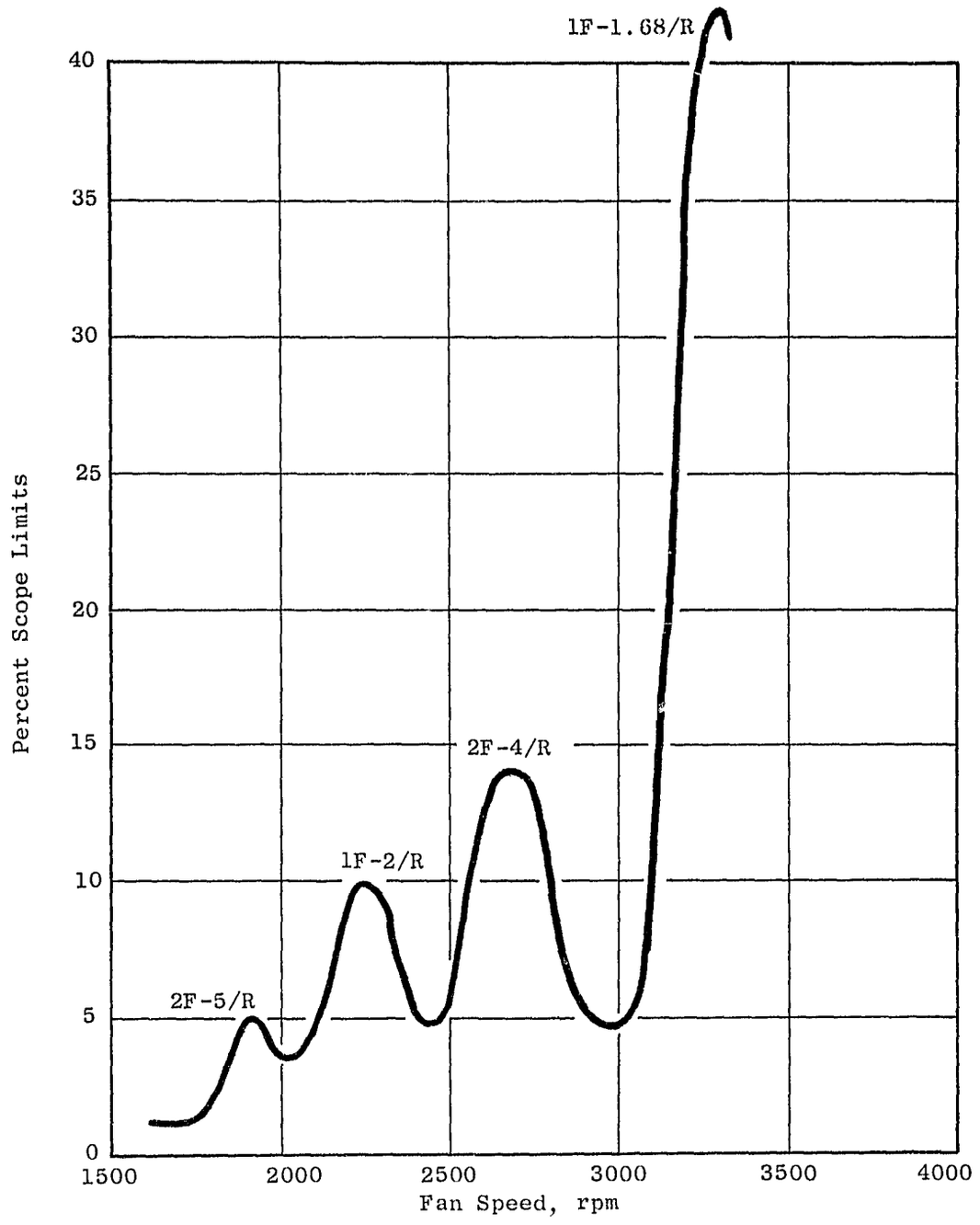

Figure 17. QCSEE OTW Fan Blade Checkout; Thrust Reverse, 115° Deflection - 11.5° Side Doors.

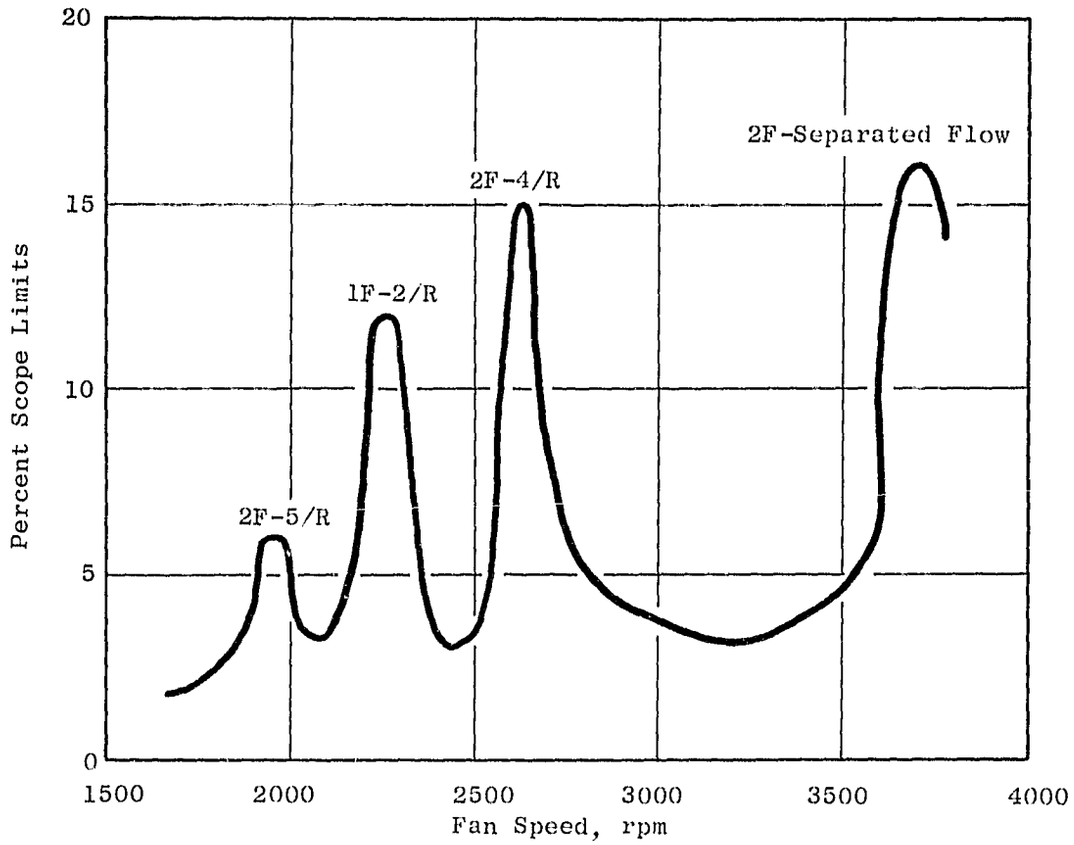

Figure 18. QCSEE OTW Fan Blade Checkout; Thrust Reverse, 105° Deflection - 0° Side Doors.

Forward Thrust - Vibratory stress levels seen during the initial testing with the bellmouth inlet were the highest of any forward-thrust configuration. Maximum vibratory stress in the instrumented blades was 32% of limits, actual stress of 128 MN/m^2 (18.5 ksi), at the 1F-2/rev crossover (Figure 13) during an engine transient with crosswinds gusting to 8.9 m/sec (20 mph). It was observed during testing that the blade stress levels showed sensitivitiy to the wind. Other prominent resonances noted during bellmouth testing were the 2F-4/rev and 3F-8/rev crossings. These maxima were less than 30% of limits; actual stresses were 93 MN/m^2 (13.5 ksi) and 30 MN/m^2 (4.3 ksi) respectively. It is probable that wakes from the four pressure rakes in the engine inlet contributed to the response of the blades in these modes.

In another test, the fan speed was set on the 1F-2/rev and 2F-4/rev crossover points and held for approximately one minute each to determine the fan blade response in other than transient conditions. At neither point did the stress level exceed 30% of limits; results are shown in Figure 14.

Three operating lines were traversed with the bellmouth inlet: A8 = 1.72 m^2 (2666 $in.^2$), A8 = 1.58 m^2 (2444 $in.^2$), and A8 = 1.9 m^2 (2947 $in.^2$). Blade stress results are shown in Figures 13, 14, and 15. As the figures show, the stress responses with the three exit areas are similar; the major stress producers are the resonant crossings of frequency and per rev lines, as predictable from a study of the Campbell diagram (Figure 6).

Figures 19 and 20 show typical stress response during bellmouth testing as reduced by the FFT analysis. Figure 19 shows the first, second, and third flexural resonances as well as the absence of first torsional response. The absence of torsional vibration was noted throughout the testing even with gages most sensitive to this mode. There was also a low level of response in the higher frequency modes typically as shown in Figure 20. Forward-thrust testing with the accelerating inlet and with the reingestion shield produced stress patterns similar to the bellmouth inlet but generally lower level; Figure 16 is typical.

The percent scope limits shown in the diagrams and quoted above are not exactly accurate in that they are the percent of limits for a single mode of vibration. Generally the blade vibrates in combined modes, but an examination of the FFT analyses shows that when the OTW fan blade is vibrating in a major mode there is very little contribution from other modes. For this reason combined-mode scope limits were not calculated.

Reverse Thrust - Prior to reverse-thrust testing, the equivalent exhaust area (A_8) of the initial reverse configuration (115° deflection, 0° side doors) was estimated. The area estimate, 1.46 m^2 (2266 $in.^2$), compared with the predicted stability boundary in Figure 9, indicated that operation in this configuration would produce blade instability in the flexural mode. This prediction was verified upon startup when stress buildup was rapid and increasing, (as shown in Figure 21), requiring a throttle chop before achieving idle speed. Stress was approximately 35% of limits and far in excess of all previously experienced starts. Also shown in Figure 21, for comparison,

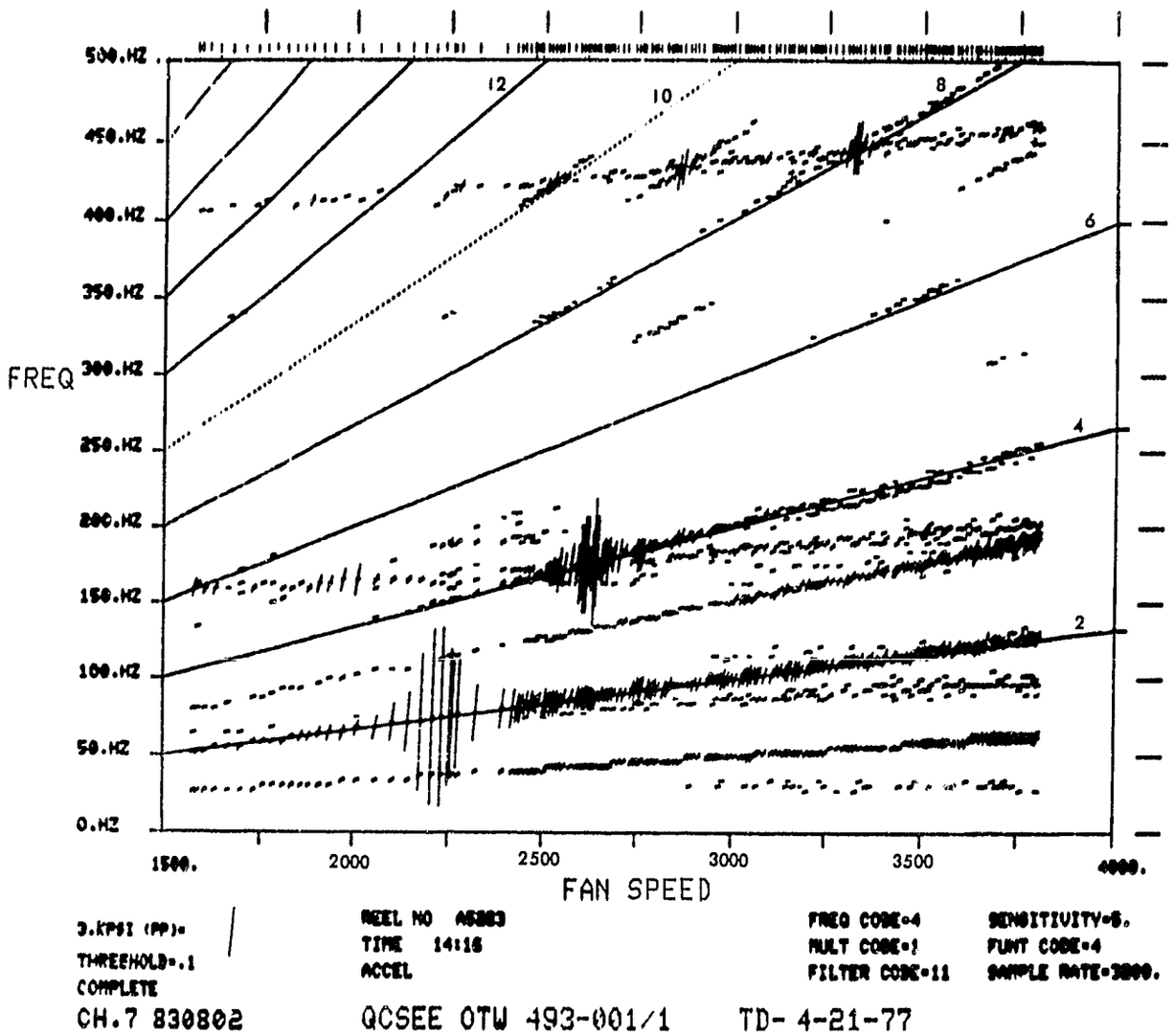

Figure 19. Typical FTT Analysis Stress Response.

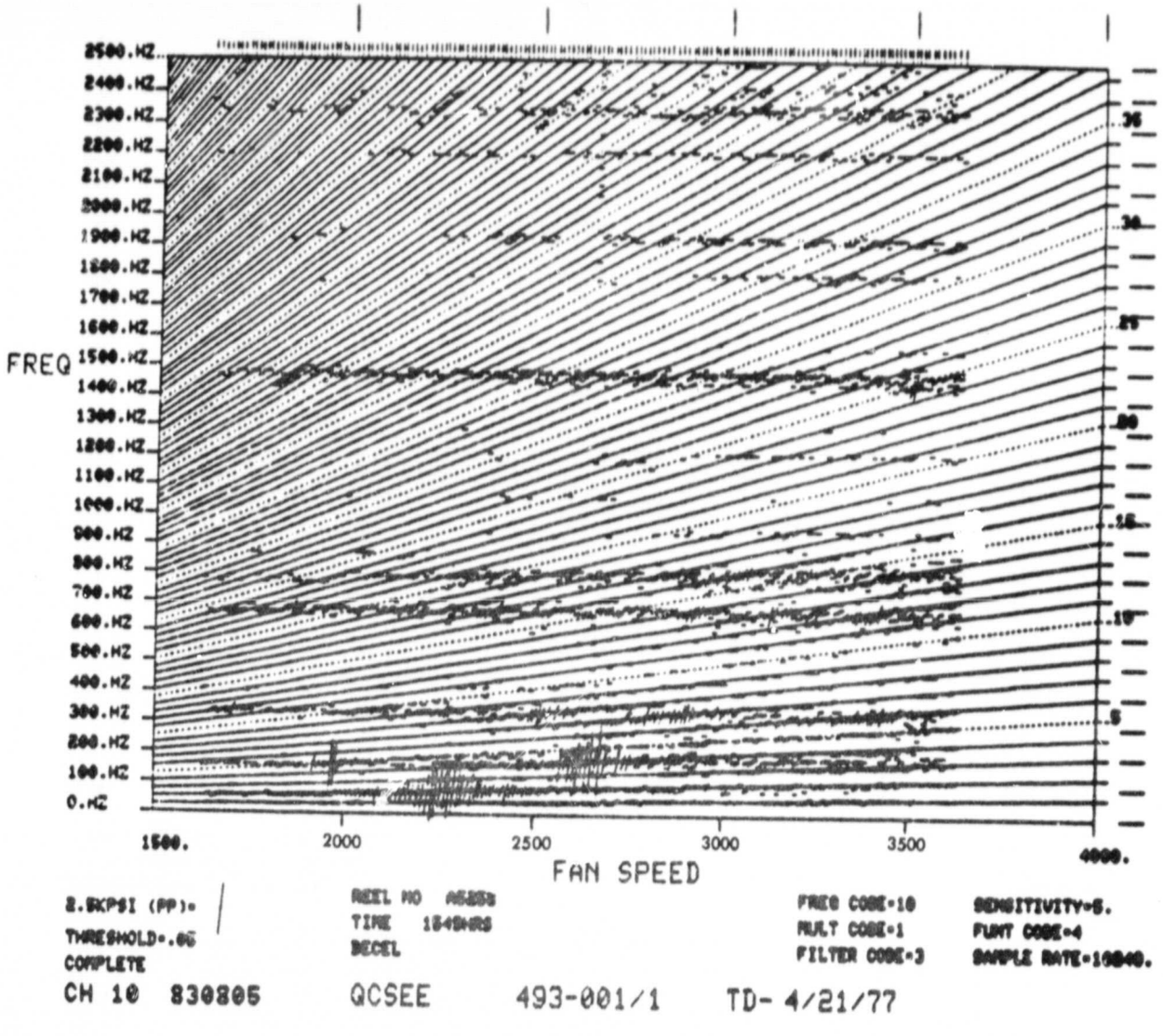

Figure 20. Typical FTT Analysis Stress Response.

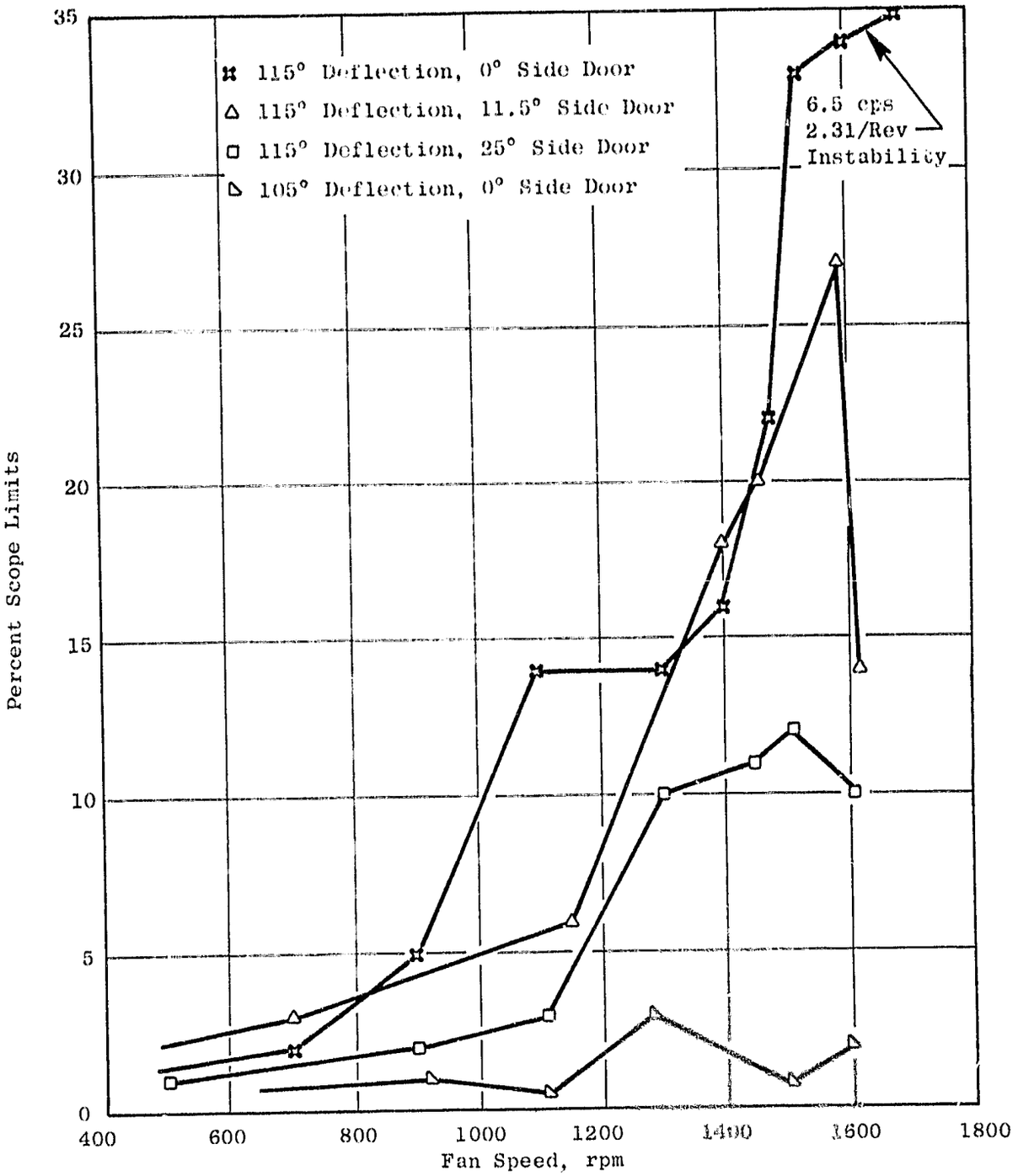

Figure 21. Fan Blade Stress at Engine Start - Thrust-Reverse Mode; First-Flexural Blade Vibratory Mode.

are other starts with less restrictive areas, including the 105° deflection 0° side door configuration where stress levels more nearly approximated that of forward modes.

Reverse-thrust testing was continued in a second, less restrictive configuration: 115° deflection, 11.5° side doors. At fan speeds above 3000 rpm the blades showed increasing stress levels with speed (Figure 17); this indicates that the blade was moving progressively into a region of instability with a nonintegral-order per rev of 1.68. A decision was made to restrict stress buildup to 40% of limits; this limit was reached at 3300 rpm, and testing of this configuration was terminated at that point.

Reverse-thrust performance objectives were met at the reverse configuration of 105° deflection and 0° side doors. Startup stresses were normal; stresses through the speed range (Figure 18) were on the order of what had been seen in forward-thrust configurations. No evidence of instability was seen.

Figure 22 is a summary of QCSEE OTW engine experience with regard to fan blade stability in terms of the reduced velocity parameter. The test data is superimposed on the predicted data of Figure 9 and shows reasonably good correlation. The two points of instability discussed above are shown in the best estimated position based on available data. The experience shown in Figure 22 indicates the need to reposition the flexural-stability boundary as shown.

4.5 OPERATING LIMITS

In the forward-thrust mode there is no restriction on fan operation in any of the configurations tested, other than limiting wind velocity to no more than 8.9 m/sec (20 mph) as was experienced in early testing. Operation at A8 less than the test 1.58 m^2 (2444 $in.^2$) increases risk because the fan operating line moves toward stall, and first-flexural instability probably occurs before stall. There is no confirmation of the location of the forward-mode stability boundary (flexural), whether it is in the same position as the reverse boundary or not, since no testing was done at A8 less than 1.58 m^2 (2444 $in.^2$). No correlation could be made between forward-mode exhaust areas and equivalent exhaust areas in the reverse mode because the configuration precluded any geometrical or aerodynamic comparison.

In the reverse-mode operation at 105° deflection, testing was done throughout the program at relatively low stress levels. Although several test points were run at the 115° deflection, 11.5° side doors, it was noted that stresses were higher than normal in this configuration throughout the test range, suggesting the proximity of the stall/stability boundary, and culminated in the instability at 3300 rpm.

Based on available test data, therefore, no restriction is placed on reverse-thrust testing at 105° deflection, but testing at 115° deflection greatly increases the risk of operating the fan blades in flexural instability.

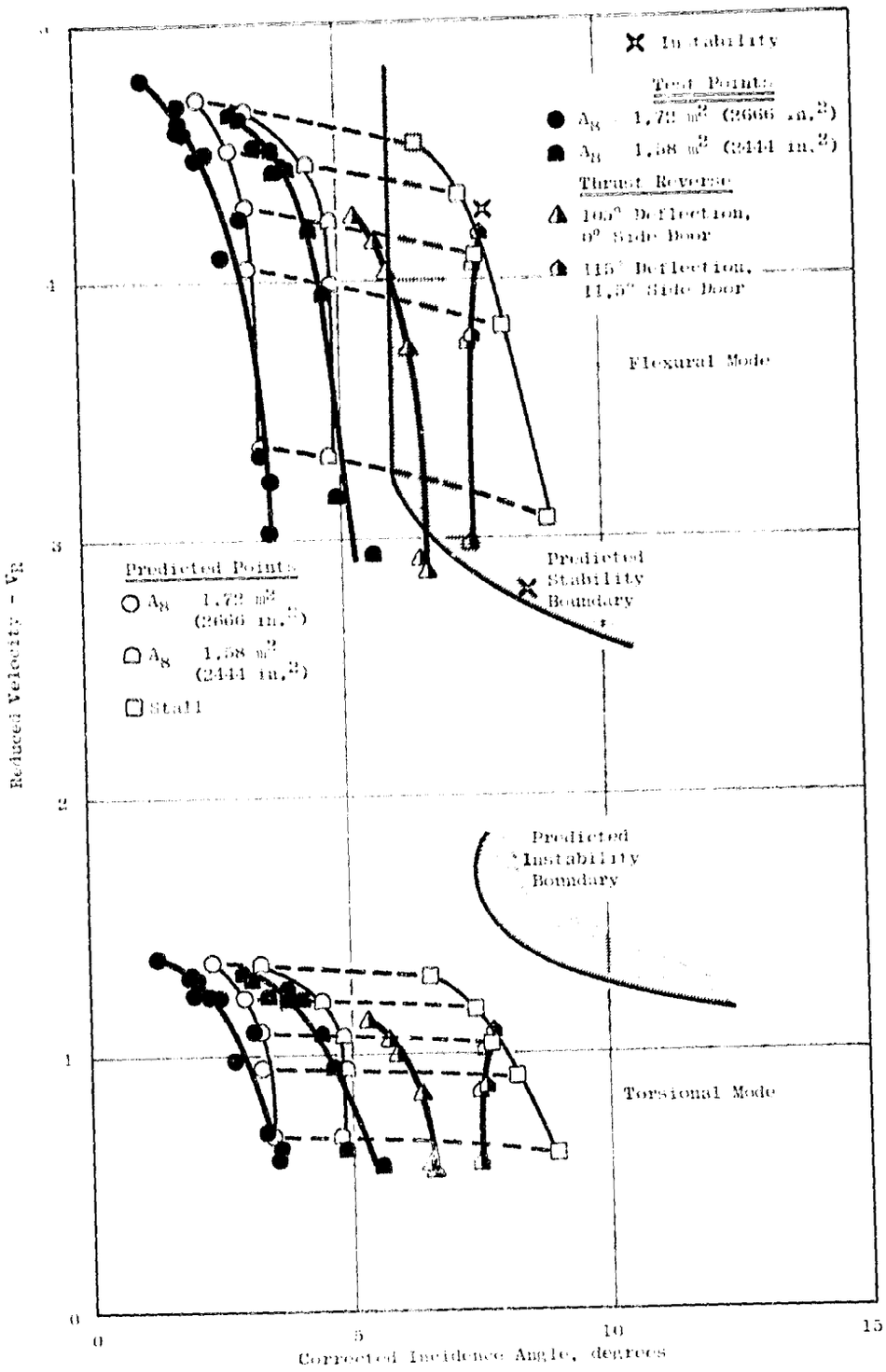

Figure 22. Corrected Fan Stability Map.

5.0 MAIN REDUCTION GEAR

The OTW engine has a star-type, epicyclic, reduction gearset in the forward engine sump to reduce the low pressure turbine speed relative to fan rotor speed. The gearset is shown schematically in Figure 23. The gearset consists of a flexibly mounted sun gear, which drives eight star gears, which in turn drive a ring gear. The ring gear is flexibly mounted to the fan shaft. Principal design characteristics are listed in Table V.

Although the engine was not disassembled for inspection of the reduction gear parts, all test operation was satisfactory. Data from bearing thermocouples, ring gear strain gages, and star gear proximity probes remained within established limits at all times.

5.1 TEST RESULTS

Gear Efficiency - Table VI shows the results of two methods of calculating power loss and efficiency of the gears. The power losses based on heat exchanger (HX) data were determined as follows:

1. Heat losses from the core engine were estimated based on F101 testing, subtracting non-QCSEE items.

2. Heat losses from the 1R and 1B bearing were calculated.

3. The accessory gearbox heat loss was determined from estimated oil flow to the gearbox based on core speed and measured oil temperature rise.

4. The main reduction gear heat rejection (plus other unknown heat losses) was determined by subtracting the sum of the above items from the total heat transferred by the heat exchanger.

The power loss based on the bearings was determined as follows:

1. Oil flow to gears was determined from the oil supply pressure at the gears.

2. The temperature rise of the oil was based on the assumption that the oil discharge temperature was equal to the maximum star gear bearing temperature, and the engine oil inlet temperature remained unchanged before it entered the gearset.

3. From this data and the specific heat of the oil, the heat losses were calculated.

From the table it is evident that an exact determination of gear efficiency is not possible. The bearing approach shows up to 0.6% higher efficiency than the heat exchanger approach. Within the accuracy of these data, the gear efficiency appears to be near 97.7% at 8352 kW (11200 hp), 3300 rpm, and "oil-in" temperature of 378 K (220° F).

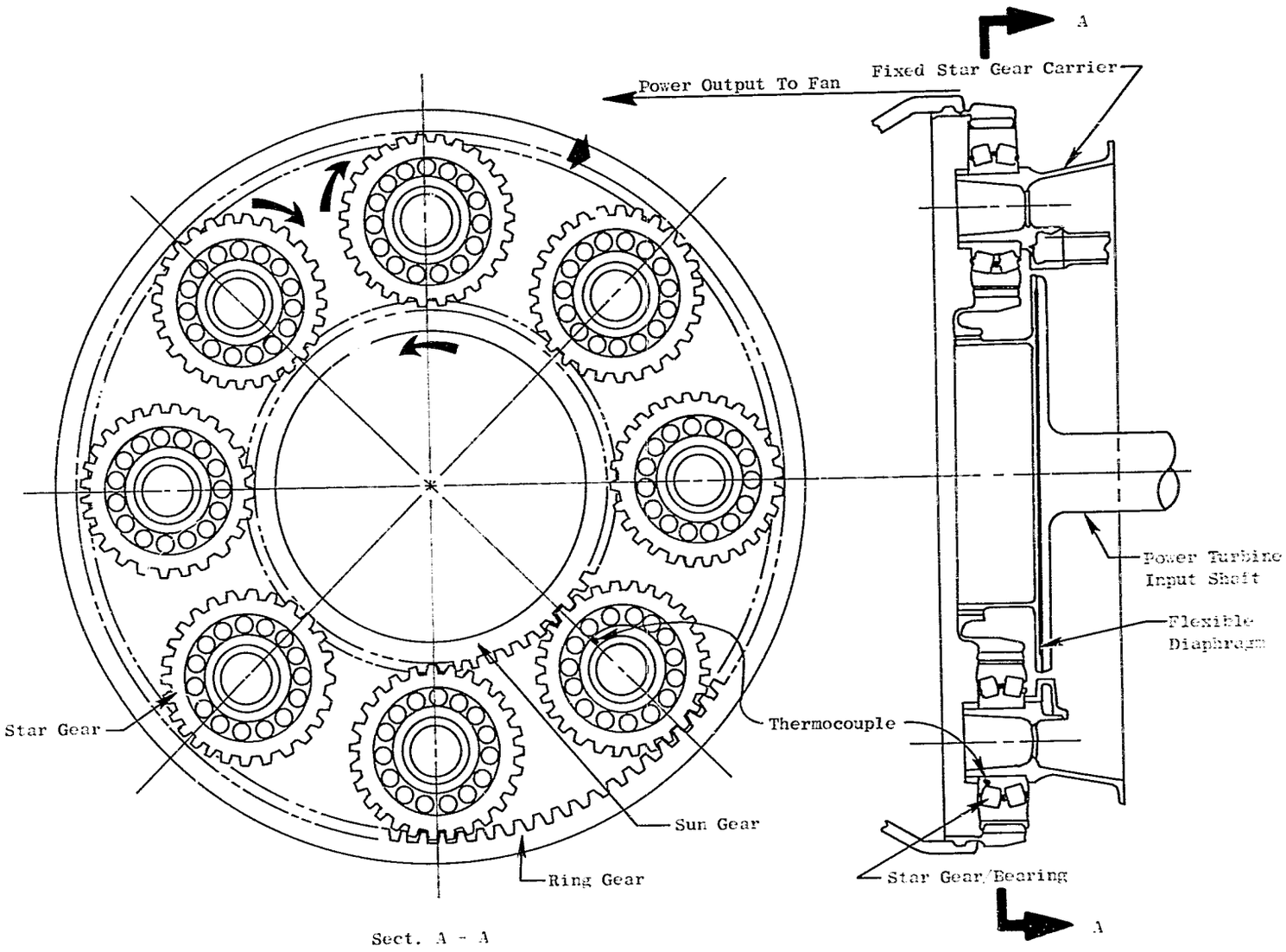

Figure 23. Main Reduction Gear Configuration.

Table V. OTW Reduction Gear Design Details.

[Takeoff, 306 K (90° F) Day]
[100% Power, 100% Speed]

Gear ratio	2.062
Turbine power	12,813 kW (17,183 hp)
Turbine speed	833.8 rad/sec (7962 rpm)
Gear pitch line velocity	119.3 m/sec (23488 ft/min)
Star gear speed	1570.6 rad/sec (14998 rpm)
Bearing load	26,845 N (6035 lbf)
Number of stars	8
Number of gear teeth	
Sun gear	81
Star gear	43
Ring gear	167
Hunting	Yes
Nonfactoring	Yes

Table VI. Main Reduction Gear Efficiency.

Fan rpm	Heat Exchanger Basis			Bearing Basis			Fan Power		Δ η
	Power Loss kW	(HP)	Eff. η	Power Loss kW	(HP)	Eff. η	kW	(HP)	
A_8 = 1.9 m^2 (2947 $in.^2$)									
3,140	211	(283)	97.12	180	(242)	97.5	7,328	(9,827)	-0.38
3,290	194	(260)	97.67	171	(229)	97.9	8,356	(11,206)	-0.23
3,670	264	(354)	97.80	202	(271)	98.40	12,406	(16,637)	-0.60
3,704	225	(302)	98.12	224	(301)	98.13	12,041	(16,147)	0.01
A_8 = 1.72 m^2 (2666 $in.^2$)									
2,908	91	(122)	98.43	128	(171)	97.79	5,790	(7,764)	0.64
3,116	169	(227)	97.60	150	(201)	97.87	7,059	(9,466)	-0.27
3,471	248	(332)	97.60	213	(286)	97.92	10,235	(13,725)	-0.32
3,647	265	(355)	97.71	228	(306)	98.02	11,567	(15,512)	-0.31
3,682	286	(383)	97.68	216	(289)	98.28	12,578	(16,867)	-0.60
3,689	258	(346)	97.72	234	(314)	97.93	11,348	(15,218)	-0.21
3,697	278	(373)	97.55	237	(318)	97.91	11,370	(15,247)	0.36
A_8 = 1.58 m^2 (2444 $in.^2$)									
3,587	274	(368)	97.7	203	(272)	98.3	11,848	(15,889)	0.60

Ring Gear Stress - Figure 24 shows the measured ring gear alternating stress as a function of speed. Also shown in the figure are the predicted stress and the allowable stress. This figure shows the stress higher than predicted but below the maximum allowable. Stresses show peaks at 2280 rpm and 2560 rpm. These correspond to areas where the fan blades pass through criticals; therefore, these higher stresses are attributed to fan loading. Figure 25 shows that the stress peaks eight times per revolution (star gear frequency). The stress variation mesh to mesh is small, showing extremely good load distribution at each star gear mesh. It was also noted that the stress races repeat exactly every 18th revolution, which is a result of the hunting tooth design bringing the same pair of teeth into contact.

Gear Wobble - During the entire test, wobble was well within the 0.0762 cm (0.030 in.) limits set from rig testing.

Star Gear Bearing Temperature - Throughout the test, star gear bearing temperatures were within the 417 K (290° F) limits. The average bearing temperature difference from oil inlet temperature is shown as a function of fan speed in Figure 26.

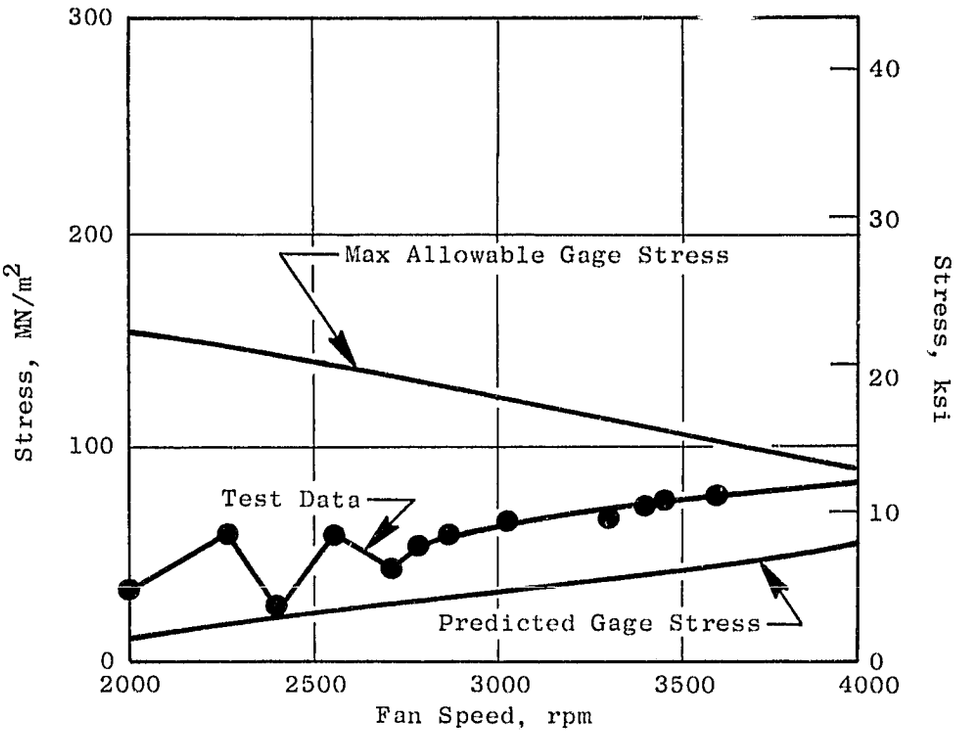

Figure 24. Ring Gear Stress Vs. Fan Speed.

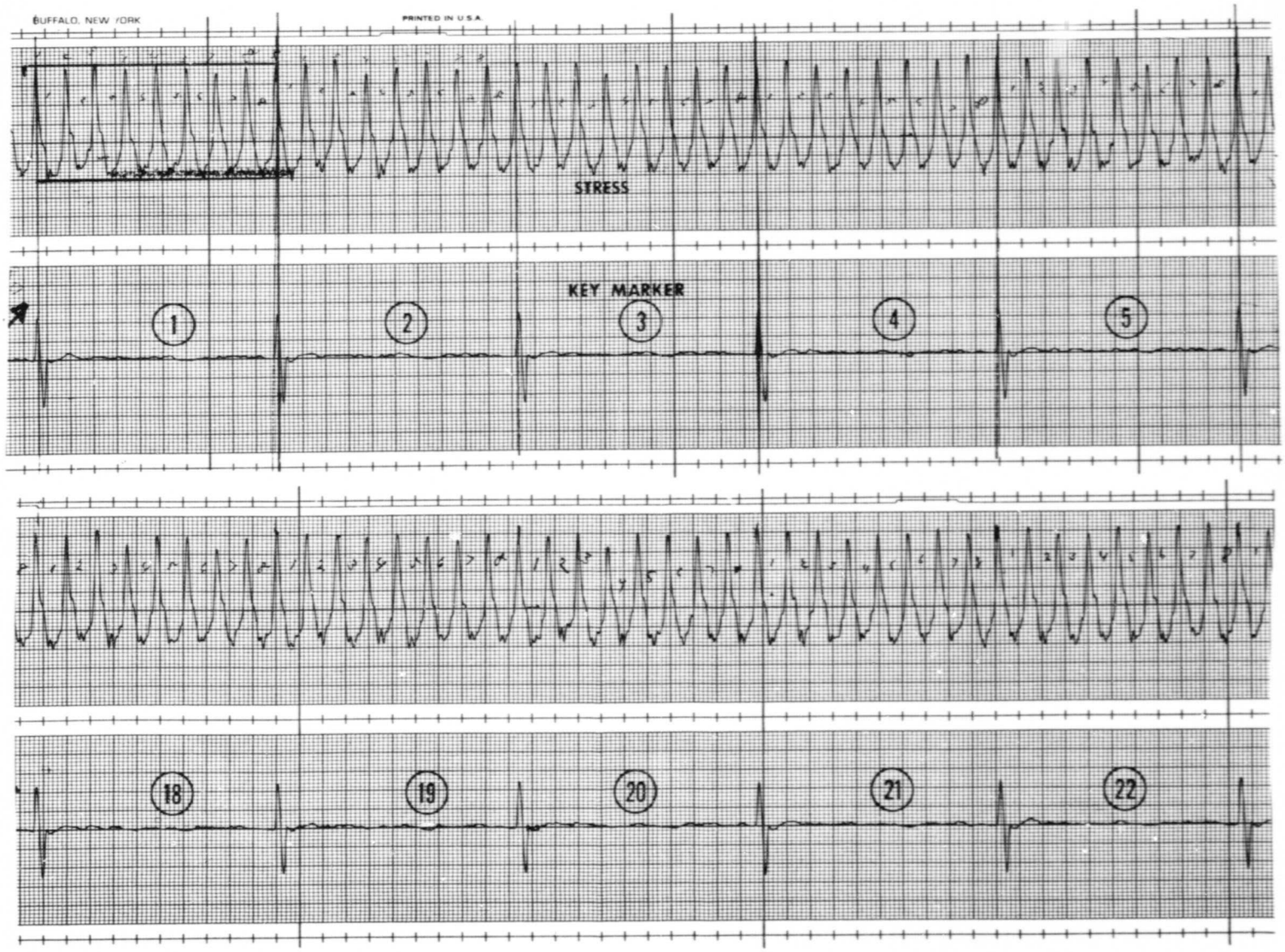

Figure 25. Ring Gear Stress Traces (NF = 3648 rpm).

Figure 26. Main Reduction Gear Bearing Average Temperature Rise.

6.0 LUBRICATION AND ACCESSORY DRIVE SYSTEM

6.1 SYSTEM DESCRIPTION

The OTW engine utilizes six main shaft bearings to support the rotating turbomachinery. The short construction of the concentric OTW rotors permits a two-bearing support system for each rotor. The No. 1B and 1R bearings support the fan rotor. The high pressure core rotor is supported by the No. 3 and No. 4 bearings. The No. 2 and No. 5 bearings support the low pressure turbine and power-transmission shaft. Both the fan and the low pressure turbine shaft are soft-coupled to the engine main reduction gear to minimize induced loads on the gears. The thrust bearings have been located in the engine forward sump to provide more precise control of fan and compressor blade clearances.

Application of a main reduction gear between the fan and low pressure turbine requires that the normal axial load "tie" between fan and low pressure turbine components be severed. As a result, the No. 2 thrust bearing must react the full aft load of the turbine without any negating forward thrust from the fan. In order to reduce the bearing load to an acceptable level, a thrust-balance cavity has been added to the rear sump. This cavity uses compressor discharge air to pressurize a balance piston, providing a forward compensating force on the turbine rotor. A high-load-capacity CF6 No. 1 thrust bearing is used in the design to react the fan axial loads.

A top-mounted accessory gearbox is driven from the core by an F101 internal bevel gearset and a long radial drive shaft. An additional F101 internal bevel gearset located in the bottom half of the engine is combined with a short radial shaft and a second bevel gearset located in the core cowl area to drive a vane-type pump that scavenges oil from both the forward and the aft sumps. This pump, along with a remotely mounted pump, scavenges the top-mounted accessory gearbox.

The lubrication system is designed on the basis of current, dry-sump technology utilizing a circulating oil system. Internal engine and gearbox passages are used wherever possible for oil delivery and return. Venting and pressurization functions also make use of internal engine passages when possible.

6.2 INSTRUMENTATION

Each sump of the QCSEE OTW engine was instrumented as follows to ensure safe operation of the engine:

1. The outer race temperature of each main shaft bearing was measured in two places.

2. The sump pressures and the carbon seal ΔP were measured for the No. 1, No. 3, and No. 6 seals.

3. Temperature in the aft sump cavity was measured.

4. The pressure and temperature were measured in the balance-piston pressurization and exhaust cavities.

5. The inner race temperature of each star gear bearing was measured.

6. The lube pressure in the manifold supplying oil to the reduction gearing was measured.

7. The lube supply and scavenge pump discharge pressures were measured.

8. ΔP across the supply filter was measured.

The accessory gearbox was instrumented as follows:

1. The internal pressure was measured in the vent tube between the gearbox and oil tank.

2. Scavenge oil temperature was measured before it entered the remotely mounted scavenge pump.

3. Gearbox surface temperature was measured close to the bottom of the housing.

The lube system package was instrumented to measure the following parameters:

1. Oil reservoir lube level

2. Oil reservoir internal pressure

3. Scavenge filter ΔP

4. Scavenge discharge temperature

5. Lube supply temperature

6.3 TEST EXPERIENCE

The sump and accessory system, with the exception of oil loss at high fan speeds, performed well throughout the test phase of the QCSEE OTW engine. No problems were encountered with scavenging the top-mounted accessory gearbox.

Main Shaft Bearings - Test limits of 450 K (350° F) were not exceeded by any of the main shaft bearings during the test program. Figures 27 through 29 show representative temperature data for these bearings as a function of

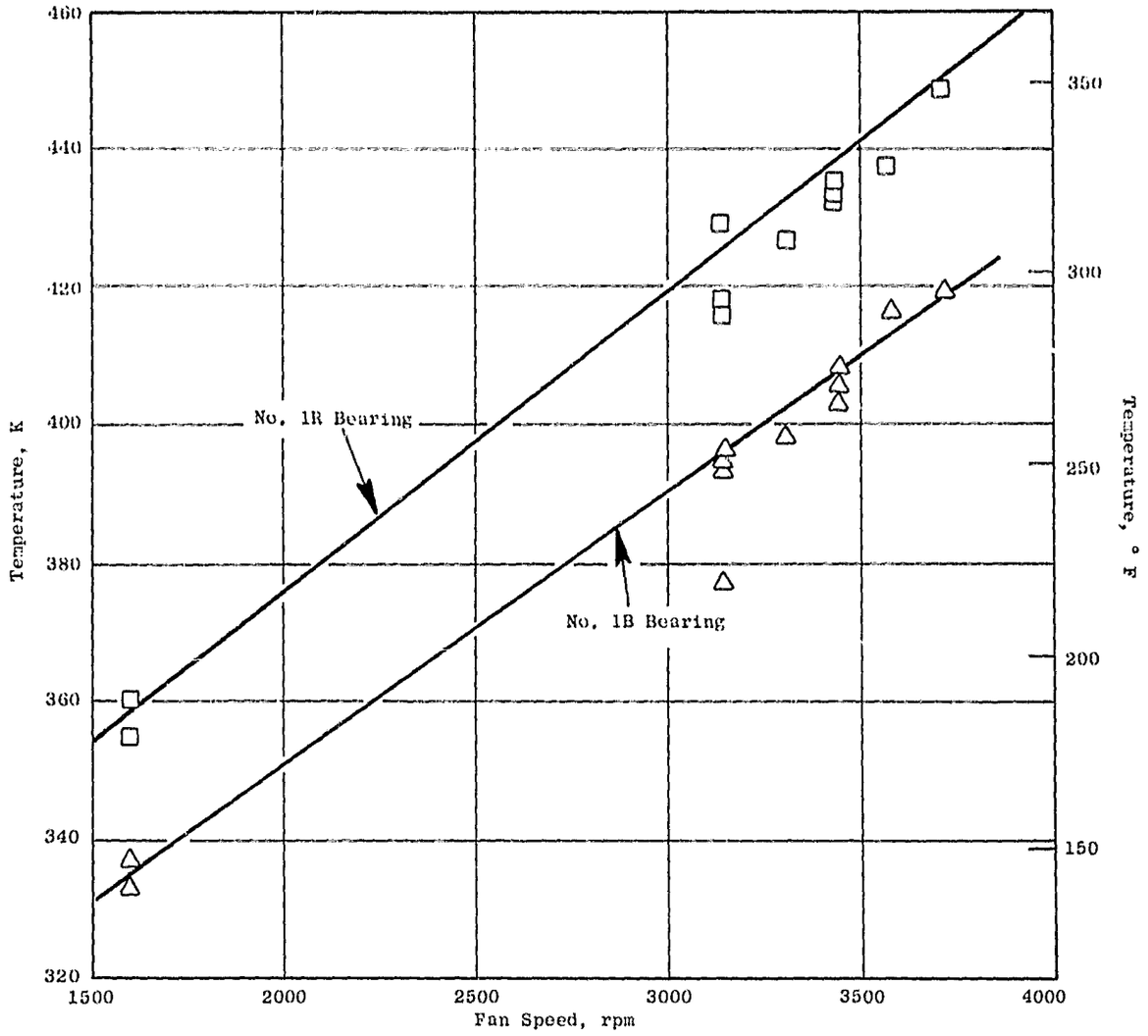

Figure 27. Outer Race Temperature Vs. Fan Speed.

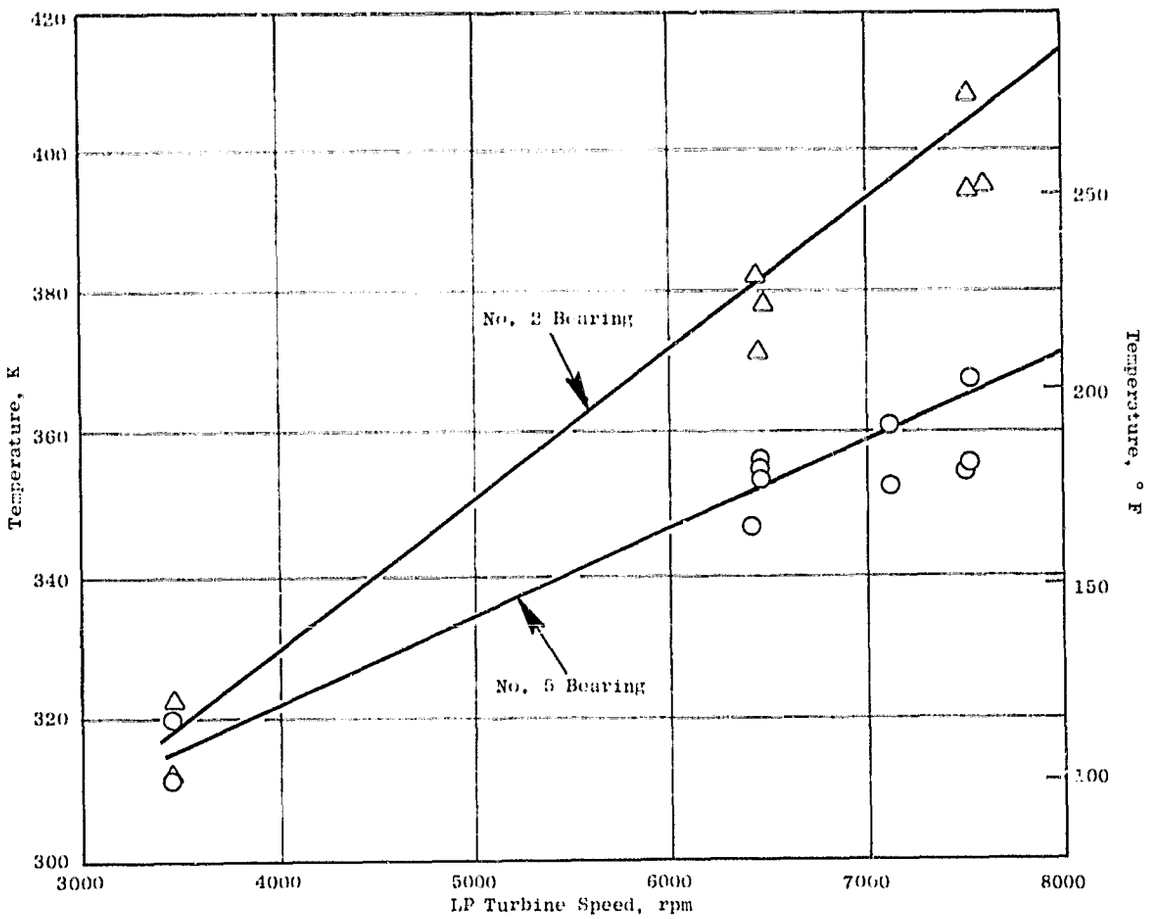

Figure 28. Outer Race Temperature Vs. LP Turbine Speed.

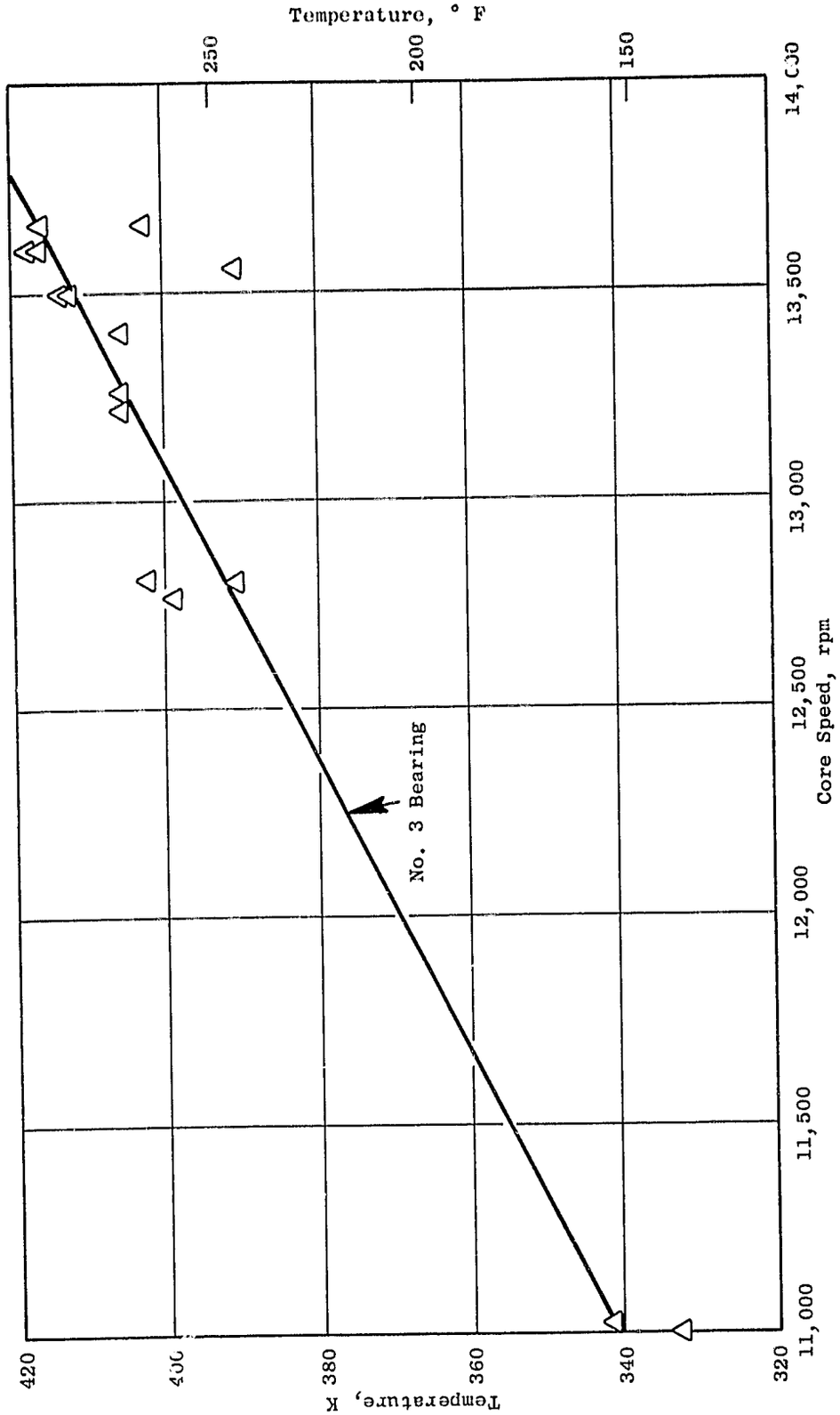

Figure 29. Outer Race Temperature Vs. Core Speed.

engine speed. The bearing with the highest operating temperature was the No. 1R roller bearing. This bearing did reach 449 K (349° F) at 3650 fan rpm. Based on projections from QCSEE UTW engine testing, this was expected; an upper temperature limit of 469 K (385° F) has been established for this bearing. This limit is based on keeping 8.3 K (15° F) below the stabilization temperature of the AISI 52100 bearing material.

Seal Pressurization - The main-shaft carbon seals are pressurized by third-stage compressor air. Figure 30 shows the seal air pressure for the No. 1, No. 3, and No. 6 seals. The No. 4 and No. 5 seal air pressures were not measured but should be between the No. 3 and No. 6 seal pressure levels. The seal pressures were adequate to prevent oil leakage at higher speed operation, but some leakage was collected in the No. 1 seal drain bottle at idle speeds.

Lube Supply and Scavenge System - Lube discharge pressure as a function of core speed is shown in Figure 31. For the OTW engine the hydraulic system make-up oil circuit used in the UTW engine was manifolded to the engine lube supply, and the bypass valve located on the lube pump was adjusted 5-1/2 turns open to achieve the required pressures and flows. The OTW engine system pressure was approximately 20.7 to 34.5 kN/m^2 (3 to 5 psig) higher than the UTW engine over the entire operating range.

Lube supply temperature was controlled by varying the water flows into two heat exchangers mounted in series. The UTW engine utilized only one heat exchanger, and during some portions of testing the maximum available water flow of 9463 cm^3/sec (150 gpm) was required to keep the star gear bearing temperatures below 403 K (265° F). Since the heat rejection of the OTW engine was expected to be higher, two heat exchangers were utilized. The maximum observed water flow required during all OTW testing was 3470 cm^3/sec (55 gpm). The scavenge pump servicing the forward sump, aft sump, and scavenge gearbox functioned well, and the combined scavenge temperature during all testing was below 394 K (250° F). The scavenge system pressure versus core speed is shown in Figure 32. Scavenge pressures were approximately 69 kN/m^2 (10 psig) higher for the OTW engine, relative to the UTW, because of added restriction of the second heat exchanger.

Accessory Gearbox Oil Scavenging - During the testing of the UTW engine, it was found that the top-mounted accessory gearbox was seriously overheating due to lack of scavenging capabilities. A remotely mounted scavenge pump was added to the accessory gearbox and the remainder of the test was completed with this fix.

The OTW engine accessory gearbox was rig-tested to establish scavenging capabilities. The test rig configuration is shown in Figure 33. It was found that if the simulated sump pressure was 4.8 kN/m^2 (0.7 psig) above the gearbox internal pressure, oil drainage from the gearbox would cease and temperatures would increase; this is indicative of flooding. The following fixes were incorporated to improve scavenging.

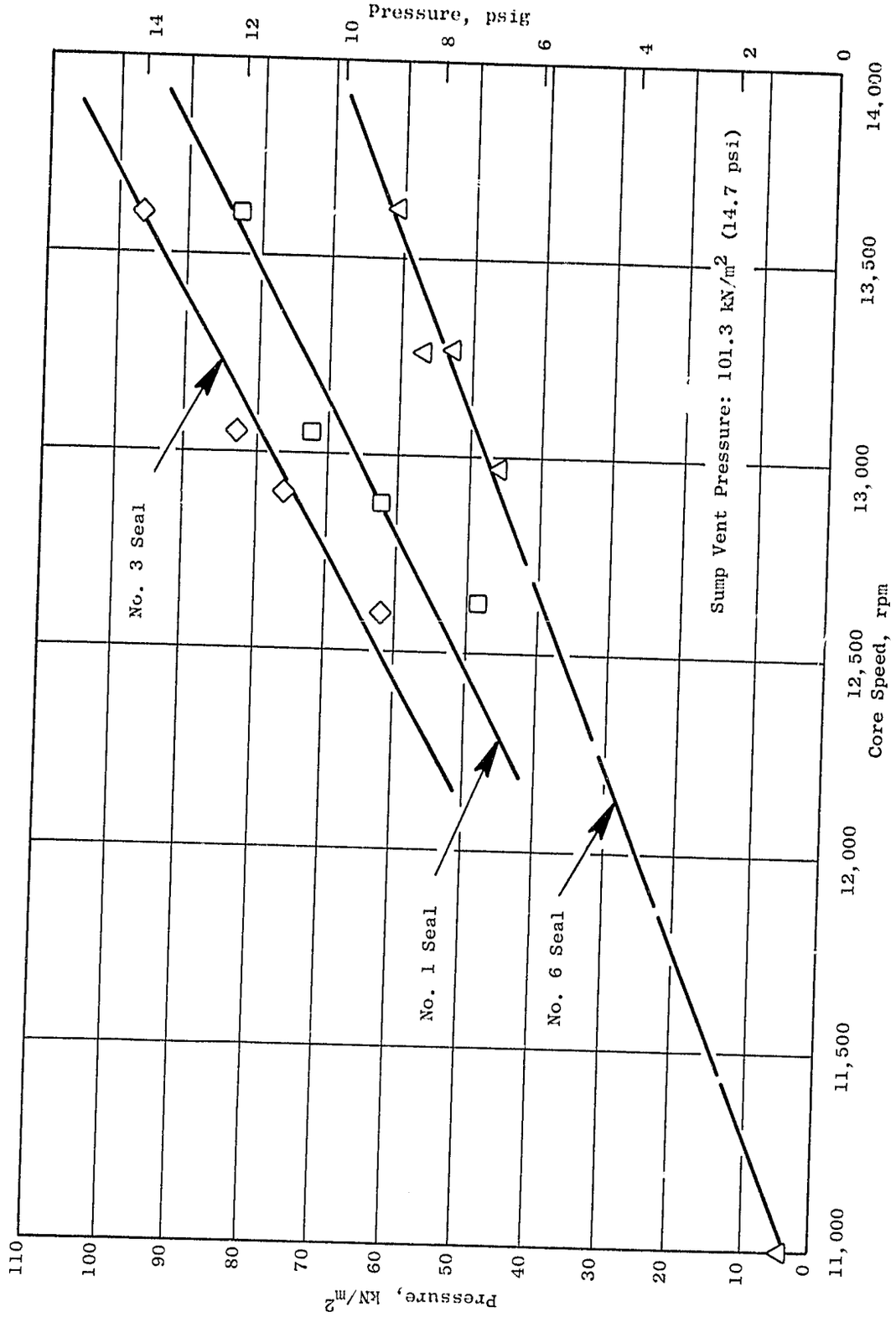

Figure 30. Seal Pressure Vs. Core Speed.

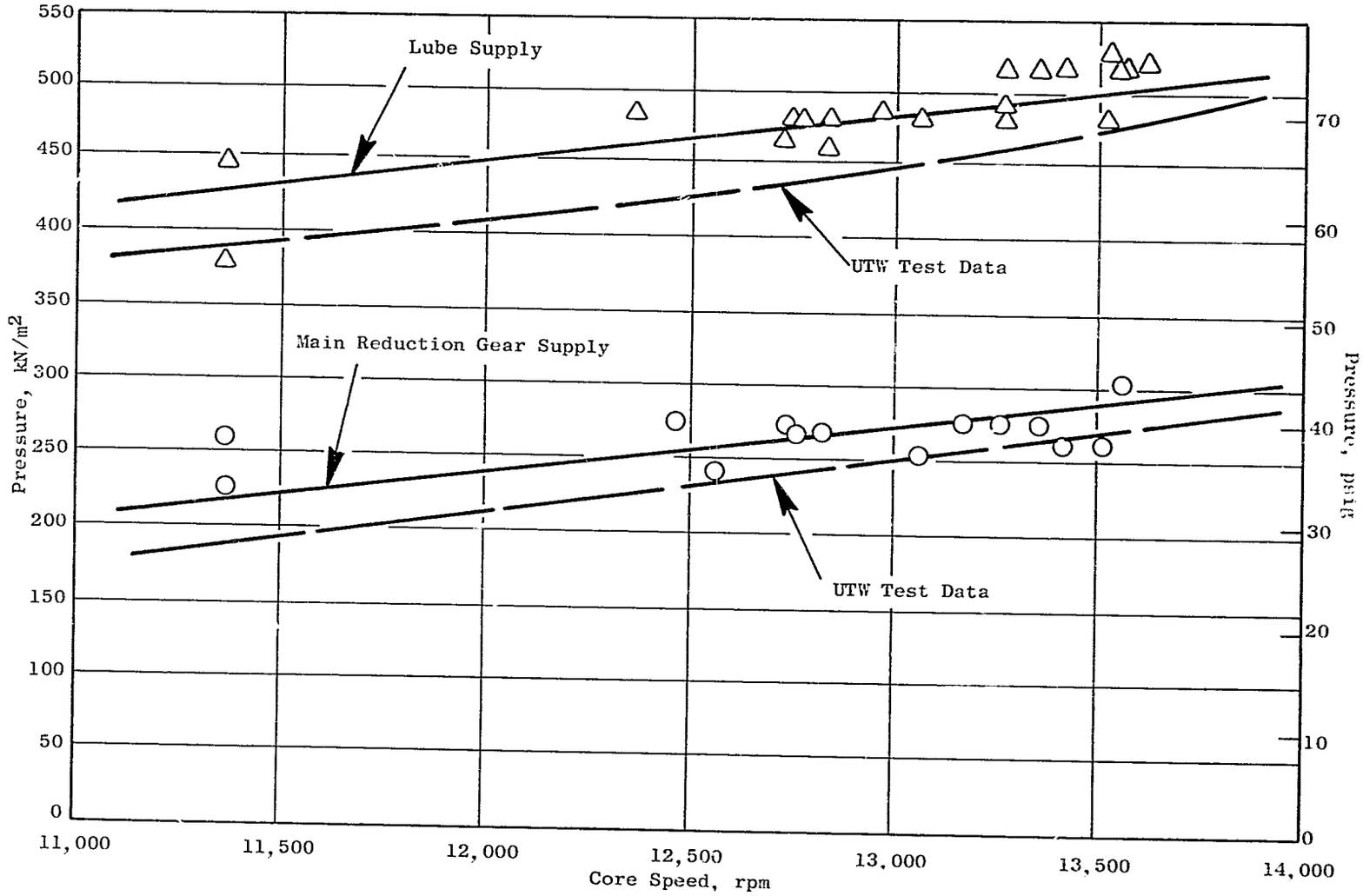

Figure 31. Lube Supply Pressure Vs. Core Speed.

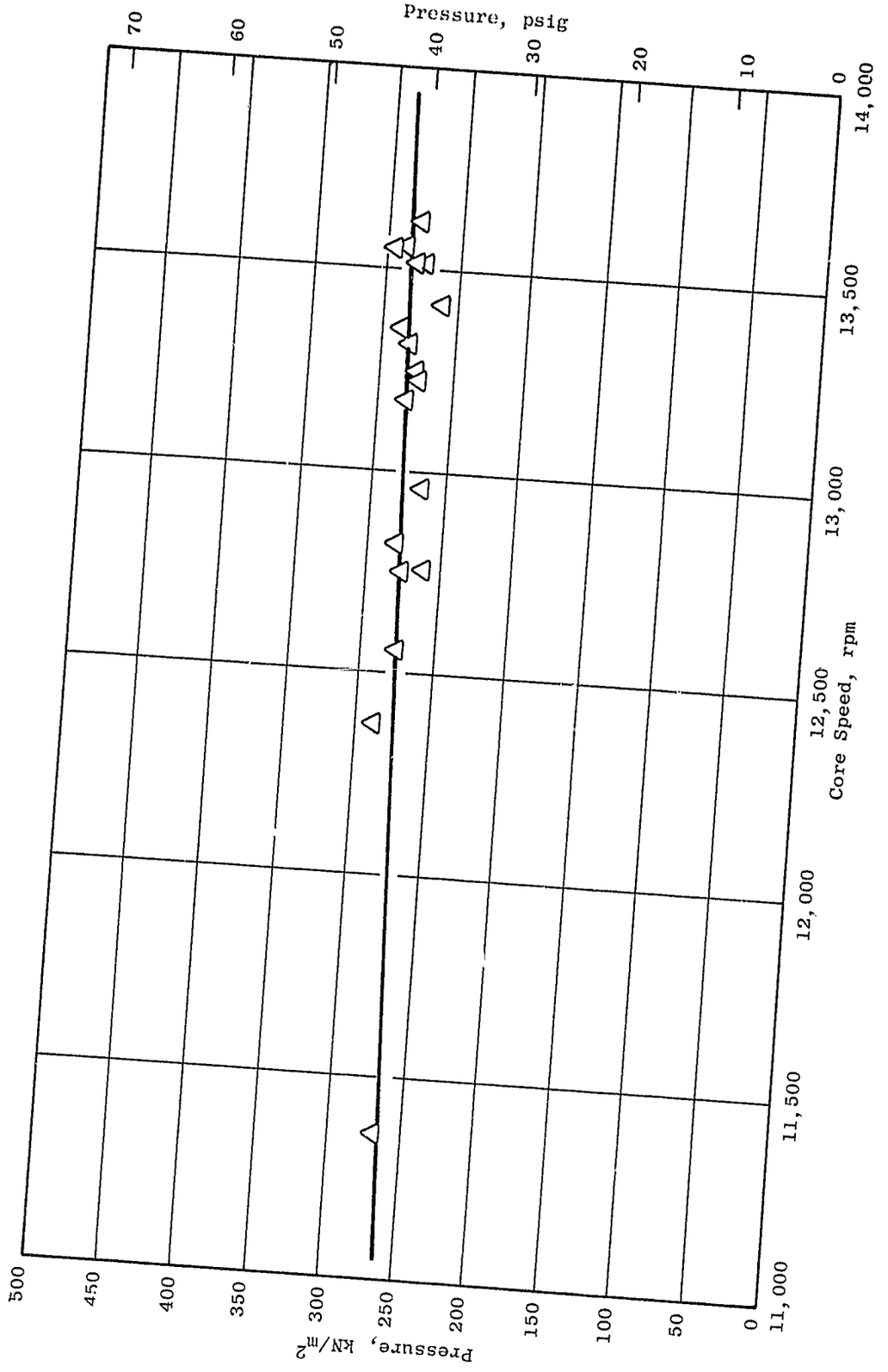

Figure 32. Scavenge Pressure Vs. Core Speed.

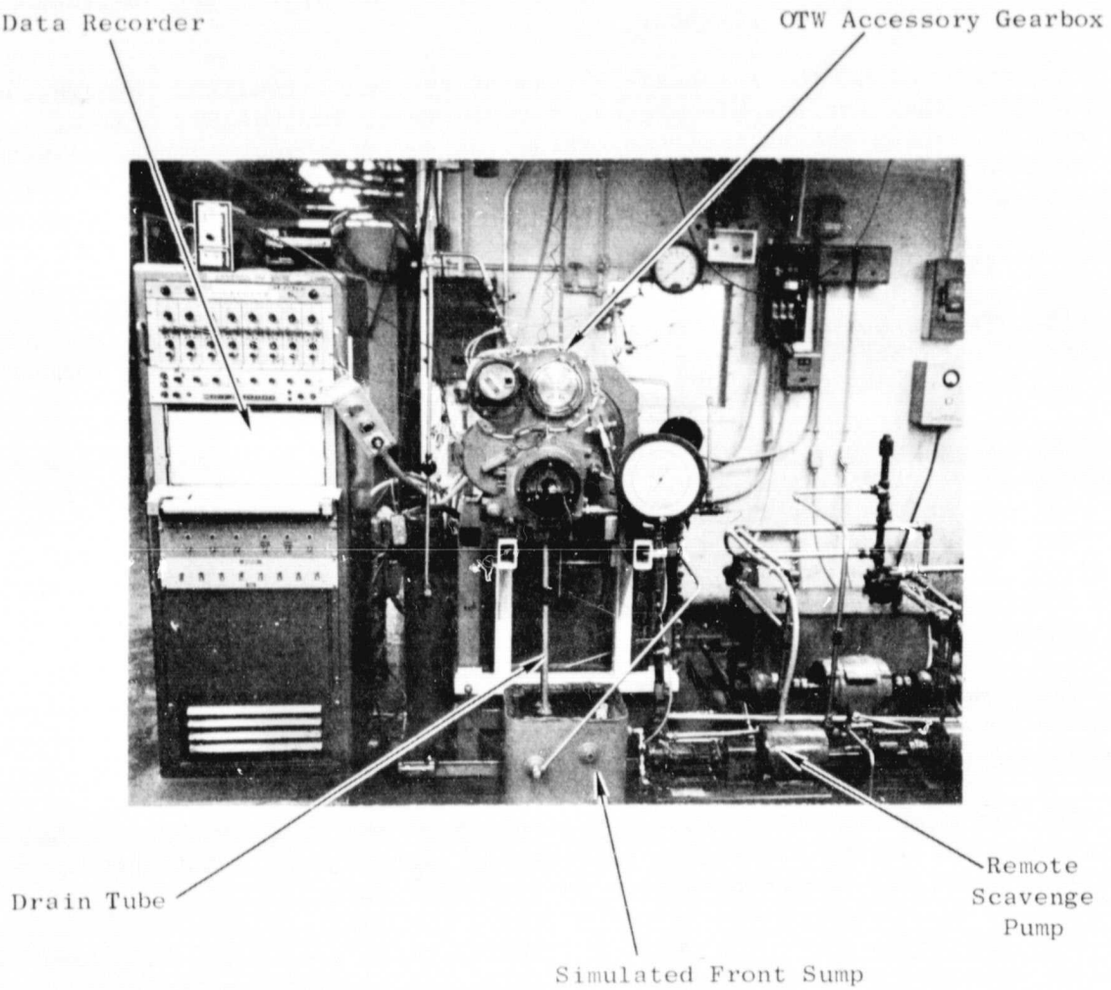

Figure 33. OTW Accessory Gearbox Test Rig Configuration.

- The remote scavenge pump gearbox port was located at the bottom of the gearbox.

- Windage shrouds were added to the vertical bevel gear and the forward side of the horizontal bevel gear.

- Holes were drilled in the horizontal bevel gear and through a vertical partition in the gear housing to improve the internal venting of the gearbox.

Figure 34 shows the temperature rise of the oil circulated through the accessory gearbox for the UTW engine, the rig test, and the OTW engine. During UTW testing the maximum temperature of the accessory gearbox scavenge oil reached 461 K (370° F) at the maximum core speed attained (13,150 rpm). The maximum scavenge oil temperature of the OTW engine accessory gearbox was 395 K (251° F) at a sustained core speed of 13,697 rpm. Transient core speeds of over 14,000 rpm were run with no problem.

The OTW gearbox temperature rise was lower than the component test below 13,400 rpm but rose above it at higher speeds. The gearbox surface temperature maximum was 369 K (204° F) for 13,697 rpm.

Oil Consumption at Higher Fan Speeds - At fan speeds up to 3400 rpm no appreciable oil loss was observed. Above this speed, in at least one test, oil was lost at the rate of 11.4 cm^3/sec (0.18 gpm). There was no apparent oil loss out the air/oil separator (based on utilizing a static air/oil separator during one test). Oil did not appear to be lost through the carbon seals; only minor leakage was noticed in the seal drain bottles mounted below the engine.

There was oil wetness in the area where the core cowl is vented upward to the accessory gearbox area, and this was especially noticed on the starter housing which overhangs this area.

At this time the exact cause and location of the oil loss has not been identified, but during all engine testing it has been only a nuisance-type problem and did not hamper obtaining desired test data.

Heat Rejection - For the QCSEE OTW engine test, two LM2500 heat exchangers mounted in series were used instead of one as used during the QCSEE UTW test. It was concluded after the UTW test that one heat exchanger would not handle the increased heat load expected for the QCSEE OTW engine.

Table VII shows the measured versus predicted heat rejection for the QCSEE OTW engine. Figure 35 also shows heat rejected to the heat exchangers as a function of fan speed.

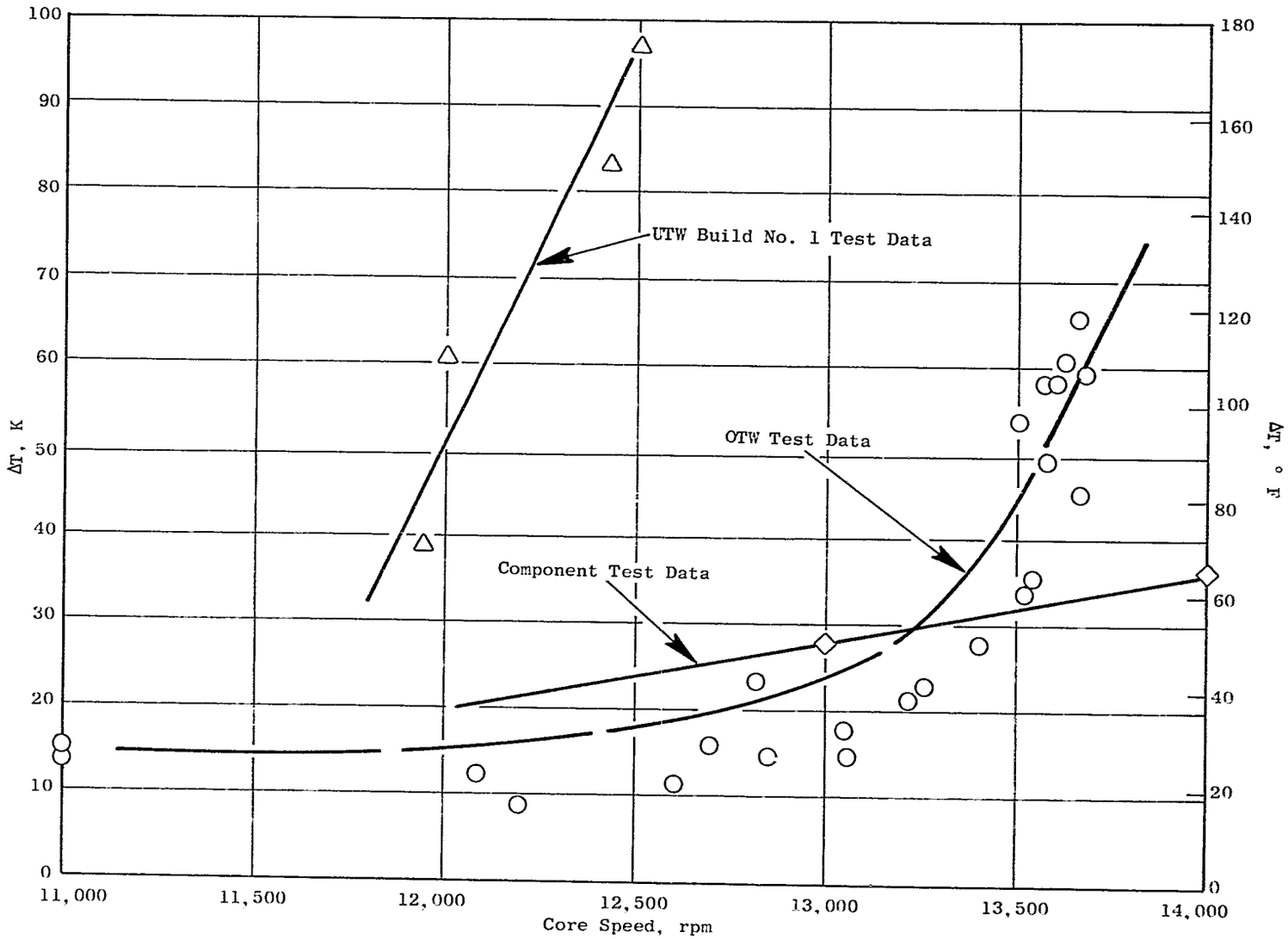

Figure 34. Accessory Gearbox Oil ΔT Vs. Core Speed.

Table VII. Engine Heat Rejection.

Parameter	* Predicted	** Measured
Core rpm (Physical)	14078	13598
Fan rpm (Physical)	3905	3670
Lube Flow	2839 cm^3/sec (45 gpm)	2524 cm^3/sec (40 gpm)
Scavenge Temperature	< 405 K (< 270° F)	< 378 K (<220° F)
Lube Temperature	< 336 K (< 145° F)	< 328 K (<130° F)
Total Engine Heat Rejection	411.3 kJ/sec (23,375 Btu/min)	369.6 kJ/sec (21,000 Btu/min)

* Takeoff 306 K (90° F) day

** ADH - 33 (4/21/77)

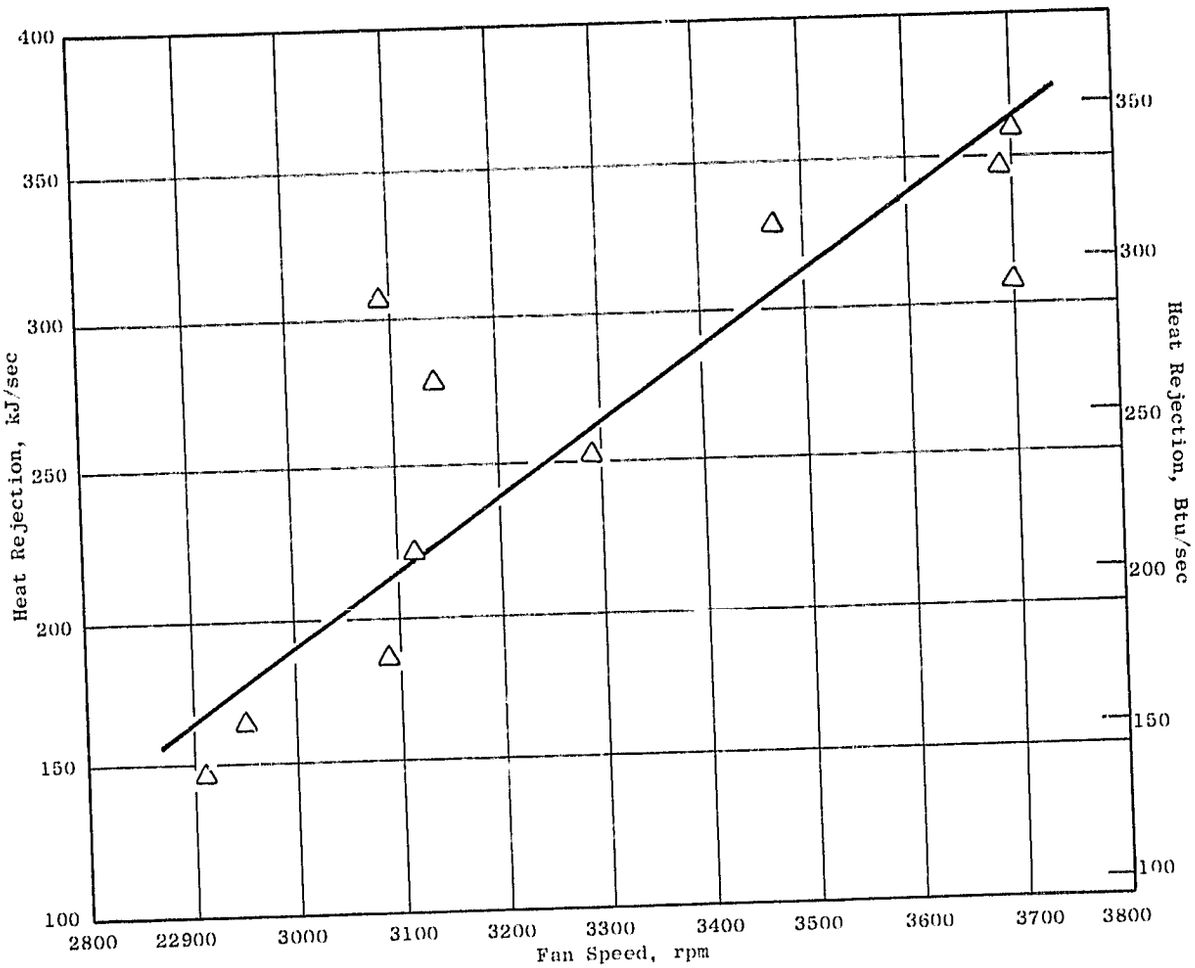

Figure 35. Engine Heat Rejection V: Fan Speed.

7.0 OTW FAN FRAME

The QCSEE integrated fan frame is a graphite/epoxy structure that incorporates the fan casing, fan bypass vanes, and core frame. It provides the primary support for the engine and is 2.00 m (78.8 in.) in diameter, 0.9525 m (37.5 in.) long, and weighed 322 kg (710 lb) at engine assembly, not including the engine mounts.

The frame was initially instrumented with a total of twelve strain gages. Eight of these were located in the engine mount area as shown in Figure 36. The other four gages were located on the fan bypass vanes as shown in Figure 37. During the test a total of nine gages were monitored, leaving the remaining three as a backup in case of gage failure. The nine monitored gages were numbers 801, 802, 803, 813, 814, 815, 816, and 817.

None of the gages in the mount area showed any significant response during engine operation. This was expected because normal operating loads are quite low compared to the five-blade-out loads for which the structure was designed. The highest stress observed during engine test was only 2% of the ultimate strength of the material. Stresses that low cannot be detected on the engine monitor scopes.

The only frame gages showing any activity during engine operation were the four working gages on the bypass vanes. All observed stresses on these vanes were low: less than 4% of the ultimate strength of the material at the worst case of fan speed of 3680 rpm and the area control doors set at an angle of 25°. The stresses became slightly less as A_8 was decreased.

It was possible, by increasing the scope sensitivity, to detect the vane natural frequencies (first flex only) as they were excited by a fan 28/rev. These frequencies were lower than expected based on bench testing of a single vane. It is probable that the actual end fixity of the vanes is somewhat less than it was for the bench test specimen which had ends cast in Devcon (a filled epoxy). The bench test results are shown in Figure 38 along with the natural frequency data obtained during engine running.

On April 4, 1977, a wet motor of the OTW was performed and then followed by two successful fire ups to idle. On the following day the engine was again successfully fired-to-idle; however, a sudden snow squall forced a shutdown almost immediately. To this point the engine was run a total of five minutes with no problems.

On April 6, 1977, the engine was fired-to-idle with no incident. The engine speed was then increased from 48% to 50%, then 65%, and finally 70%, and throughout this run a steady drop in oil level was recorded. At 70% fan speed the engine was shut down to investigate the oil loss. During coast down, oil was seen gushing out of the "D" nozzle exhaust and core doors. Since no definite leak path was found, two subsequent dry motors were performed with the cowling doors open; but again, the oil leak could not be isolated.

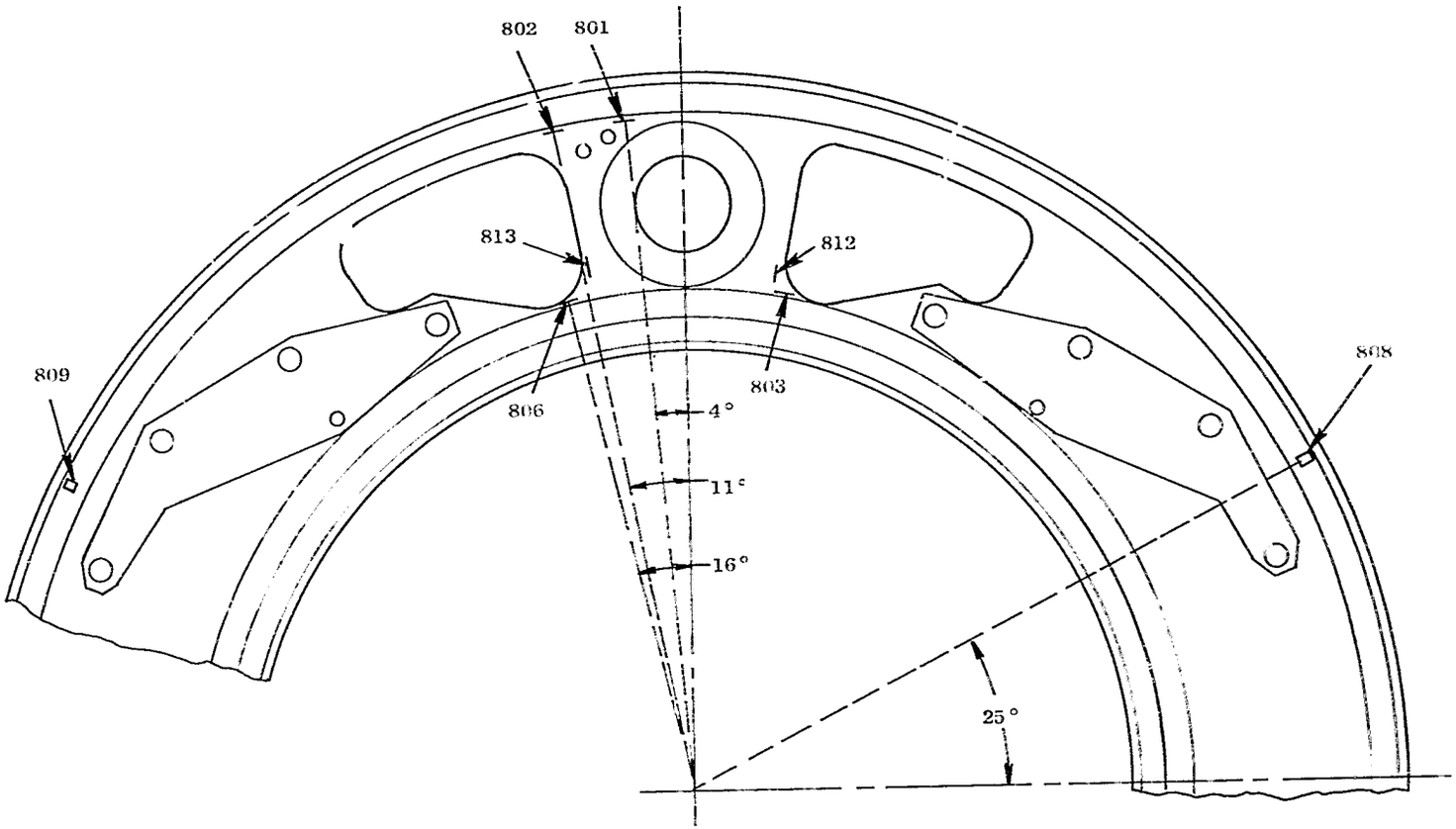

Back of Aft Wheel Splitter Ring - Mount Area

Gages are Symmetrical About Vertical Centerline

Note: Gages 808 and 809 are located on the fan flow splitter surface 10.16 cm (4 in.) forward of the vane trailing edge.

Figure 36. Strain Gage Locations for OTW Fan Frame, Mount Area.

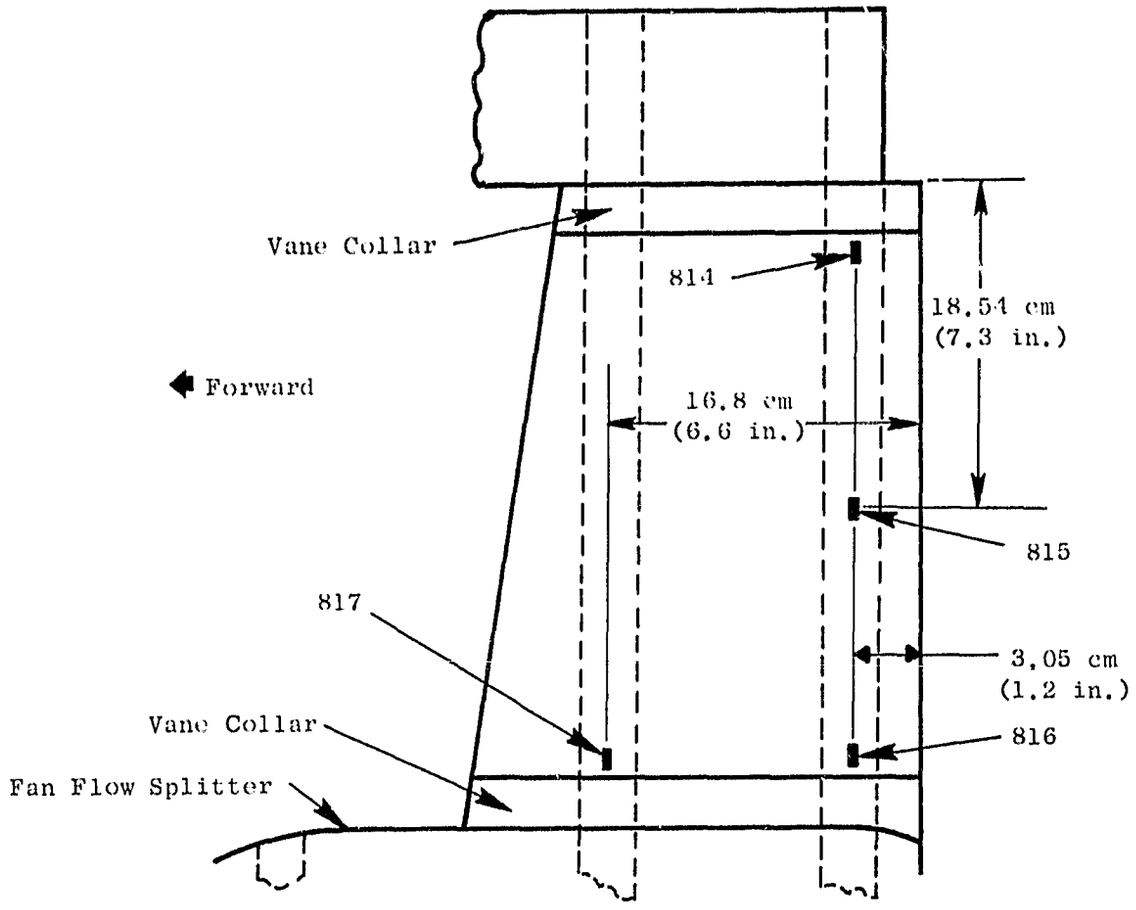

NOTES:
1. All gages are on the concave side of the vane.
2. Gages 814, 816, and 817 are to be 1.5 cm from vane collars.

Figure 37. Strain Gage Locations for OTW Fan Frame, Bypass Vanes.

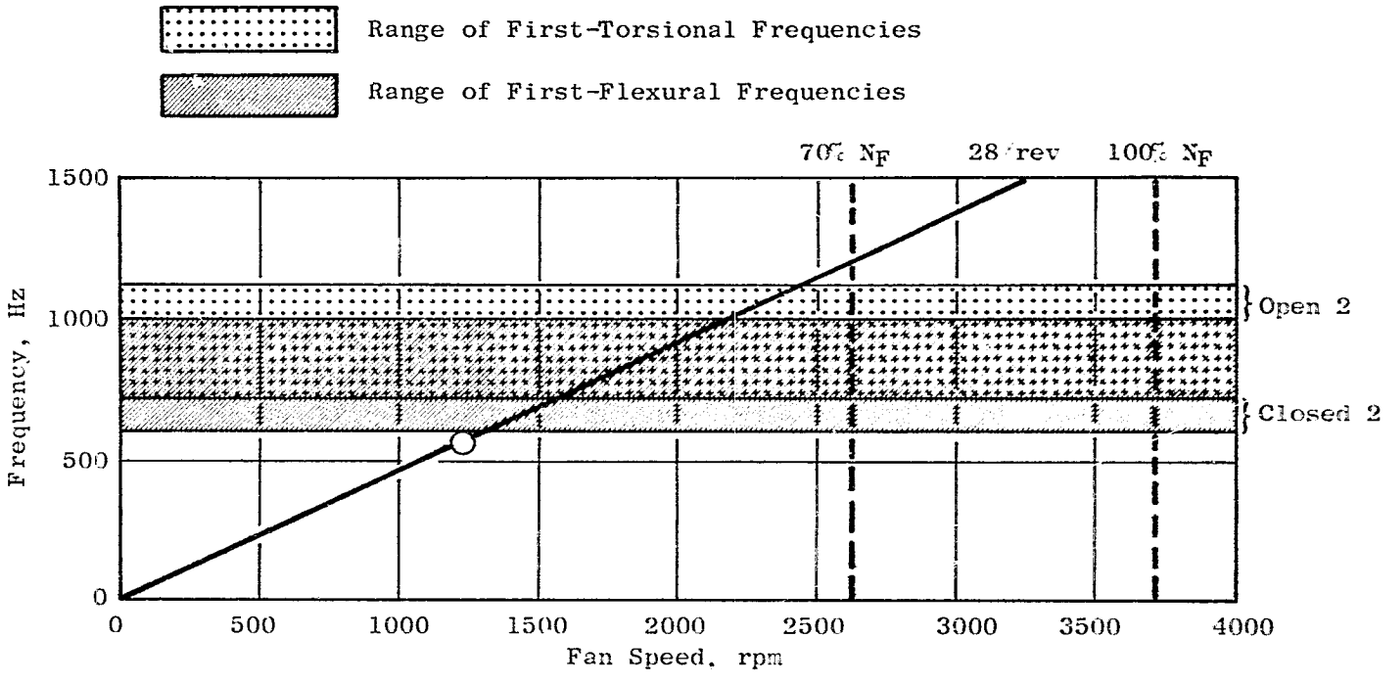

Natural Frequencies for the Closed 2 Vane Were Obtained from Bench Tests.

Natural Frequencies for the Open 2 Vanes Were Extrapolated Analytically from Closed 2 Data.

Results of Engine Tests: Closed 2 Vane First Flex at N_F = 1300 rpm and 564 Hz.

Figure 38. Natural Frequencies of QCSEE Bypass Vanes.

After several days of meticulous inspection and cleaning, the engine was dry motored on April 14, 1977. This run provided the first positive indication that oil was leaking from the midspan bearing region in the frame pylon. A small portion of the concave pylon panel was removed, and the interior of the pylon was borescoped. This operation further isolated the oil leak to the upper region of the drive shaft shroud tube. This region was cleaned with MEK, and then Furance 9210 adhesive was injected into this region. Another dry motor was performed, and an additional leak was found in the region of the oil-in line in the 10 o'clock core frame strut. A hole was cut into the top of the splitter flow-path panel above the oil-in tube location, and Furance 9210 adhesive was injected around the tube to plug two holes that were emitting oil. The engine was again motored, and no leaks were evident. The pylon skin and splitter skin were then repaired to patch up the access holes used for the Furane sealing operations.

On the following day the engine was fired to idle, and after 30 minutes of running at idle, approximately 0.004 m^3 (1 gallon) of oil was lost. After this run oil was identified on the left side (aft looking forward) of the fan frame under the core cowl and aft of the middle "wheel" inside the frame. The right side had no evidence of leakage.

The next operation consisted of pressurizing the forward sump and accessory gearbox with 6.9 kN/m^2 (1 psig) of helium gas. A helium detector discovered a leak beneath the accessory gearbox drain cup. Oil was then forced into the accessory gearbox through the auxiliary scavenge line by reversing the auxiliary scavenge pump motor polarity. Oil was then seen running out of the acoustic treatment on either side of the pylon and down the inside of the pylon. Material was removed from around and under the gearbox drain cup; this uncovered a large cavity filled with oil. A boroscope was then inserted into the cavity; it was found to extend under the cup and along the entire length. After this trouble-shooting, the following repairs were made:

- The core strut cavity at top vertical and between the middle and aft wheels was filled with Furance 9210 adhesive to a depth of approximately 2.54 cm (1 inch).
- The gap around the PTO shroud tube at the midspan bearing was sealed with Dow Corning 94-009 Flurosilicone.
- The entire frame pylon cavity was filled with Furance 9210 adhesive.
- The entire region around and under the gearbox drain cup at top vertical was filled with Furane 9210 adhesive.

Following the exhaustive repairs, a helium-leak check was conducted with no leaks detected. Following the helium-leak check, three deliberate floodings of the accessory gearbox were performed with no indication of any oil leakage. A three-minute dry motor was then performed with the core cowl doors open, and again no oil leak was visible.

On the following day the engine was fired to idle for 30 minutes with no register of any oil loss through the tube level indicator. The engine was shut down and inspected. A careful, visual inspection revealed no oil leaks. On April 21, 1977 the OTW was fired to idle and ran for several hours with no loss of oil from the frame. This run completed the mechanical check-out, and all engine running from this point continued without incident.

In summary, no structural problems or unexpected stresses were encountered during engine testing. The vane natural frequencies were somewhat lower than predicted and caused no problems. Several oil leaks were found in the frame during engine operation but these were repaired on the test stand.

8.0 NACELLE COMPONENTS

8.1 INLET

Two boilerplate inlet configurations were tested. The NASA Quiet Engine "C" bellmouth inlet was used for aerodynamic engine mapping and baseline acoustic evaluation, and the boilerplate high Mach number inlet for the UTW engine with bulk-absorber, acoustic-suppression panels was used for aerodynamic and acoustic evaluation. The boilerplate inlet was not instrumented for mechanical data. No problems were encountered during the test.

8.2 CORE COWL COOLING

During mechanical checkout in the forward-thrust mode, thermocouples on the core cowl skin indicated temperatures in excess of 460 K (370° F) aft of the fire seal. This was above the temperature that would ensure a safe, long-term operating environment for the epoxy resins used in the construction of the acoustic and hard-wall panels. Additional cooling, using shop air, was introduced under the cowl and distributed around the circumference of the engine by addition of a manifold placed just aft of the treatment panels. Holes were located in the manifold to allow the cooling air to scrub the cowl skin in the area of the treatment panels; this maintained skin temperatures under 450 K (350° F) for all test configurations.

Prior to testing the composite core cowl, the severity of the environment it will be exposed to was ascertained; a small (10 × 10 cm) test panel representative of the design and construction of the composite cowl was made and placed under the boilerplate cowl at top-vertical centerline just aft of the treatment panels. One thermocouple was attached to the test panel; temperatures in excess of 811 K (1000° F) were recorded during the test. The condition of the panel after test verified the high temperature recorded by the thermocouple. A major portion of the panel had all resin burned out of the graphite skin and HRH-327 honeycomb core. It is believed that this area, beneath the boilerplate metal apron, is not representative of the temperature the composite cowl will see during test because skin thermocouples on the boilerplate cowl were indicating temperatures under 450 K (350° F). As a precaution, additional cooling air manifolds will be installed beneath the composite cowl, and an insulation blanket will be added to protect the aft section of the cowl.

8.3 "D" SHAPED EXHAUST NOZZLE AND THRUST REVERSER

The exhaust nozzle was tested in the closed position and the reverser in the open position with adapters which provided for a 105° and 115° rotation of the blocker door. Bolt-on sideplates and a 0.6 lip/throat extension were used to simulate the configuration of the flight reverser in the fully deployed position. The exhaust nozzle/thrust reverser was not instrumented. No mechanical problems were encountered during test.

9.0 DIGITAL CONTROL SYSTEM

9.1 TEST SUMMARY

The QCSEE OTW experimental engine was controlled with a full-authority, engine-mounted, digital control. The digital control received and processed power-demand commands, which were multiplexed from the control room, and engine-state data from engine-mounted sensors to control engine fuel flow and to schedule the core compressor stator vanes. A photograph of the engine-mounted digital control is shown in Figure 39.

The control incorporated a power management system whereby closed loop control of the thrust parameter (corrected fan speed) was maintained by regulating fuel flow. The engine thrust demand, which was set in the control room as a percent of rated power, was multiplexed to the digital control and was interpreted as a percent of scheduled corrected fan speed. This corrected-speed demand was converted to physical fan speed and compared to actual fan speed. The speed error was integrated to zero by controlling engine fuel flow. The core compressor stators were scheduled as a function of corrected core engine speed. Scheduled vane angle was compared to actual vane angle, and the error was integrated to zero.

In addition to the basic control mode described above, the digital control incorporated transient fuel schedules for engine acceleration and deceleration, a calculated turbine inlet temperature limit for turbine protection, a corrected core speed limit for core overspeed protection, a control-room-adjustable idle speed limit for experimental engine flexibility, and a core stator reset function for rapid transient response. All of the above logic and schedules were incorporated into the digital control memory.

For additional protection of the experimental engine, two major safety functions were incorporated in the system components. The digital control package incorporated a separately powered analog system which would cut off engine fuel flow if fan speed or the rate of change of fan speed exceeded prescribed values. The hydromechanical fuel valve, which was a modified F101 main fuel control, incorporated a core speed governor whose speed limit was a function of hydromechanical power-lever input.

The digital control also incorporated two automatic failure detection and corrective action concepts and provisions for monitoring and displaying forty-eight engine and control parameters. The first failure detection and correction concept consisted of monitoring selected engine parameters such as vibrations, engine oil temperature and pressure, and computational tests on the digital control. In the event that an engine parameter exceeded a defined level or the digital control failed to pass the computational test, a defined corrective action for experimental engine protection was implemented. The second failure detection and correction concept provided protection for failed digital-control-system sensors (i.e., PS3, N_1, N_2, etc.). The concept incorporates a simplified dynamic model of the engine. Sensed engine

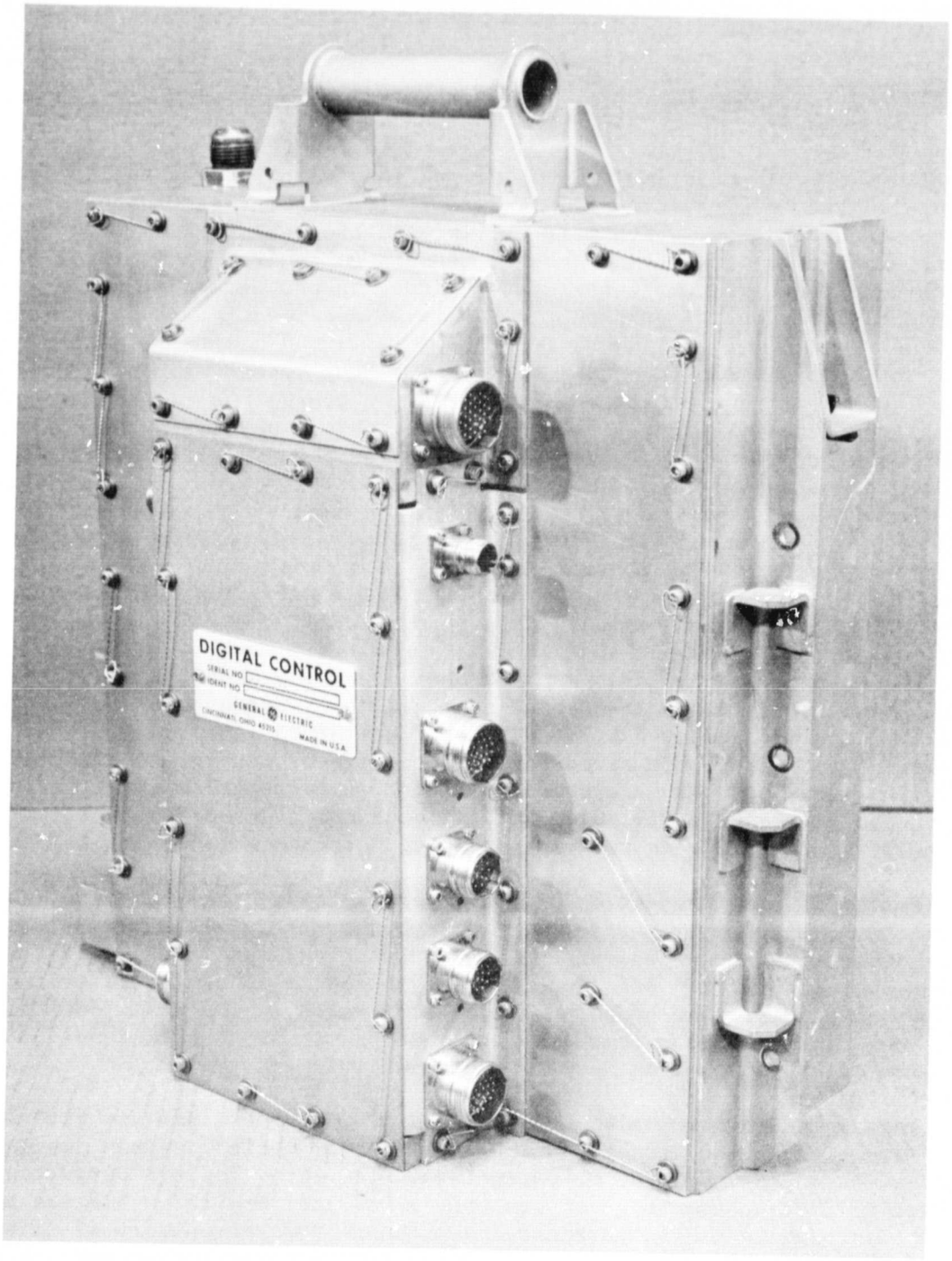

Figure 39. QCSEE Digital Control.

parameters are calculated and compared with measured values. If the measured value differs from the computed values by a prescribed amount, the computed value is used for engine control.

The full-authority, engine-mounted, digital-control system was installed and active throughout the complete OTW engine test. Total test time was 58 hours and 19 minutes. The digital control performed satisfactorily throughout the engine test. Observation of the engine on test and detail data analysis showed the following:

- Smooth, cool, engine starts. Typical time to idle after ignition was 25 seconds.
- Stable corrected fan speed control. Corrected fan speed was held within ±0.1 percent. Transient data recording revealed fan speed holding capability of ±3 rpm.
- Accurate fan speed scheduling.
- Accurate measurement of fan inlet temperature and accurate computation of core compressor inlet temperature.
- Accurate scheduling of core compessor stators. Measured stator angle matched scheduled angle within ±0.5 degrees.
- Stable control on all control system limits ($N2/\sqrt{\theta}$, $T41C$).
- Reasonably accurate computation of turbine inlet temperature, and satisfactory control on the turbine temperature limit. Digital-control-computed T41 read 5 to 16 K (9° to 29° F) higher than performance-calculated T41 at high temperature levels.
- Fast transient response capability. Contract commitment of one-second response from 62% to 95% thrust was met.

9.2 SYSTEM DESCRIPTION

An interconnection schematic of the overall digital control system, showing the various components, is shown in Figure 40. The digital control is the heart of the system. The control system block diagrams which define the detail control schedules and logic are shown in Figures 41 and 42. Figure 41 defines the control laws for fuel control, and Figure 42 defines the control laws for core stator control. As shown in Figure 41, the primary mode of operation is fan speed control. Fuel flow is modulated to maintain the desired corrected fan speed unless it is overriden by a core speed, turbine temperature, deceleration schedule, acceleration schedule, or idle speed limit.

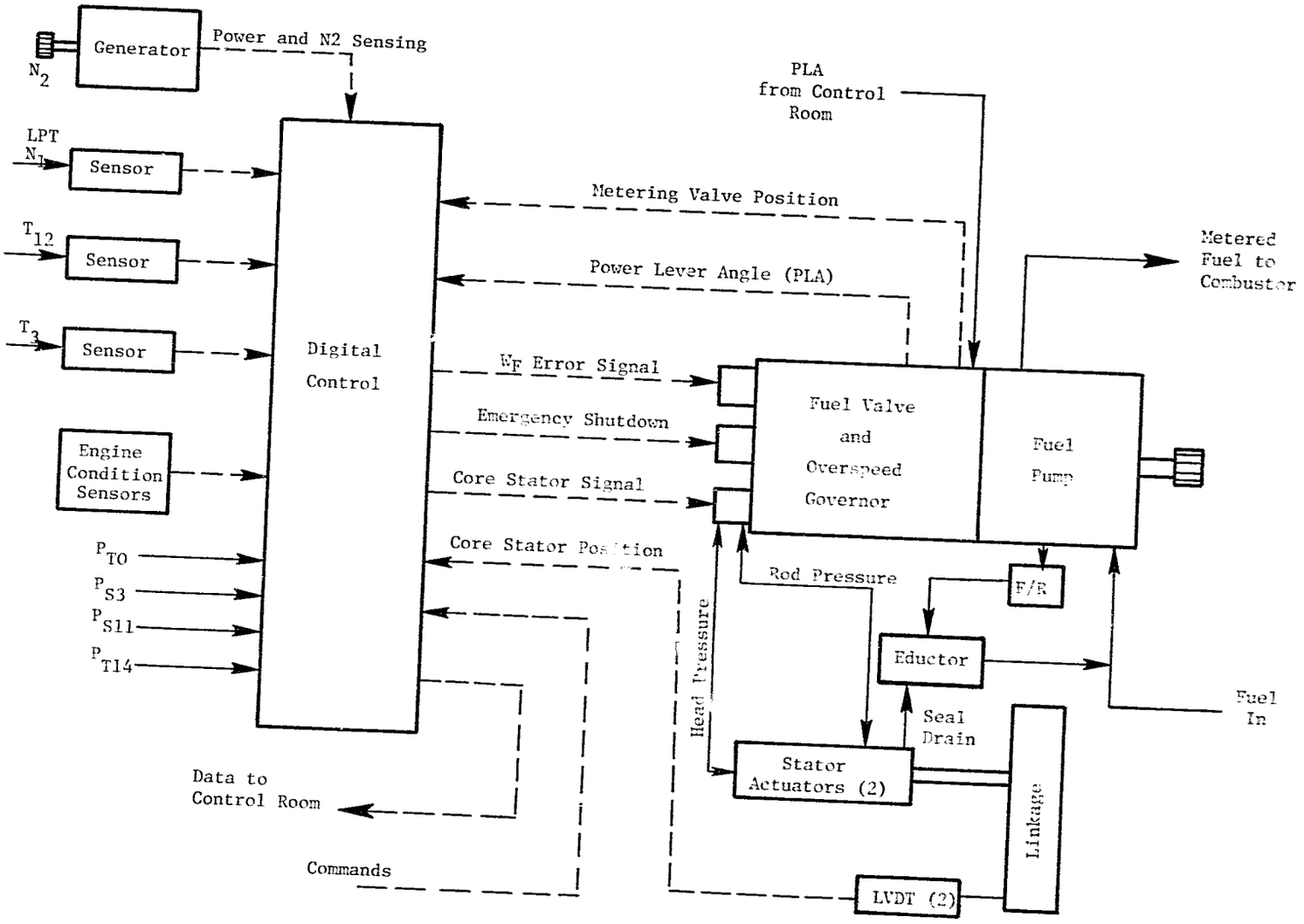

Figure 40. Digital Control System Schematic.

All of the control logic, schedule equations, failure detection, and data transmission are incorported in the digital control program memory. The program memory contains 4075 words and has an iteration time of 13.5 milliseconds.

The fuel valve and overspeed governor was a modified F101 hydromechanical control. This is a bypassing-type control with an isochronous governor. For this test the normal scheduling functions of the hydromechanical control (i.e., acceleration schedule, stator schedule) were disabled to allow these functions to be performed by the digital control. The fuel valve incorporated electrohydraulic torque motor servovalves to serve as the interface between the electrical and hydromechanical parts. A rotary variable-differential transformer (RVDT) was linked to the metering valve and provides fuel flow indication. The hydromechanical overspeed limit was set by positioning the mechanical power-lever angle (PLA) in the control room. In addition to setting the overspeed governor, the PLA also operated a positive fuel shutoff in the hydromechanical fuel valve. After initial engine checkout, the PLA was set at a high-speed point to prevent interference with engine control by the digital system.

The hydromechanical control was mounted on an F101 fuel pump, a centrifugally boosted, positive-displacement, vane pump. Pump discharge flow was delivered to the control through the mounting interface, and the control returned excess fuel to the vane element inlet through a bypass valve.

In order to achieve the operational flexibility required by the QCSEE program, the commands to the digital electronic control were introduced through control room elements shown on Figure 43. The interconnect unit, operator panel, and engineering panel were actually peripheral elements of the digital control. They provided means for the engine operators to introduce commands, to adjust various control constants, and to monitor control and engine data.

9.2.1 ENGINE CONTROL SENSORS

The digital control used engine-mounted sensors for system inputs. The engine variables sensed by the control system are shown schematically in Figure 44 and discussed briefly below.

Core Speed This speed was sensed electrically, by measuring the output frequency of the generator which supplied digital control computer power, and was sensed mechanically by a rotational input from the accessory gearbox to the hydromechanical fuel valve.

Low Pressure Turbine Speed - This speed, proportional to fan speed, was sensed by a stationary, magnetic pickup located near a multitoothed disk which rotated with the LP turbine shaft.

FOLDOUT FRAME

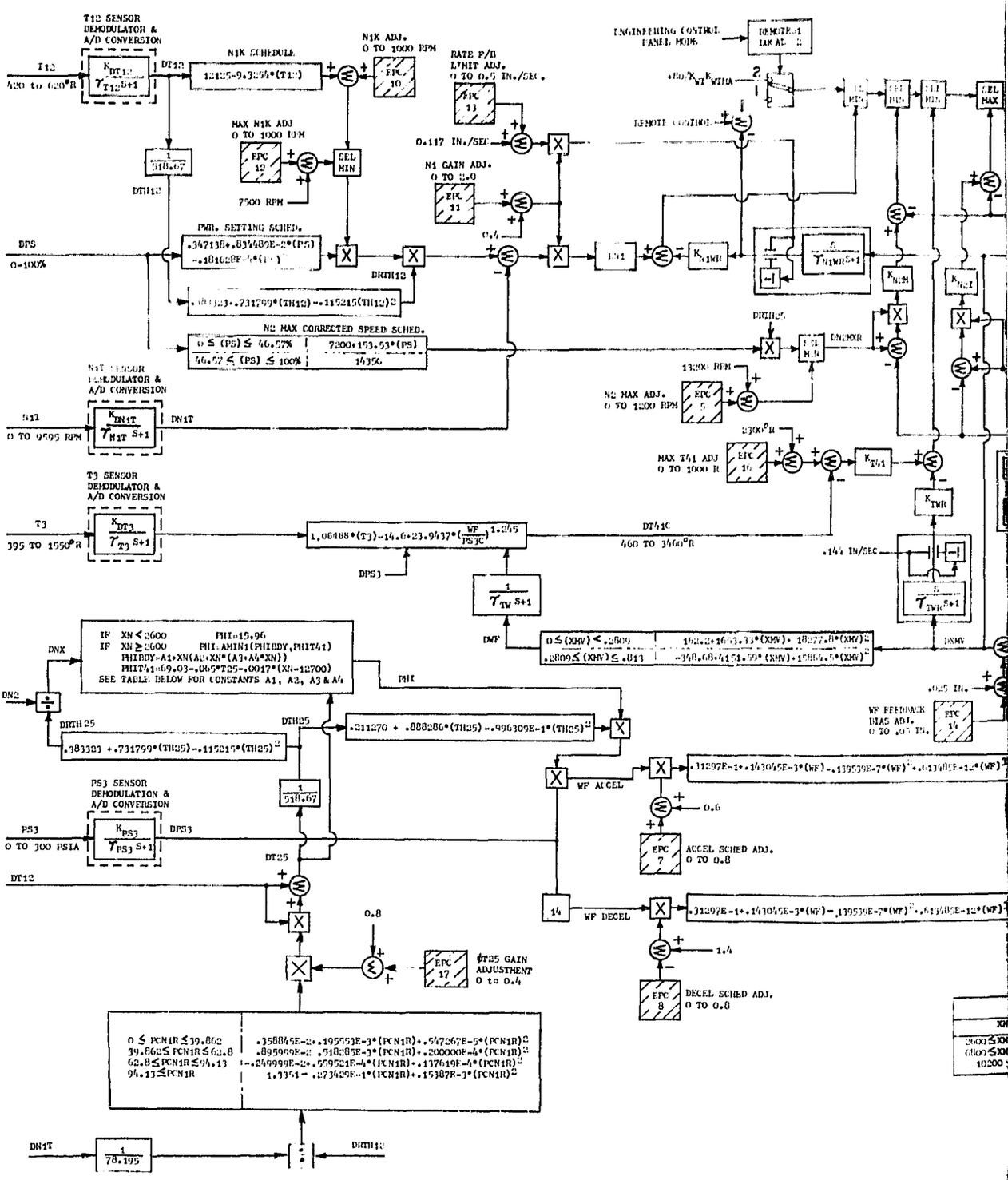

Figure 41. QCSEE OTW Fuel Flow Contre

PRECEDING PAGE BLANK NOT FILMED

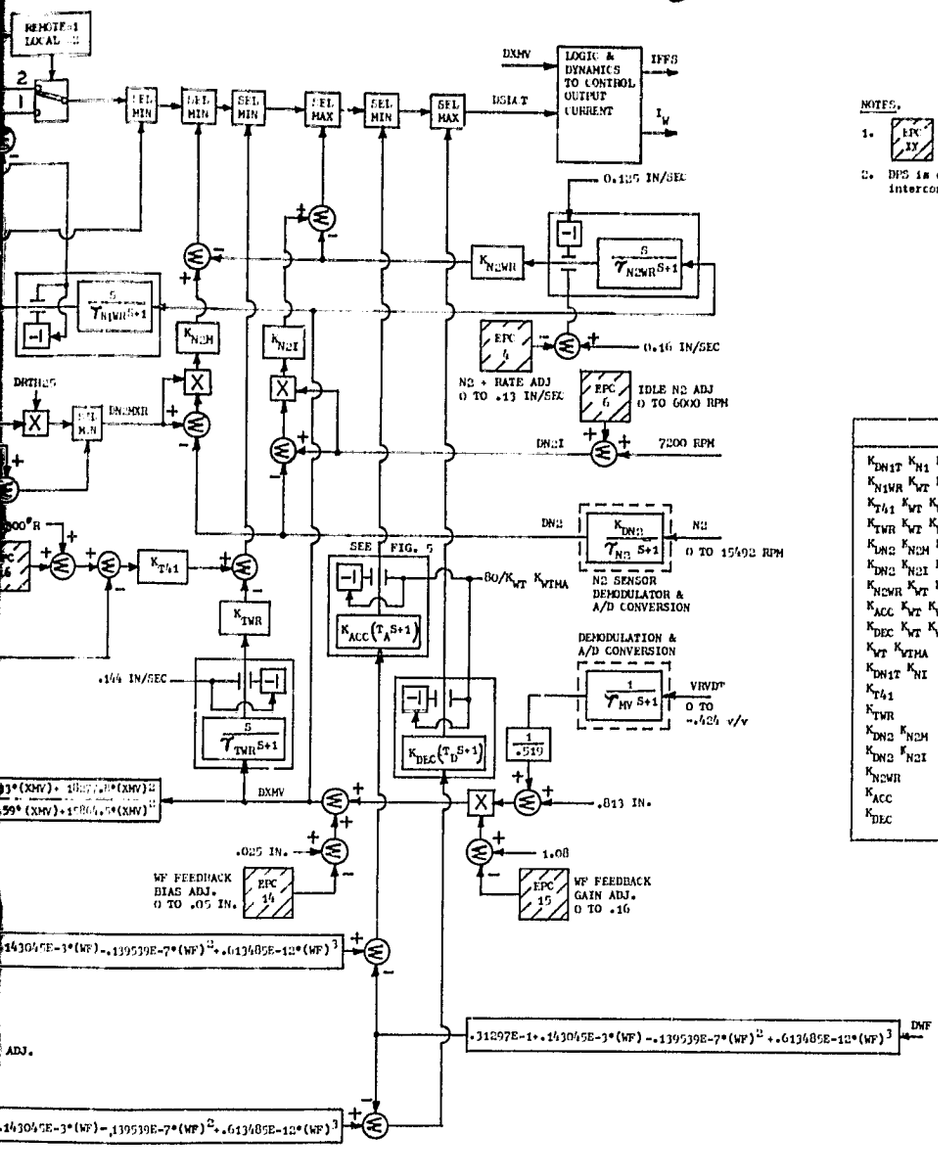

NOTES.

1. EPC YY — Denotes potentiometers on engineering panel
2. DPS is digital power demand setting from interconnect unit

DIGITAL GAINS	
K_{DN1T} K_{N1} K_{WT} K_{WTMA}	0.1225 MA/RPM
K_{N1WR} K_{WT} K_{WTMA}	164.3 MA/IN/SEC
K_{T41} K_{WT} K_{WTMA}	5.354×10^{-2} MA/ R
K_{TWR} K_{WT} K_{WTMA}	32.85 MA/IN/SEC
K_{DN2} K_{N2M} K_{WT} K_{WTMA}	2.967×10^{-2}MA/RPM@DN2MXR=11200RPM
K_{DN2} K_{N2I} K_{WT} K_{WTMA}	1.618×10^{-2}MA/RPM@DN2I=7200RPM
K_{N2WR} K_{WT} K_{WTMA}	164.3 MA/IN/SEC
K_{ACC} K_{WT} K_{WTMA}	405.7 MA/IN
K_{DEC} K_{WT} K_{WTMA}	405.7 MA/IN
K_{WT} K_{WTMA}	7.566
K_{DN1T} K_{N1}	1.619×10^{-2}
K_{T41}	6.9437×10^{-3}
K_{TWR}	4.3417
K_{DN2} K_{N2M}	3.9215×10^{-3}@DN2MXR=11200RPM
K_{DN2} K_{N2I}	2.1384×10^{-3}@ DN2I=7200RPM
K_{N2WR}	21.709
K_{ACC}	53.62
K_{DEC}	53.62

"A" CONSTANT TABLE				
XN	A1	A2	A3	A4
$2000 \leq XN < 6800$	.42118701E2	-.25707055E-1	.74804485E-5	-.56754241E-9
$6800 \leq XN < 10200$	-.19708559E3	.86346402E-1	-.10384008E-4	.39665754E-9
$10200 \leq XN$	.36912564E3	-.80113589E-1	.59159283E-5	-.13263709E-9

TIME CONSTANTS FREQUENCY RANGE .01 TO 10.0 HERTZ	
SYMBOL	VALUE, SEC.
T_{T12}	≤ 6.0*
T_{N2WR}	0.5
T_{N1WR}	0.5
T_{N1T}	≤ 0.01
T_{N2}	≤ 0.01
T_{T3}	$(T_{th} + T_{S/D})$ **
TA	0.05
T_{MV}	≤ 0.01
T_D	0.05
TWR	0.10
T_{TW}	0.05
T_{PS3}	≤ 0.02

* @ 10 PPS/FT^2 AIR FLOW DENSITY

** $T_{th} = .952 \frac{W_3^2}{65.29}$

** $T_{S/D}$ 0.02

E OTW Fuel Flow Control Block Diagram.

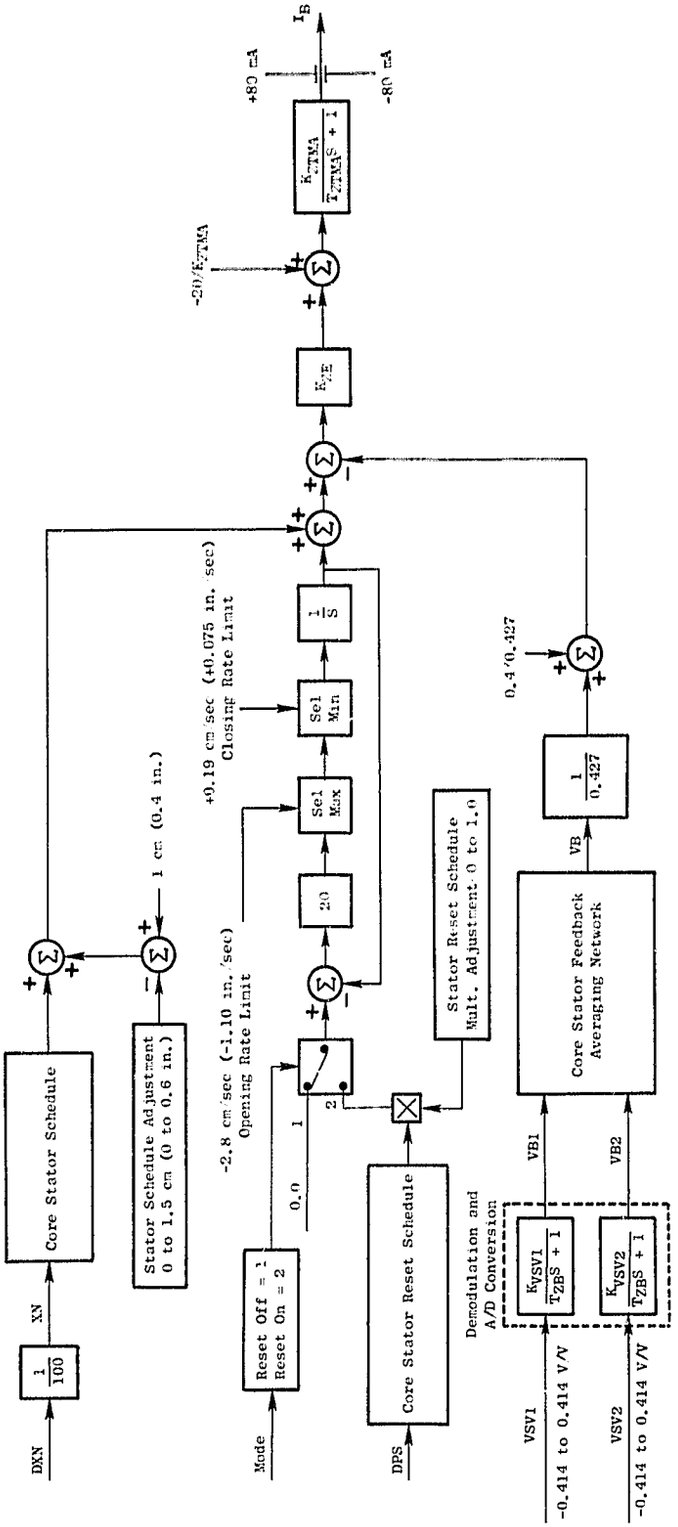

Figure 42. QCSEE OTW Compressor Stator Control Block Diagram.

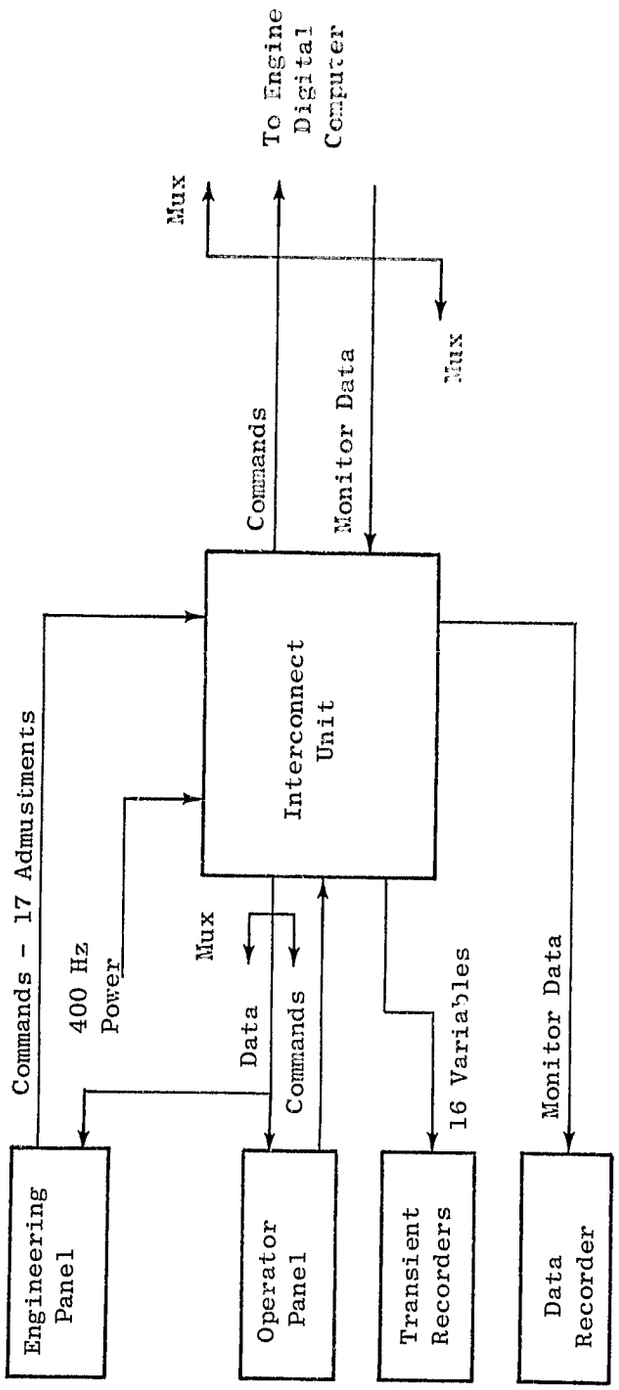

Figure 43. Control Room Elements of QCSEE Digital Control.

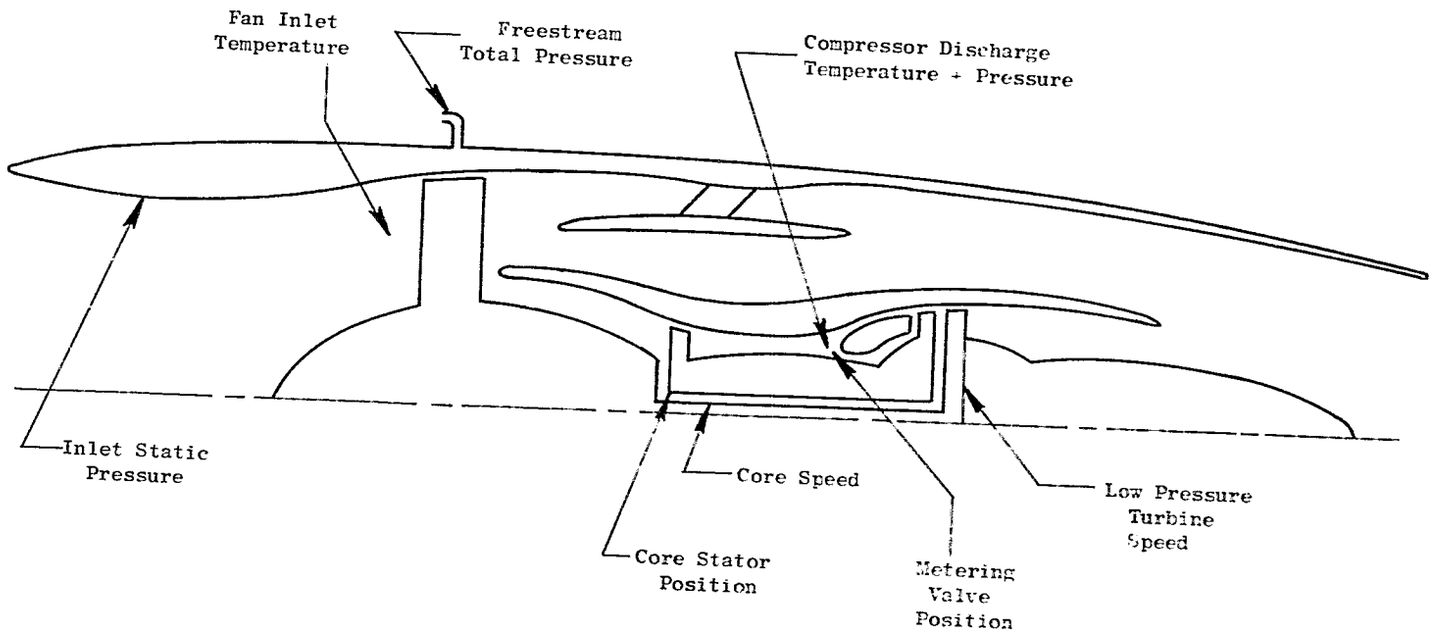

Figure 44. Sensed Engine and Control Variables.

Core Stator Position - Sensed electrically through an electrical, position transducer attached to the stator-actuation linkage.

Compressor Discharge Pressure - Sensed through a static pressure tap in the entrance to the engine combustor and piped to a pressure-to-electrical transducer in the digital control.

Compressure Discharge Temperature - Sensed by chromel-alumel thermocouple at the entrance to the core combustor.

Metering Valve Position - This was used as a measure of fuel flow in the digital control and was sensed with a transducer (rotary differential transformer) in the hydromechanical fuel valve.

Engine Inlet Static Pressure - Sensed through two static taps in the inlet duct wall and piped to one side of a differential pressure transducer in the digital control. The taps were located in a position near the inlet throat at an X/L position of 0.4.

Fan Inlet Temperature - Sensed by an electrical-resistance, temperature detector protruding through the inlet wall into the airstream.

Freestream Total Pressure - Sensed at the digital control as ambient total pressure for this static engine testing. A pressure-to-electrical analog transducer provided the signal to the digital control.

9.2.2 Control and Engine-Variable Monitoring

The digital control system also included provisions for monitoring control and engine variables. Core speed, fan speed, power demand, failure indication, core stator angle, corrected fan speed, and calculated turbine inlet temperature were displayed continuously on the operator panel. Other parameters were provided for continuous recording on transient data recorders, and all transmitted data were recorded on an automatic printer. Table VIII shows a list of recorded data and the conversion factors to engineering units. The purpose of this monitoring function was to demonstrate the digital control capability to process and transmit data and to incorporate an integrated, engine-conditions-monitoring system.

9.2.3 Failure Detection and Correction

One objective of the QCSEE Program digital control technology development was to utilize the inherent abilities of a digital computer to record and compare large amounts of data for engine-condition monitoring and fault correction.

Table VIII. OTW Digital Readout Conversions.

Channel	Parameter	Parameter to XXXX	Units	XXX to Parameter
00	VSV TMC	20.475 (mA + 100)	mA	0.04884 XXXX - 100
01	FICA XNL	0.4096 (XNL)	rpm	2.4414 XXXX
02	WF TMC	20.475 (mA + 100)	mA	0.04884 XXXX - 100
03	WF*	0.4095 (WF)	pph	2.442 XXXX
05	VSV	4449.276 (V/V + 0.414) + 208	V/V	0.0002247 (XXXX - 208) - 0.414
06	FMP*	5.11875 (FMP)	psia	0.19536 XXX
07	T41C	1.1835 (T41C)	° R	0.8449 XXXX
08	ΔP/P	2047 (ΔP/P)		0.0004885 XXXX
09	$\sqrt{012}$	2048 $\sqrt{012}$		XXXX/2048
10	PD	40.95 (PD)		0.02442 XXXX
11	PLA	28.3385 (PLA) + 204	degrees	0.035288 (XXXX-204)
12	N1	0.8798882 (N1)	rpm	1.136508 XXXX
13	N3	0.2643299 (N2)	rpm	3.783151
14	FICA XNH	0.1024 (XNH)	rpm	9.765625 XXXX
19	T12	20.475 (T12 + 40)	° F	0.04884 XXXX - 40
20	PTO	215.5263 (PTO)	psia	0.0046398 XXXX
21	P14-PTO	341.25 (P14-PTO)	psid	0.0029304 XXXX
22	PTO-PS11	341.25 (PTO-PS11)	psid	0.0029304 XXXX
23	PS3	13.65 (PS3(	psia	0.07326 XXXX
24	MVP	4531.3653 (MVP) + 204	in.	0.0002206 (XXXX - 204)
25	VSV 1	4449.275 (V/V + 0.414) + 208	V/V	0.0002247 (XXXX - 208) - 0.414
26	VSV 2	4449.275 (V/V + 0.414) + 208	V/V	0.0002247 (XXXX - 208) - 0.414
27	FICA T3S	0.640 (T3S)	° R	1.5625 XXXX
28	FICA ZWF	0.2048 (ZWF)	in.	0.00048828 (XXXX)
29	T3	3.54545 (T3 + 65)	° F	0.28205 XXXX - 65
30	DWF	0.302214 (DWF)	pph	3.3089 XXXX
32	FICA ZBETA	819.2 (ZBETA)	in.	0.0012207 XXXX
33	WF Temp*	13.65 (TEMP)	° F	0.07326 XXXX
34	VSV	63 (VSV + 5)	degrees	0.015873 XXXX - 5
35	T56	2.0475 (T56)	° F	0.4884 XXXX
36	Oil Inlet Temperature	16.38 (TEMP)	° F	0.06105 XXXX
37	Scav. Temperature	11.7 (TEMP)	° F	0.08547 XXXX
38	Oil Pressure 2	27.3 (PRESS)	psig	0.03663 XXXX
39	Scav. Oil Pressure	27.3 (PRESS)	psig	0.03663 XXXX
40	T25*	20.475 (T25)	° F	0.04884 XXXX
41	P5*	163.8 (P5)	psia	0.006105 XXXX
42	GB brg. Temperature	13.65 (TEMP)	° F	0.07326 XXXX
43	Horiz. Vibs	81.9 (VIBS)	mils	0.01221 XXXX
44	Vert. Vibs	81.9 (VIBS)	mils	0.01221 XXXX
45	FICA T56S	0.640 (T56S)	° R	1.5625 XXXX
46	FICA PS3	5.12 (PS3)	psia	0.1953125 XXXX

The OTW control system incorporated two active fault detection and correction concepts. The features of the first are discussed below.

A fault light on the operator panel indicated when one or more of the faults had occurred, and a digital indicator on the engineering panel identified the fault or faults. A switch was available on the engineering panel to deactivate each of the features except the fan overspeed emergency shutdown.

Engine Vibration - Engine horizontal and vertical vibrations were sensed if both exceeded 1 mm (40 mils), fuel flow was reduced to set idle core speed.

Loss of Command Data Link - Among the set of digital commands that were transmitted respectively in series from the control room to the engine-mounted, digital-control computer was a test word. An error to this word at any time caused the control to revert to the last valid set of commands received and to continue operation at this condition until the fault was corrected.

Computer Fault - The program memory in the digital control computer included test elements which, if found to be incorrect for two successive iterations through the program, would interrupt the control outputs, cause fuel flow to drift downward, and cause core stators to close.

Fan Overspeed Emergency Shutdown - If the LP turbine (fan) speed signal exceeds an absolute maximum limit, or if it increased at a rate indicating a loss in turbine load, an electrical signal from the digital control to the hydromechanical control caused flow to be shut-off immediately. All elements of this feature were electrically isolated from the remainder of the system so that it also protected against digital-control-system faults which might cause overspeed.

Core Stator Transducer Failure - The signals from the two core-stator-position transducers are normally averaged by the digital control. However, if the signals differ by 2.5° or more the control uses the signal with the largest voltage level, discarding the other on the premise that the transducer producing the lower voltage may well have failed because the predominant failure mode for such transducers is loss of signal.

Lube Supply Temperature - If this temperature exceeds 355 K (180° F) the engineering panel fault light illuminates, but there is no automatic corrective action.

Gearbox Bearing Temperature - If this temperature exceeds 402 K (264° F) the engineering panel fault light illuminates, but there is no automatic corrective action. This function was also observed during engine test.

Computer Timing Failure - The digital control includes redundant oscillators for timing in both the engine-mounted computer and in the control room portion of the control. An oscillator failure in the former will illuminate

the fault light on the engineering panel, and fault in the latter will illuminate a light on the interconnect unit in the control room.

A second failure detection and correction strategy is incorporated in the QCSEE OTW digital control. This strategy allows continuing control of the engines in the event of a control system sensor failure. An extended Kalman filter is used to provide the best estimate of the state of the engine based on currently available sensor outputs. Should a sensor failure occur, the control is based on the best estimate rather than the sensor output. The extended Kalman filter consists of essentially two parts: a nonlinear model of the engine and update logic which causes the model to track the actual engine. To allow implementation, approximations are made to the feedback-gain matrix which result in a single feedback matrix which is suitable for use over the entire flight envelope. An overall block diagram of this failure detection and correction strategy is shown in Figure 45.

9.3 ENGINE CONTROL SYSTEM TESTING

The engine was successfully started and operated to maximum allowable power under control of the engine-mounted, full-authority, digital control. Both steady-state and transient operation were conducted. The two electrically controlled variables, fuel flow and core stator angle, were stable and accurate. A total of 42 starts were made, and the total time on the digital control was 58 hours and 19 minutes. All primary control-system objectives were met. In subsequent paragraphs, data-analysis results are presented.

9.3.1 Engine Starting

One of the major functions of the full authority digital control is fuel flow scheduling during an engine start. Fuel flow scheduling is a nonlinear function of core speed (N2), compressor inlet temperature (T25), compressor discharge pressure (PS3), and engine fuel flow as sensed by the digital control.

The fuel-scheduling parameter (ϕ) is a function of WF, PS_3, and T_{25}; it is scheduled as a function of corrected N2. It (ϕ) is a constant for corrected core speeds below 2600 rpm and is a third-order polynomial whose coefficients are a function of corrected core speed for speeds above 2600 rpm. For high speed operation the basic fuel schedule parameter may be overriden by an alternate parameter, which is a function of T_{25}, to limit engine turbine inlet temperature (T_{41}). The digital control program is designed to select the minimum fuel-schedule demand to prevent over-temperature. The fuel-schedule parameter is multiplied by an emperical, corrected-temperature function, to obtain fuel flow over compressor discharge pressure (WF/PS3), and multiplied by PS_3 to define the fuel flow limit. This fuel flow limit is compared to actual fuel flow to establish a fuel flow error signal. The fuel flow error, with appropriate dynamic compensation, acts to limit fuel flow during transients. All of the above logic is

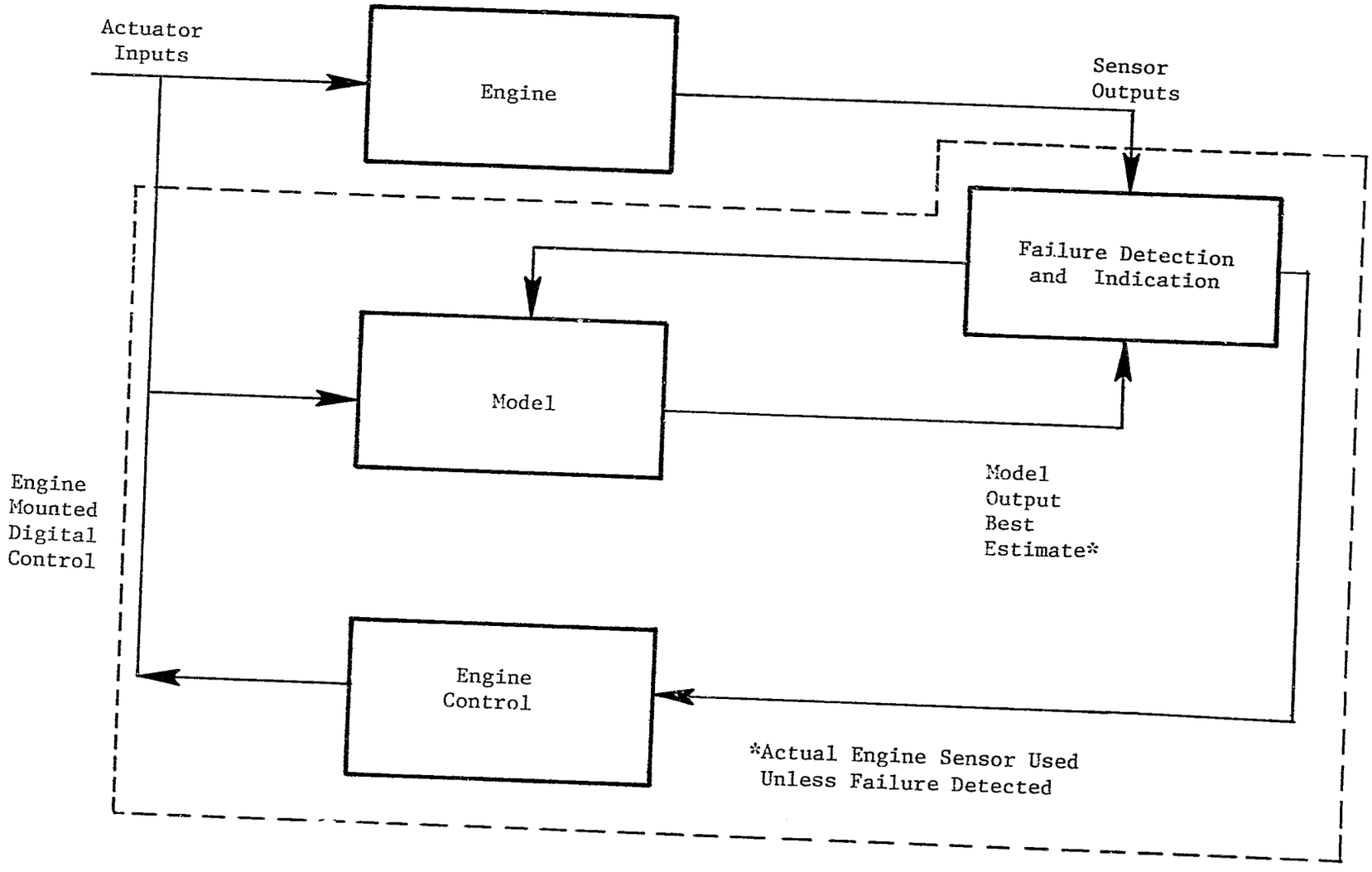

Figure 45. Block Diagram of the Failure Detection and Correction Strategy.

incorporated into the digital control program memory. The nominal fuel schedule parameter is shown graphically in Figure 46.

The data plotted on Figure 46 were extracted from digital data recordings on start number three. On this start the nominal acceleration schedule had been increased by eight percent; therefore, most of the data is above the nominal schedule after light-off. The reason for the transient drive-down in the fuel scheduling parameter right after combustor ignition is not understood. One possible explanation would be a transient increase in PS_3, due to ignition, which would appear as a decrease in WF/PS_3. Another explanation would be transient lag in measured fuel flow. Further testing in the starting region would be desirable.

The engine was started by motoring-up on the air starter until the digital control was in electrical regulation. Observation of operator panel data indicated that the control went into electrical regulation at approximately 3000 rpm (21%) core speed versus a component requirment of 25% core speed. After achieving digital control regulation, the engine was motored to approximately 4000 rpm at which time the stopcock was opened and the ignition was energized. The combustor lit approximately 5 seconds after the stopcock was opened, and the engine achieved idle speed 25 seconds after light-off. Turbine discharge temperature rise was smooth during the start, and no overtemperature indications were observed. Figure 47 shows a typical start.

9.3.2 Corrected Fan Speed Schedule

As noted above, the primary mode for the digital control is to vary fuel flow to hold a corrected fan speed demand. Corrected fan speed was selected as the prime control parameter because it is closely related to engine thrust.

As shown in Figure 41, the corrected fan speed schedule is a function of the maximum corrected fan speed and the power demand. The maximum corrected fan speed limit is a fixed value or a function of fan inlet temperature. The control is designed to select the minimum of the two limits. This schedule provides a constant thrust rating up to the rated fan inlet temperature. To provide experimental engine flexibility, both of these schedules were adjustable from the engine control room.

Table IX compares schedule corrected fan speed with actual corrected fan speed for a series of power-demand settings. As shown in the table, there is excellent correlation between the scheduled and actual values. The minor variation is thought to be nonlinearities in the potentiometer used to set the fan speed schedule limits.

9.3.3 Steady-State Stability

To evaluate the steady-state control characteristics of the installed, full-authority, digital-control system, transient data was recorded on

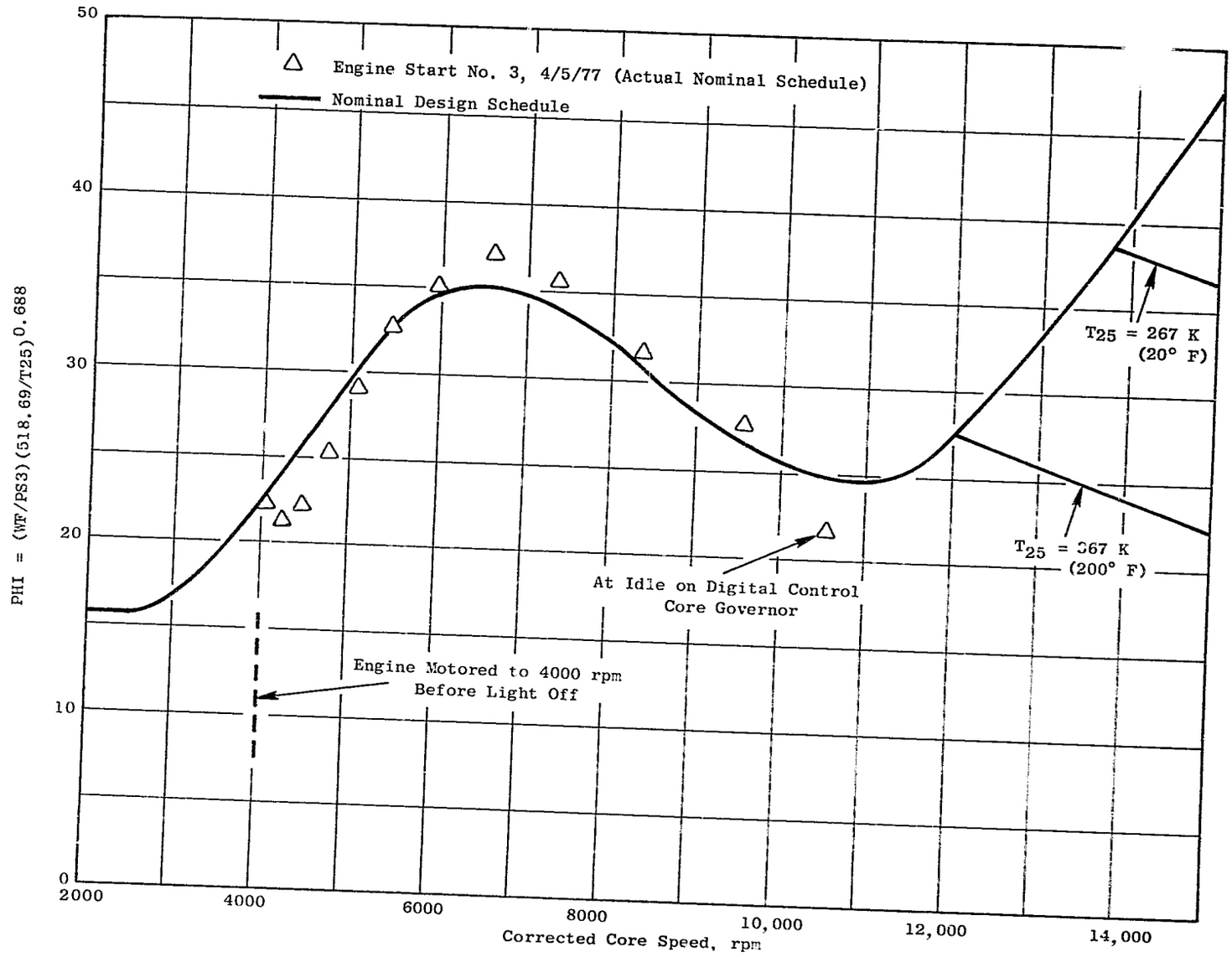

Figure 46. Nominal Acceleration Schedule.

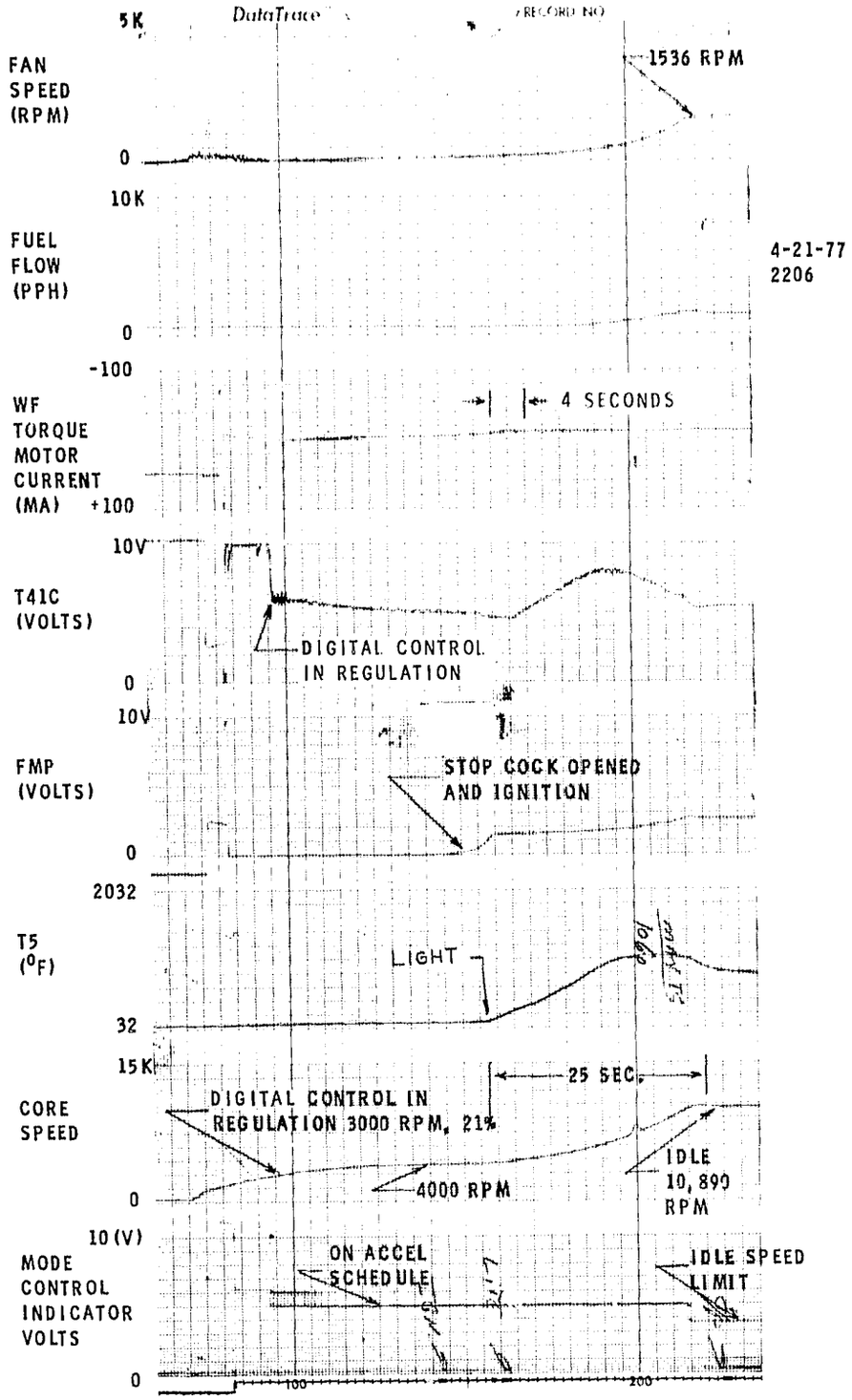

Figure 47. Typical Engine Start.

Table IX. Corrected Fan Speed Schedule.

Point Number	Power Demand %	Scheduled Corrected Fan Speed rpm	Actual Corrected Fan Speed rpm	Delta	
				rpm	%
1	44.73	2638	2639	+ 1	+0.04
2	58.28	3018	3023	+ 5	+0.17
3	74.46	3396	3403	+ 7	+0.21
4	83.43	3591	3599	+ 8	+0.22
5	85.42	3649	3651	+ 2	+0.05
6	89.86	3614	3602	-12	-0.33
7	93.84	3690	3676	-14	-0.38

NOTES:

1. After point 5, fan speed schedule was adjusted to provide a new limit.
2. Points 1-5 are running on schedule slope.
3. Points 6 and 7 are running on schedule flat.

several parameters during steady-state ADH readings. Data was taken over a range of operation on core speed governing, fan speed governing, and T41C governing. The general characteristics were the same for all control modes. Figure 48 shows a transient recording on steady-state fan speed control at a base-point fan speed of 3646 rpm. The figure shows excellent control with steady-state peak-to-peak variations of:

- fan speed ±3 rpm
- fuel flow ±18.1 kg/hr (±40 pph)
- calculated T41 ±7.8 K (±14° R)
- core speed ±30 rpm

9.3.4 Fan Inlet Temperature Measurement

The digital control uses fan inlet temperature (T12) as an input to the corrected fan speed schedule ($N1/\sqrt{\phi}$) and as an input to the compressor inlet temperature calculation.

On the experimental engine, T12 was measured using four temperature rakes with each rake containing five thermocouple elements. This data was recorded and, after correcting for bad thermocouples, was averaged to provide the ADH reading for T12. The digital control uses a single, resistance-type sensor for measuring T12. It is located at approximately the eleven o'clock position in the inlet.

The digital control data and the ADH data were examined and compared for thirty-five valid ADH cases. Close agreement between the ADH data and digital control data was obtained for the forward operating mode. In the reverse mode the digital control sensor generally read higher than ADH. Maximum variation was +4.5 K (8° F). Table X shows the average difference and the standard deviation on the difference as a function of inlet configuration and operating mode. Figure 49 compares the digital control sensor data with the average ADH T12 data. Figures 50 and 51 show the temperature error as a function of inlet temperature and corrected fan speed. All of the data show the higher temperature readings in reverse. Figure 51 indicates that the temperature distortion increases with corrected fan speed or thrust level. With further study, this error could be used to advantage because the higher T12 results in a higher T25. This higher T25 results in a lower corrected core speed, causing the stator to close, with a possible automatic improvement in core stall margin in reverse.

9.3.5 Calculated Compressor Inlet Temperature

The digital control system uses compressor inlet temperature (T25) as an input to the acceleration schedule calculation ($WF/PS_3\ \theta^{0.688}$), and to core

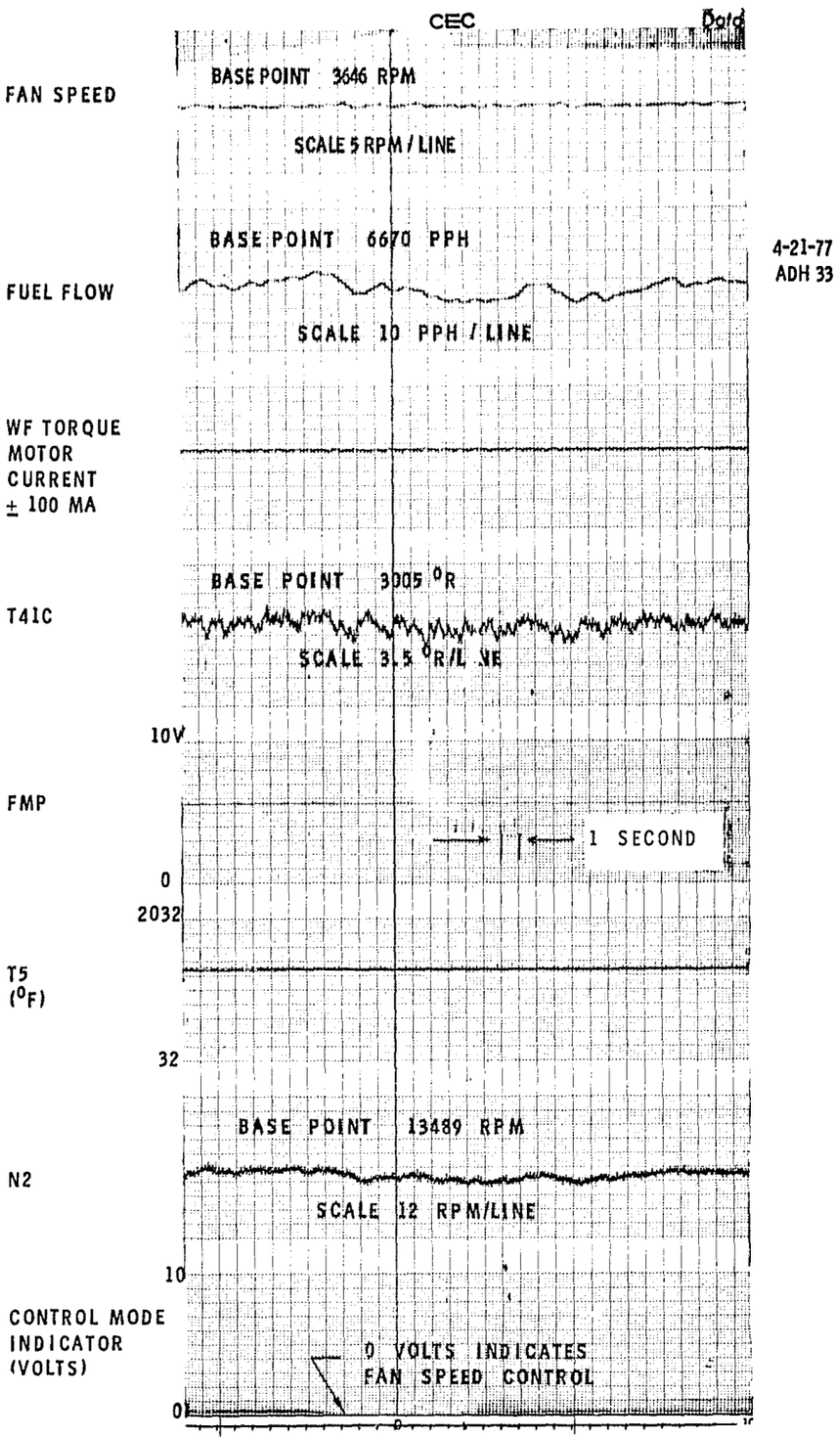

Figure 48. Control System, Steady-State Stability.

Table X. Fan Inlet Temperature Average Error.

Configuration	Average Error, K	
	Mean	Standard Deviation
Bellmouth Inlet, Forward	+0.21	0.46
Flight Inlet, Forward	-0.10	1.0
Flight Inlet, Reverse	+1.76	1.77

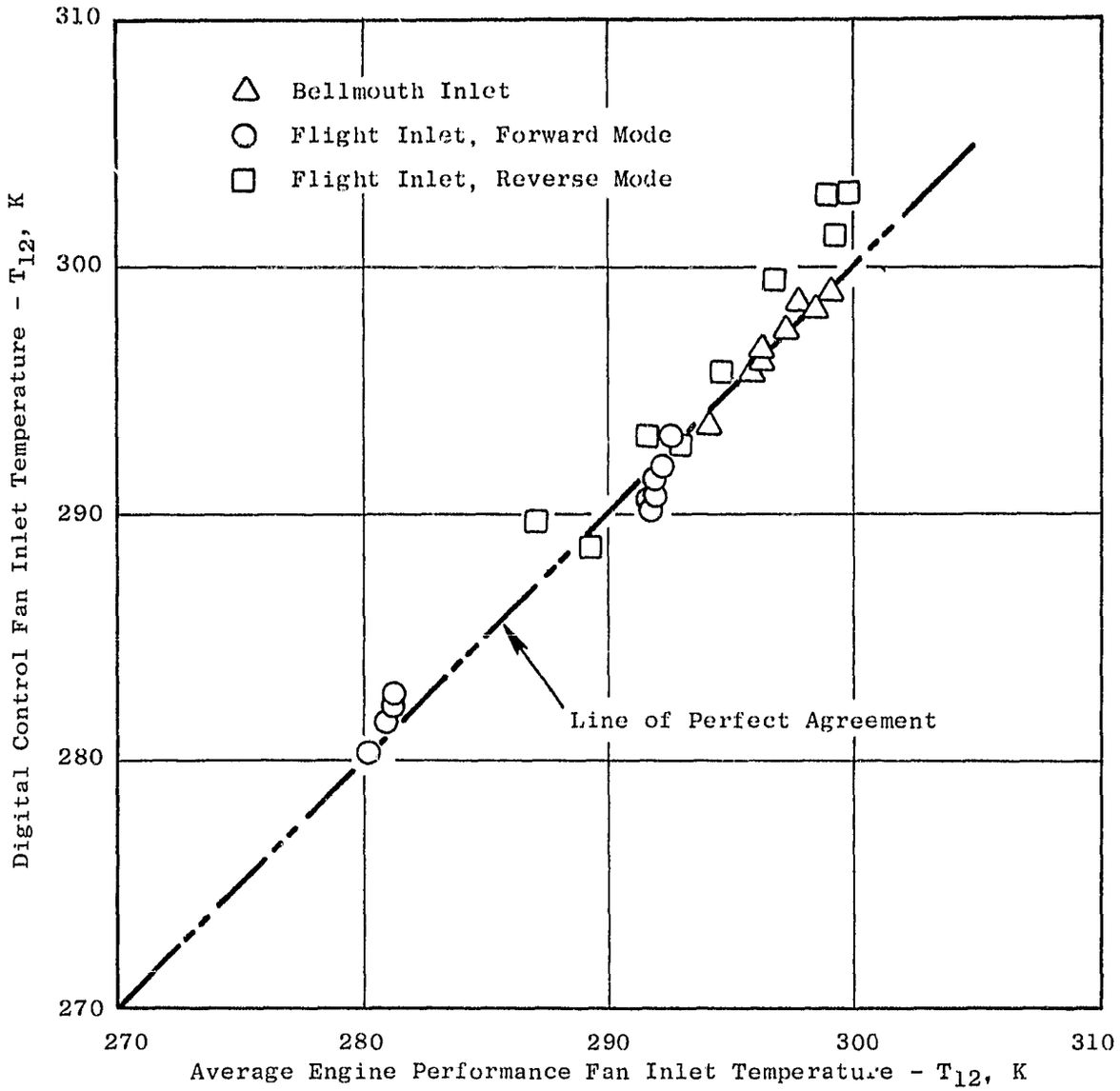

Figure 49. Comparison of Fan Inlet Temperature Measurement.

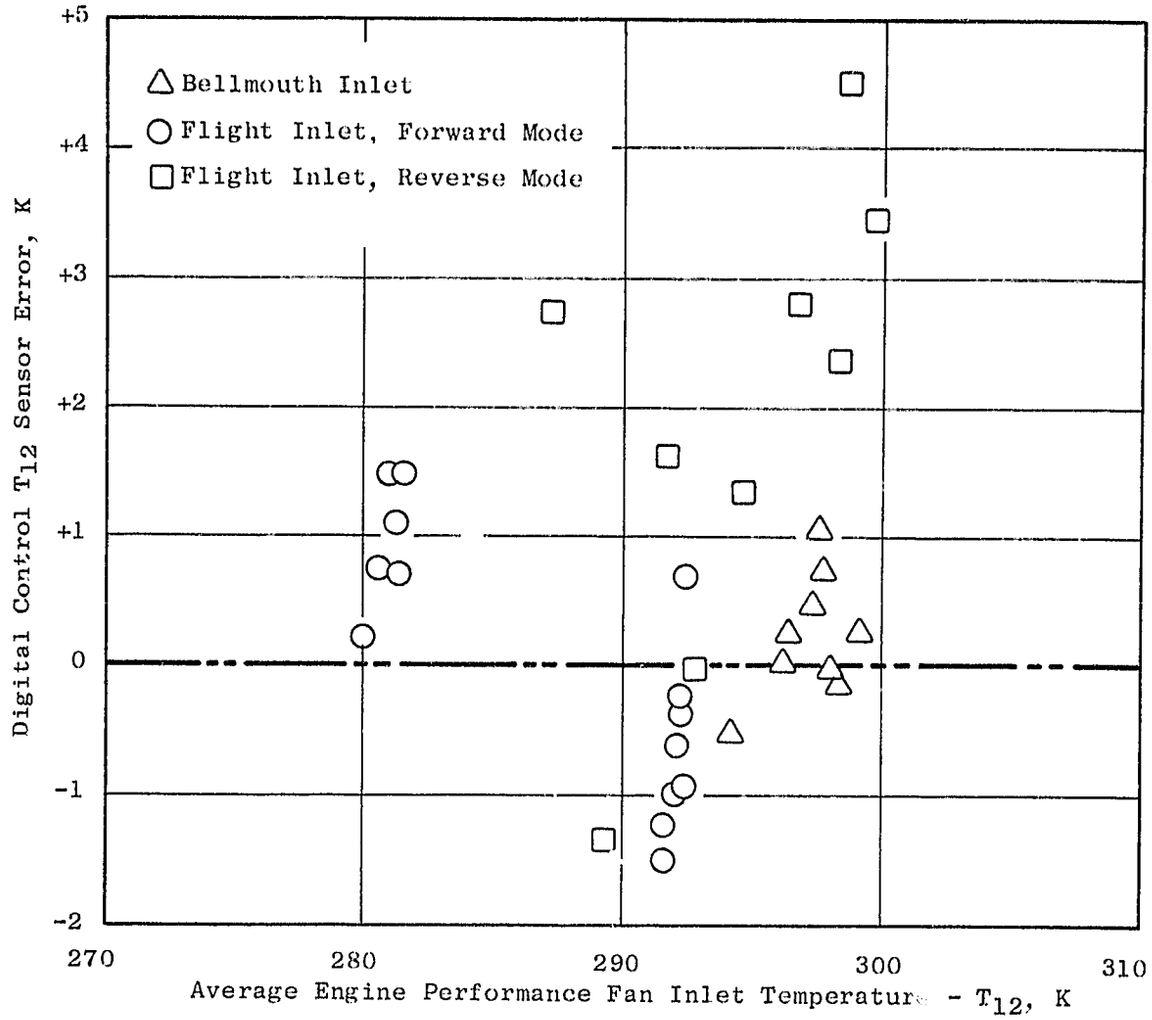

Figure 50. Fan Inlet Temperature Sensor Error.

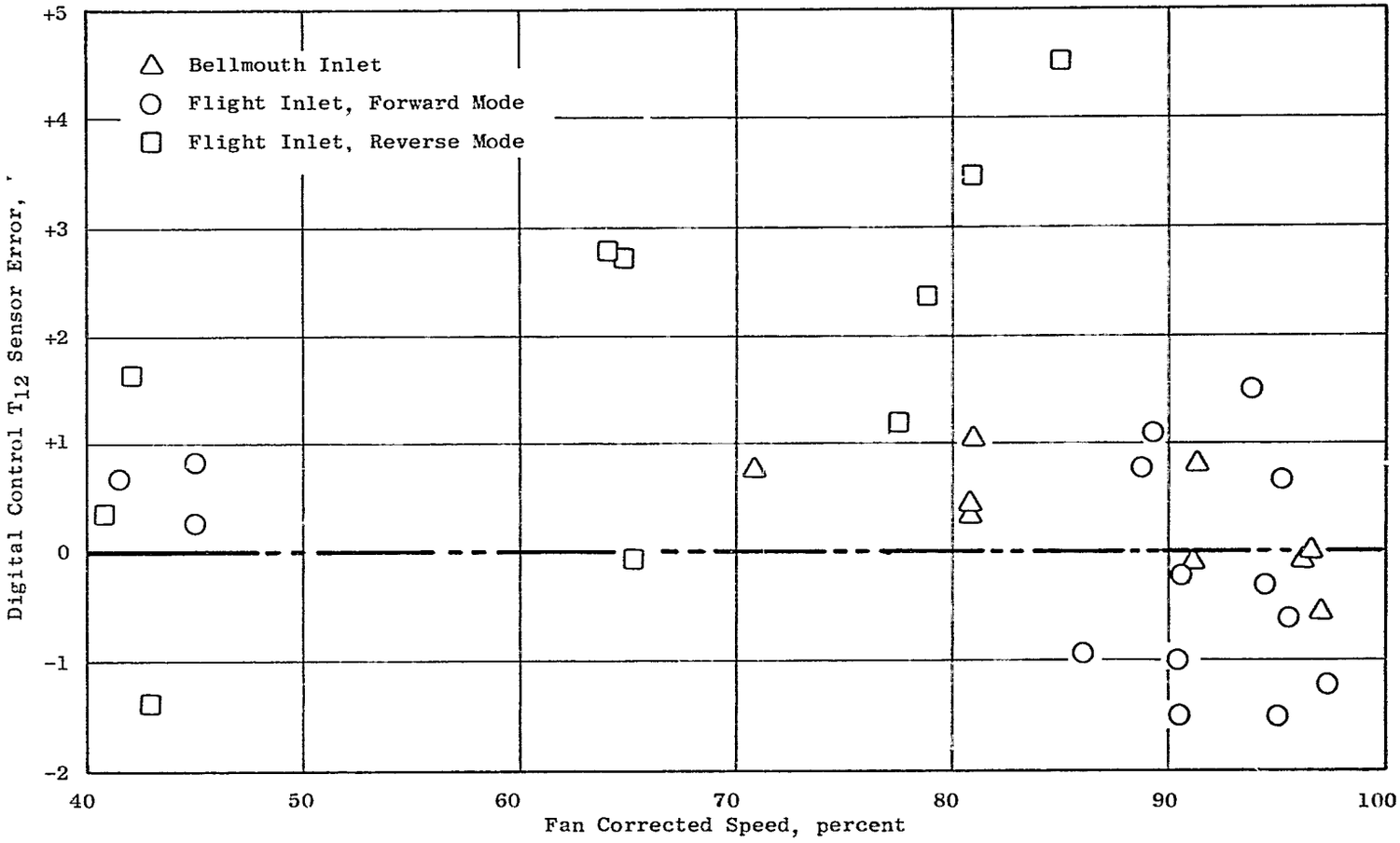

Figure 51. Fan Inlet Temperature Sensor Error.

stator/corrected core speed schedule calculation ($N2/\sqrt{\theta}$), where Theta (θ) is T25/518.67. In this digital control system, T25 is calculated from fan inlet temperature (T12) and fan speed (N_1) rather than being measured. This design feature eliminates a temperature sensor, associated amplifier, and electrical harness and will improve reliability and reduce cost if an accurate temperature can be calculated. Compressor inlet temperature is calculated from T25 = T12 + T12 × ϕT25 where ϕT25 is calculated from the following equation:

$$\phi T25 = a_1 + a_2 \ (PCN_1R) + a_3(PCN_1R)^2$$

where the coefficients in the above equation are dependent upon the corrected fan speed (PCN_1R) level.

On the experimental engine, T25 was measured using three temperature rakes with each rake containing five thermocouple elements. This data was recorded and then averaged to provide the ADH T25 reading. The digital control recorded N_1 and T_{12}. This data was reviewed and T25 was calculated for 35 valid ADH cases for comparison. For these 35 cases the average T25 and calculated T25 agreed closely; the average difference between ADH and calculated T25 was -1.7 K (-3° F) with a standard deviation on the data of 1.7 K (3° F). Figure 52 compares the calculated and measured T25. Figure 53 shows the error between the calculated and measured value, and Figure 54 shows the percent error in calculated T25 as a function of corrected fan speed. This last figure indicates that an equation coefficient change may be in order for the high corrected fan speed region.

The results obtained with this one test indicate that calculation of compressor inlet temperature is feasible; however, additional tests should be considered with fan distortion conditions.

9.3.6 Core Compressor Stator Control

The digital control schedules compressor core stator angle as a function of corrected core speed. The basic schedule is part of the digital control memory, and schedule values are determined from the calculated core speed. Core corrected speed is calculated from a measured core speed, fan speed, and fan inlet temperature. Core inlet temperature is calculated as discussed in Section 9.3.5. The scheduled stator angle is compared with the actual angle which is measured by an LVDT attached to a master bellcrank on the compressor core, and any error is integrated to zero.

Figure 55 shows the steady-state core stator schedule and core stator angle data recorded during the engine test by the digital control system. As shown on the curve, the control system scheduled the stators within 0.5 degrees of the scheduled value. This is considered to be excellent performance and demonstrates the digital-control accuracy.

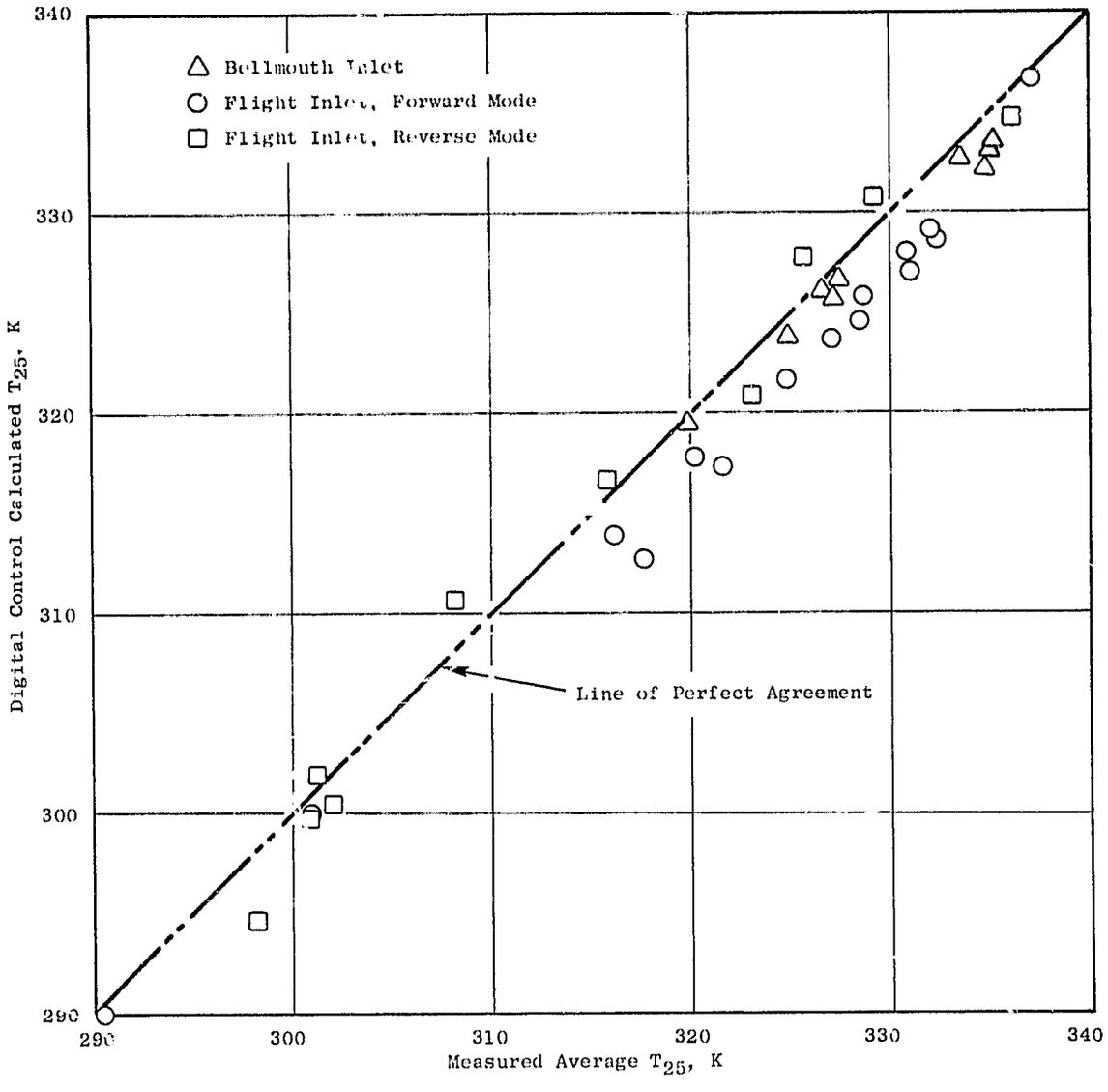

Figure 52. Comparison of Calculated and Measured Compressor Inlet Temperature.

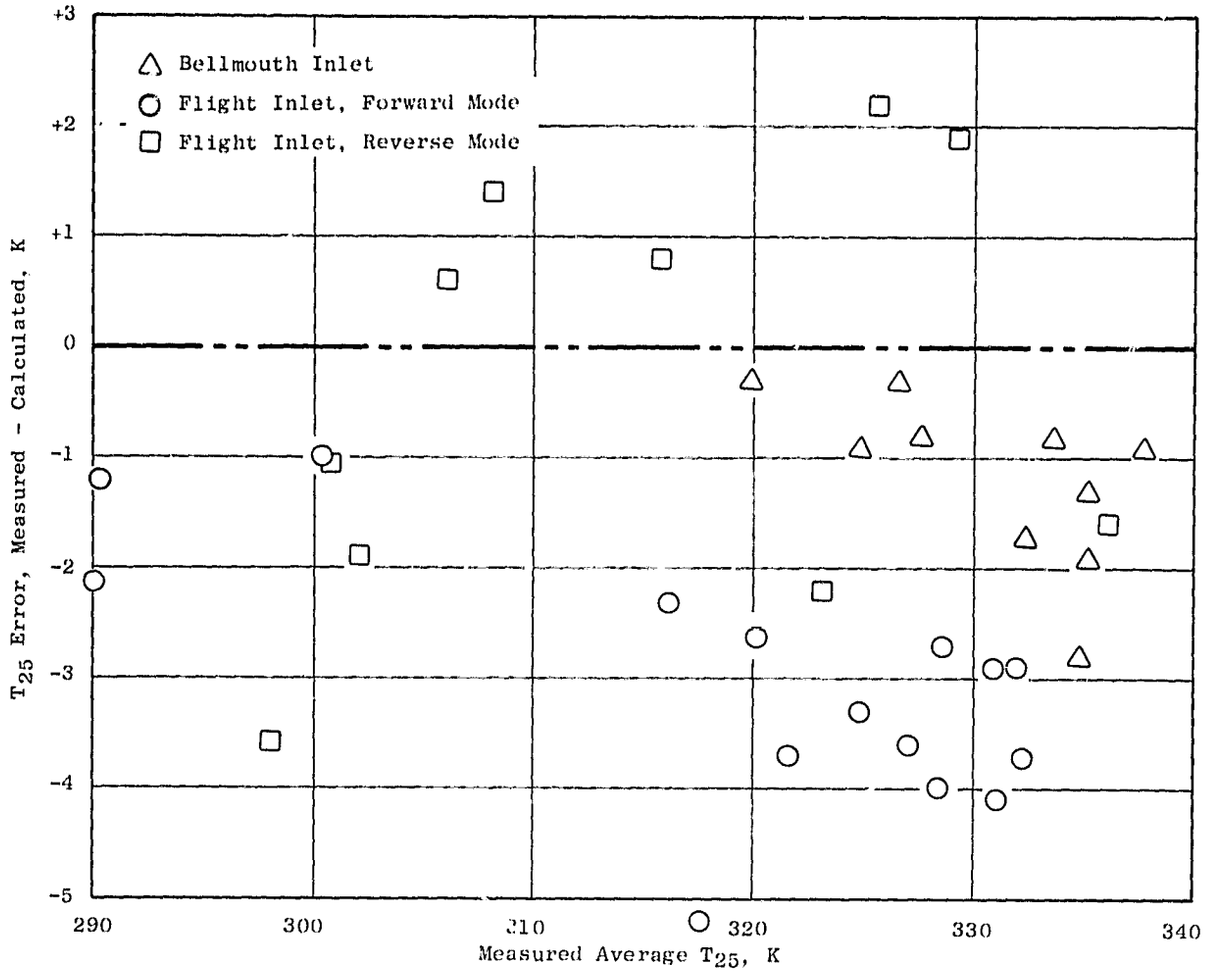

Figure 53. Compressor Inlet Temperature Error.

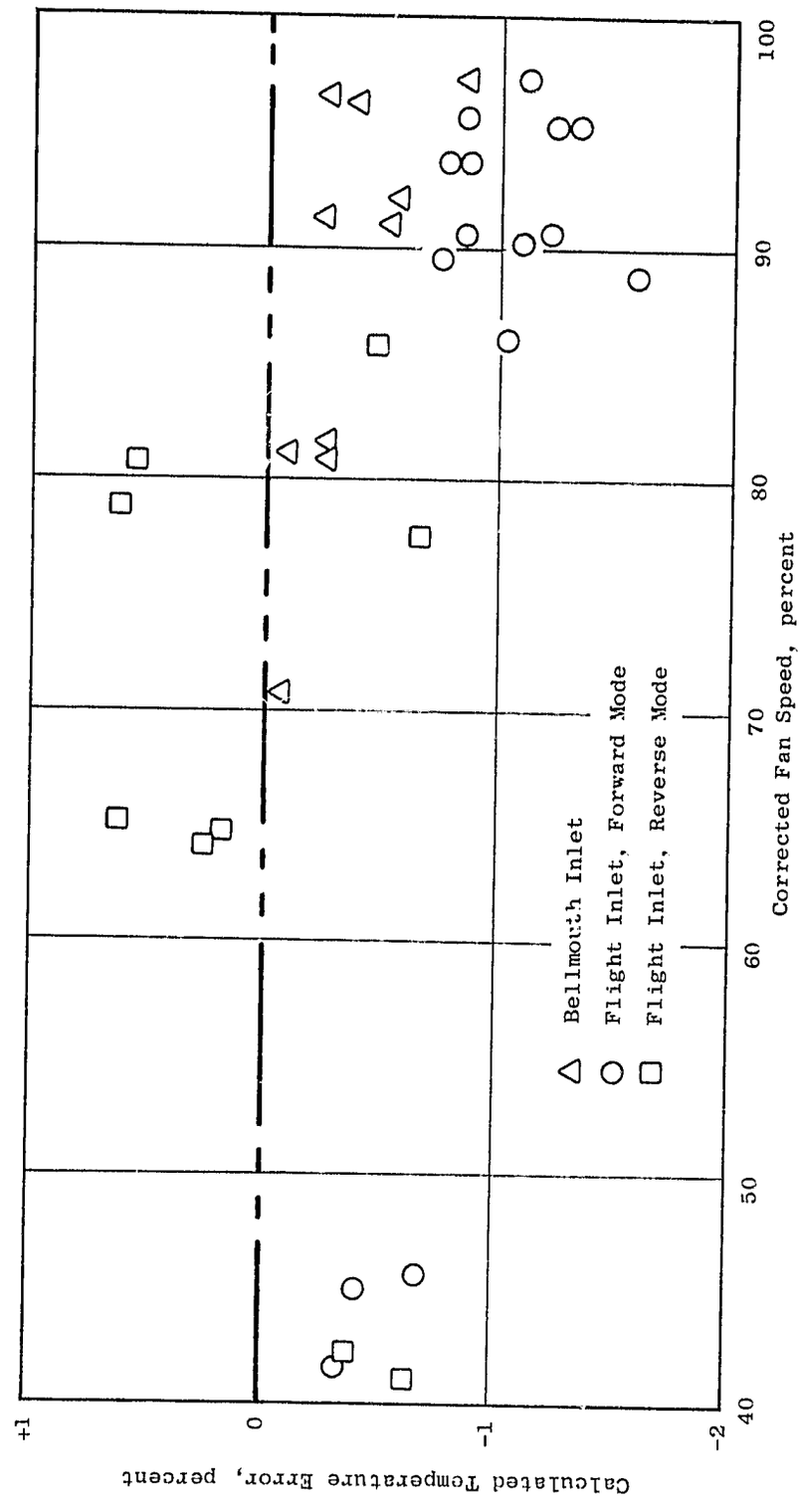

Figure 54. Calculated Compressor Inlet Temperature Error.

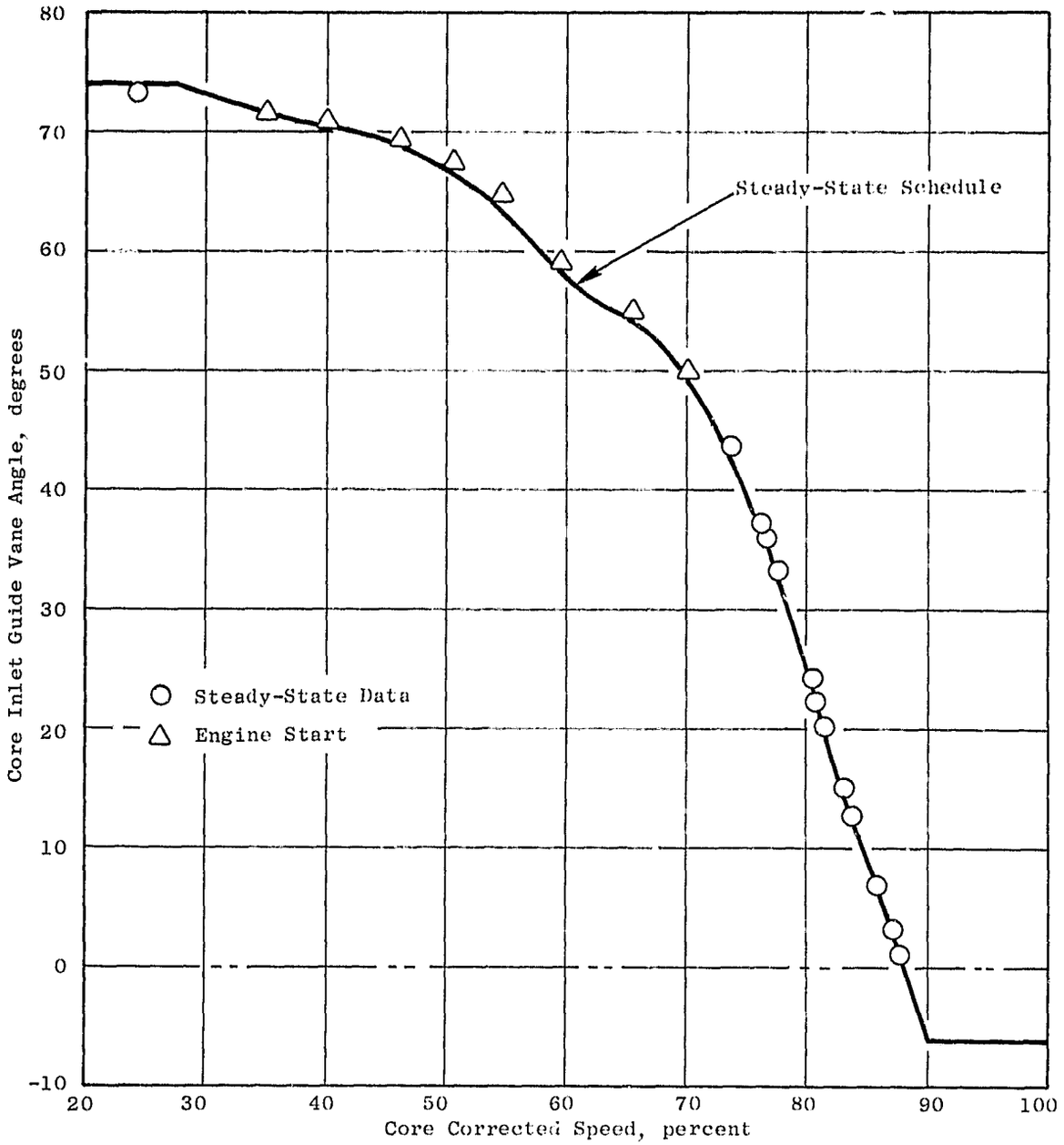

Figure 55. Core Stator Control Performance.

9.3.7 Steady-State T41 Limit

The digital control calculates turbine inlet temperature (T41C) as a function of compressor discharge temperature (T3), compressor discharge static pressure (PS_3), and fuel metering valve position (XMV), which is proportional to fuel flow, per the following equation:

$$T41C = -14.6 + 1.06468\ (T3) + 23.9437\ (WF/PS3)^{1.245}$$

where fuel flow (WF) is a function of XMV as shown below:

for low fuel flow (XMV < 0.2809)

$$WF = 162.2 + 1653.33(XMV) + 18277.8(XMV)^2$$

and for high fuel flow ($0.2809 \leq XMV \leq 0.813$)

$$WF = -348.68 + 4151.59(XMV) + 15864.5(XMV)^2$$

The above equations are incorporated into the digital control program memory, and the sensed parameters are part of the engine control system as noted above. A comparison of T41C as calculated by the digital control using the above equations and hand calculation of T41C using the input data to the digital control is shown in Table XI. The data tabulation indicates that the digital control is accurately calculating the turbine inlet temperature from the input data.

Turbine inlet temperature is also calculated during engine test data reduction for engine performance analysis. The performance data T41 (ADH values) is calculated from measured values of compressor discharge static pressure (PS3), compressor discharge temperature (T3), and measured fuel flow (WF). These measured values are corrected to the actual compressor discharge station in the cycle deck. It should be noted that these are different sensors from those used in the control system. The measured values (T3, PS3, and WF) are manipulated along with an assumed airflow, combustor efficiency, and combustor pressure drop to generate a turbine flow function. This calculated flow function is compared with a cycle deck flow function, and the data is iterated until the flow function balances. The T41 is then calculated from the flow function.

Figure 56 compares T41C as calculated by the digital control with T41C calculated from performance data. This figure, along with the associated data, indicates that the digital control is calculating a high value of turbine inlet temperature. The variation with engine performance data ranges

Table XI. Digital Control Turbine Inlet Temperature Computation Comparison.

ADH No.	$T_{41}C$* K	$T_{41}C$** K	Difference	
			K	%
74	1589	1591	2	0.13
75	1681	1683	2	0.13
76	1041	1043	2	0.19
80	1513	1515	2	0.13
82	1664	1667	3	0.18
96	1470	1468	-2	0.14
102	1308	1307	1	0.08

* $T_{41}C$ as calculated by Digital Control.

** $T_{41}C$ hand-calculated using Digital Control input data.

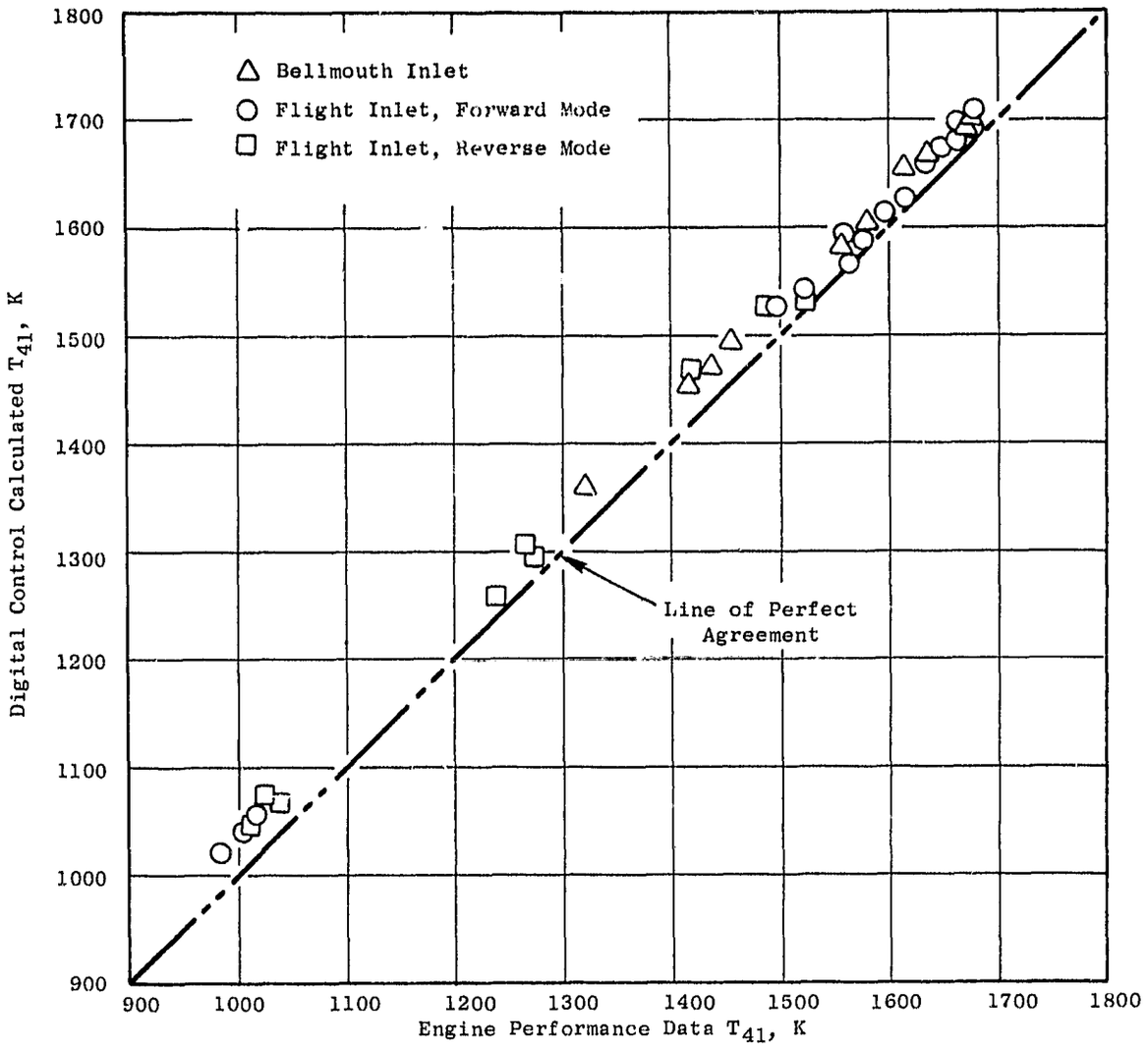

Figure 56. Comparison of Calculated Turbine Inlet Temperature.

from 52 K to 6 K (94° F to 11° F) from idle to takeoff power. This variation in calculated temperatures is caused by several factors as noted below:

- Nonsynchronization of instantaneous data.
- Variation in actual engine turbine nozzle area.
- Variation in input data (PS3, T3, WF), primarily fuel flow.

During the steady-state engine testing the standard procedure was to take a digital-control-data reading as soon as the engine was on point and at the beginning of the ADH data reading which was taken after a three-minute stabilization period. The resulting T41C data were averaged and compared with the ADH reading. Since the control system is modulating fuel flow to maintain fan speed, there is a high probability that the fuel flows recorded by the digital control and the ADH system would be different and would contribute to a T41C variation. This error-contributing factor was recognized during the test, and for several data points multiple digital data readings were taken during the four-minute ADH reading. Table XII shows the results for three data points. For ADH reading number 81, sixteen digital readings were taken during the ADH reading, and the average digital control T41C was within 6 K (11° F) of the ADH reading. It is interesting to note, for that data point, the total spread in the instantaneous T41C was +12 K and -13 K (+22° F and -23° F), and one standard deviation on the data was 7.6 K (13° F).

Table XIII compares ADH T41 with a T41 calculated from the digital control equation but using the ADH input data. As shown in the table, the variation between calculation methods ranges between 0.6 and 1.2 percent. A substantial part of this variation is due to turbine area differences. The coefficients in the digital control were based on the engine technical requirements cycle deck, and this data implied a specific value for turbine area. The coefficients were not updated to reflect the actual, experimental-engine hardware. In contrast, the engine performance calculations utilized the measured value of turbine area. A comparison of technical requirement cycle data and experimental engine data indicates a variation of approximately 0.8% difference in turbine area. Application of this factor to the digital control T41C equation would reduce the coefficient of the third term in the equation and eliminate most of the error between the calculation methods.

The third contributing factor in variation between digital control T41C and performance T41C is the variation in sensor input. Table XIV shows the difference between digital control and ADH T3 sensors. The table also shows the percent error in the T3 sensor. This percent error tabulation assumes that the true T3 is the average of the ADH and the digital control T3's. The average T3 error for 35 data points was -0.46%. This percent error is used later to determine the effect on T41C. Table XV shows data similar to the above on the PS3 sensors. The average PS3 error for 25 valid data points was -0.36%. Table XVI shows fuel flow data; it assumed that the true fuel flow is represented by the ADH data since it is based on two turbine-type

Table XII. Comparison of Calculated Turbine Inlet Temperature Average Digital Control $T_{41}C$ Minus ADH $T_{41}C$.

ADH* Reading Number	ADH $T_{41}C$ K	Digital Control $T_{41}C$ K	No. Digital Control Readings	Temperature Difference	
				K	%
77	1616	1628	13	+12	0.74
80	1498	1514	8	+16	1.07
81	1561	1566	16	+ 5	0.32

*ADH - Automatic data handling system.

Table XIII. Comparison of Turbine Inlet Temperature Calculation Methods.

ADH No.	ADH T_{41}* K	Digital Control T_{41}** K	Temperature Difference	
			K	%
74	1579	1596	+17	1.1
75	1664	1684	+20	1.2
77	1616	1635	+19	1.2
78	1661	1680	+19	1.1
81	1561	1577	+16	1.0
82	1636	1654	+18	1.1
83	1677	1696	+19	1.1
103	1573	1582	+ 9	0.6
104	1489	1498	+ 9	0.6
109	1559	1569	+10	0.6
110	1648	1659	+11	0.7
111	1678	1690	+12	0.7

* T_{41} calculated by iteration method.

** T_{41} calculated with digital control equation using ADH data.

Table XIV. Digital Control Compressor Discharge Temperature Sensor (T_3) Error.

ADH No.	ADH T_3, K	Digital Control T_3, K	Average T_3, K	% Error Digital Control T_3
74	702	696	699	-0.43
75	733	723	728	-0.69
76	713	707	710	-0.47
80	682	676	679	-0.49
82	725	716	720	-0.62
95	611	606	608	-0.37
96	663	663	663	0
102	616	608	612	-0.64

Table XV. Digital Control Compressor Discharge Static Pressure Sensor (PS_3) Error.

ADH No.	ADH PS_3 kN/m^2	Digital Control PS_3 kN/m^2	Average PS_3 kN/m^2	% Error Digital Control PS_3
74	1474.2	1471.4	1472.8	-0.09
75	1627.9	1621.0	1624.5	-0.21
76	519.2	513.0	516.4	-0.67
80	1345.2	1331.4	1338.3	-0.52
82	1581.0	1585.9	1583.9	+0.13
95	831.5	920.5	926.0	-0.60
96	1210.8	1195.6	1203.2	-0.63
102	899.8	884.6	892.2	-0.85

Table XVI. Digital Control Engine Fuel Flow Sensor (WF) Error.

ADH No.	ADH WF kg/hr	Digital Control WF kg/hr	Digital Control WF Error %	Number of Digital Control Readings
74	2752	2748	-0.15	1
75	3194	3207	+0.41	5
76	611	623	+1.96	1
80	2366	2362	-0.17	8
82	3046	3119	+2.40	1
95	1378	1415	+2.67	1
96	1987	2052	+3.25	1
102	1310	1352	+3.22	1

flow sensors which read within 0.5 percent of each other. The large variation in fuel flow indication by the digital control is probably associated with nonsynchronization of the ADH and digital control fuel flow readings.

The effect on T41 due to sensor errors can be determined from the following equation:

$$\%T41 = (k_2\ T3/T41)(\%T3\ \text{error}) + (k_3\ k_4/T41)(WF/PS3)^{k_4}(\%WF\ \text{error})$$
$$-(k_3 k_4/T41)(WF/P3)^{k_4}(\%\ PS\ \text{error})$$

where k_2, k_3, and k_4 are the coefficients in the digital control T41C equation and the percent sensor errors are shown in Tables XIV, XV, and XVI. Table XVII shows the effect of sensor errors on the overall T41 calculation.

9.3.8 Thrust Response

One of the major control system objectives in the QCSEE program was to design a system which would provide fast thrust-response capability. The QCSEE engine is designed for a powered-lift aircraft, and NASA studies have shown that fast engine-thrust response is required for aircraft control and/or wave-off. The basic requirement placed on the engine was to achieve a thrust response of 1.0 second between 62 and 95% thrust. This is approximately 50% faster than current engines.

Since the QCSEE OTW engine has a fixed-pitch fan, the options to achieve fast thrust response are limited. System design studies showed that the basic engine thrust-response requirement could be met by resetting the core compressor stators at the approach-power setting. The mechanization of this concept on the experimental engine is shown in Figure 42. As shown in the figure, the core stators are set as a function of power demand. The core stator reset switch and schedule adjustment were incorporated for experimental engine flexibility.

The results of the transient response test on the QCSEE OTW engine are shown in Figures 57, 58, and 59. Figure 57 is a transient data recording showing selected engine parameters as a function of time; the time scale is 50 mm/sec. As shown in the figure, the overall thrust requirement of 62 to 95% thrust in one second was met. Zero time is at the point of power-demand movement. Figure 58 compares thrust-response data with the thrust-response requirement. Although portions of the test-result curve are below the requirement, the overall thrust-response objective was met. Figure 59 shows thrust-response time as a function of acceleration-schedule adjustment and core stator reset. An acceleration-schedule adjustment of 10 percent above nominal was required because the actual engine operating line as related to acceleration-schedule parameters was higher than predicted. No adverse turbine temperature overshoots were observed with this acceleration-

Table XVII. Contributions To Calculated Turbine Inlet Temperature Error.

ADH No.	ΔT_4 K due to T_3 error	ΔT_4 K due to WF error	ΔT_4 K due to PS_3 error	Total ΔT_4 K
74	-3.1	- 1.4	+0.94	- 3.6
75	-5.4	+ 4.9	+2.3	+ 1.8
76	-2.4	+11.2	+4.0	+12.8
80	-3.5	- 1.7	+4.0	- 1.2
82	-4.9	+26.6	-1.5	+20.2
95	-2.4	+21.5	+4.9	0
96	0	+29.8	+5.7	+35.5
102	-4.2	+25.8	+6.8	+28.4

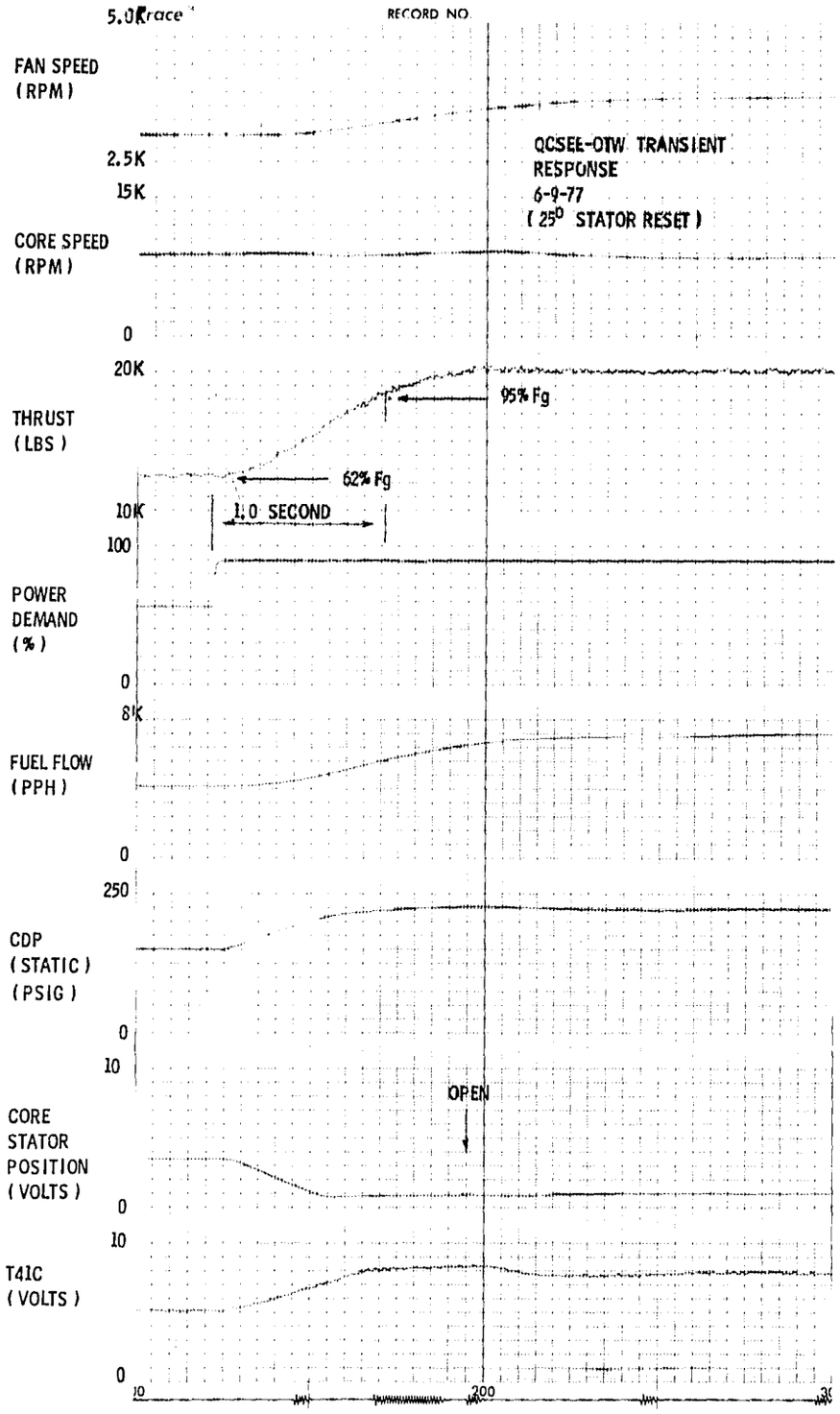

Figure 57. Transient Response.

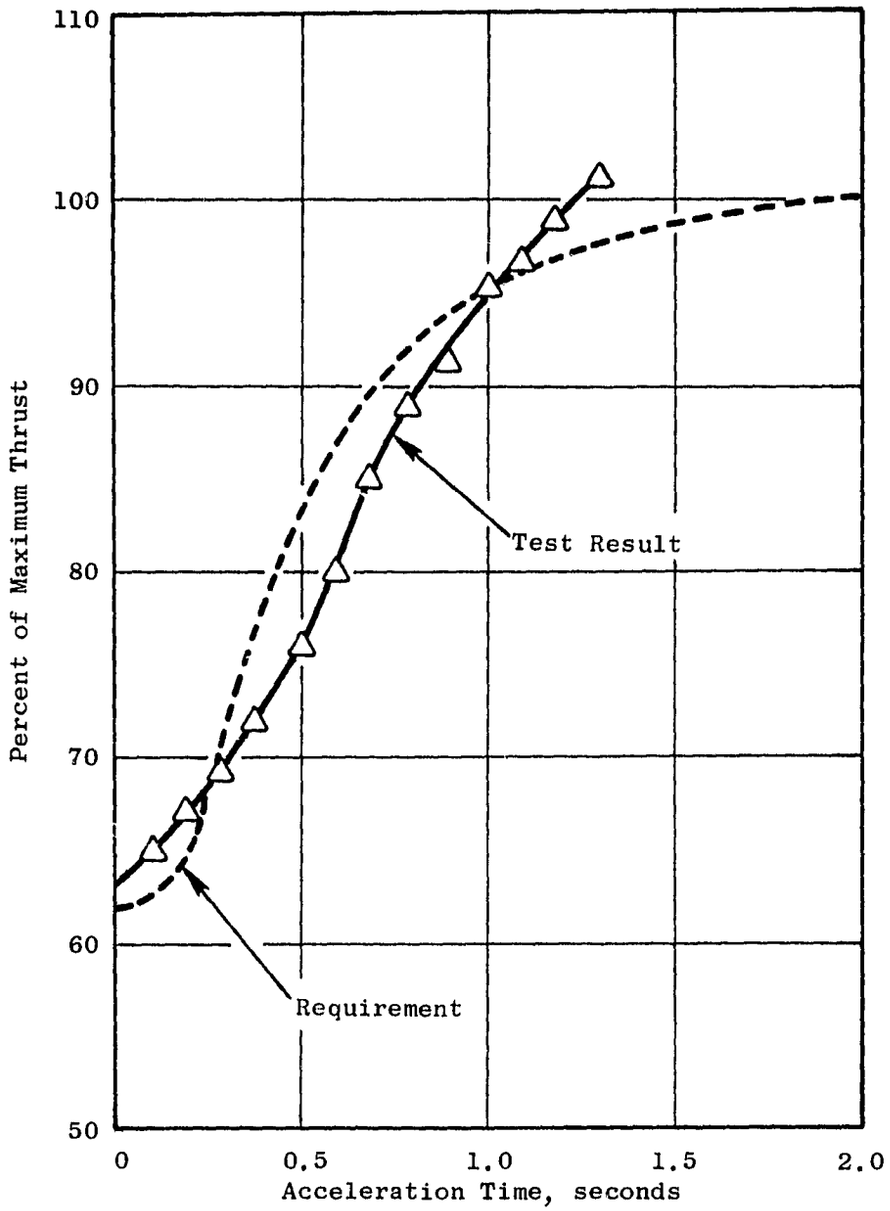

Figure 58. Engine Thrust Response.

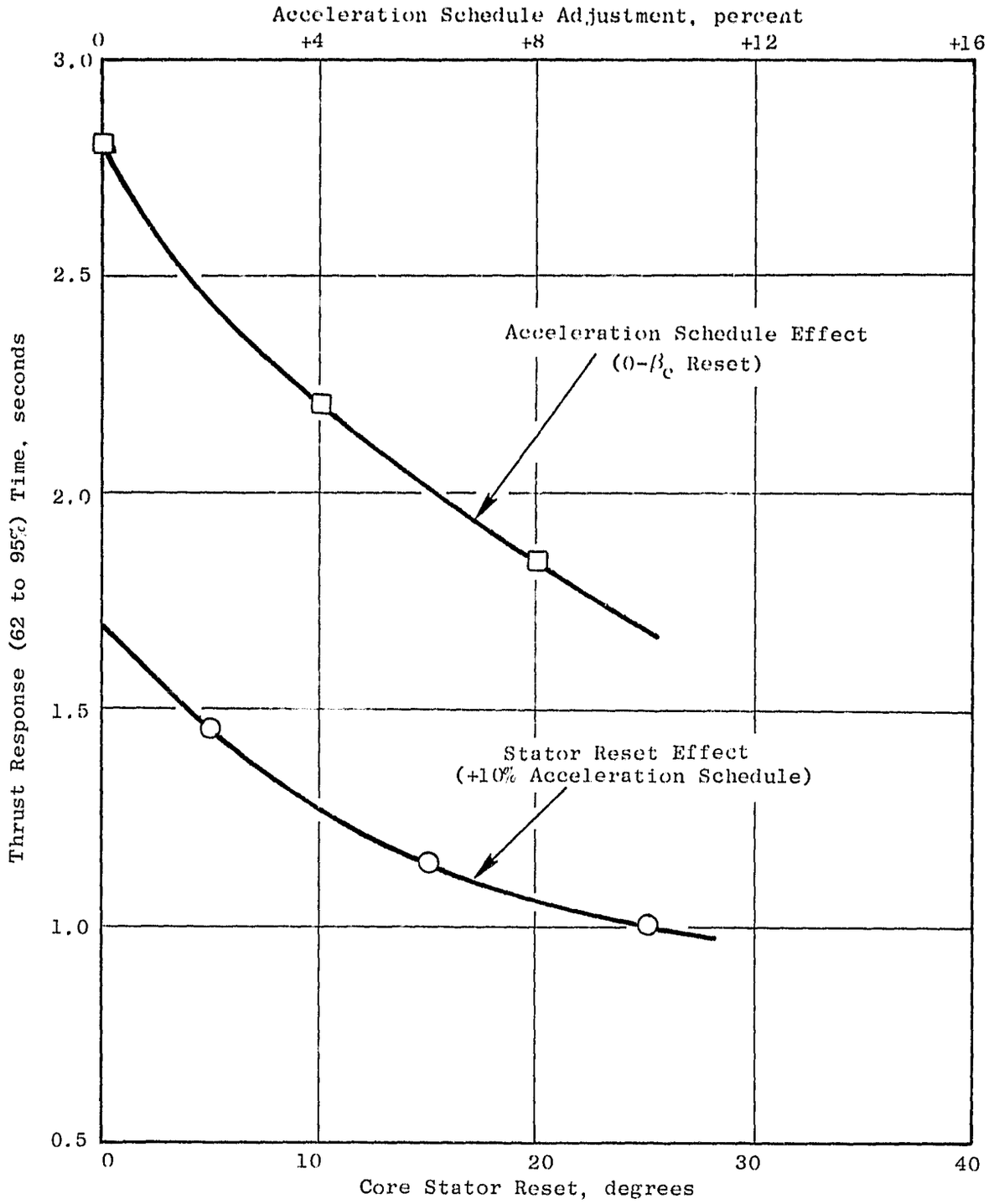

Figure 59. Transient Thrust Response.

schedule adjustment since turbine temperature was limited by the control-calculated T41. As shown on Figure 59, the thrust-response requirement was met with 25 degrees of core stator reset and an acceleration-schedule adjustment of 10 percent.

The OTW engine incorporated titanium fan blades and, as a result, had a relatively high moment of inertia. It is planned that the flight-design engine would incorporate composite fan blades. This reduction in inertia would improve transient thrust response by approximately 0.2 seconds.

These initial tests on thrust response were successful, and the basic response requirement was met. However, additional tests which would optimize the acceleration schedule and stator reset schedule are in order to define the engine-response capability.

9.3.9 Failure Detection and Correction

As noted above, the QCSEE OTW digital control incorporates two failure detection and correction concepts. The first concept functioned properly throughout test and provided a fault warning to the engine operator if an out-of-limit condition existed. When this occurred, appropriate corrective action was taken. The second concept, which is called Automatic Failure Indication and Corrective Action (FICA), consists of extended Kalman-Bucy filter, nonlinear engine model, and updated procedure. It has the capability to substitute calculated best estimates for a failed control-system sensor. Tests on this concept were partially successful.

The FICA system incorporates two override switches. Switch number one arms the system to allow the nonlinear model to be updated by the engine sensors. Switch number two arms the system to allow automatic sensor placement if the error between the calculated and measured sensor values exceeds prescribed limits. The objective of the engine level tests were three-fold:

1. To evaluate the filter to determine update capability.

2. To evaluate the system armed for automatic sensor replacement.

3. To evaluate the system performance with simulated sensor failures.

The first two objectives were accomplished.

With switch number one on and switch number two off, the engine was operated from idle to maximum power both for steady-state and for transient conditions. Over most of the speed range the FICA error word showed that the filter tracked the engine, both steady-state and transient, within the FICA tolerance bands. Over the core engine speed range of 13,350 to 13,550 rpm there were repeated failures of the filter to track properly as indicated by the FICA error word. Generally, these failures occurred on an increase in speed. In each case, the filter recovered tracking without operator action.

Examination of recorded data leads to the conclusion that there is a specific error in the filter or the digital-control coding. Table XVIII shows a comparison of measured and calculated values for the control-system sensors.

With both switches on, and at the operating point selected, the failure detection and correction system functioned properly. That is, there was no indication of an error or sensor substitution. On slow accelerations the filter failed to track and, since switch number two was on, there was an improper substitution for engine sensors. When this occurred, switch number one and switch number two were deactivated. Analysis of the recorded data indicates an error in the model definition or digital-control coding. The basic concept, however, appears to be sound. Further data analysis is in process and additional tests are planned.

Table XVIII. Comparison of Measured and Calculated Engine Parameters.

Reading No.	N_1, rpm		N_2, rpm		PS_3, kN/m^2		T_3, K		MVP, cm		C, cm		T_5, K	
	M	C	M	C	M	C	M	C	M	C	M	C	M	C
69	1592	1602	10889	10879	505	503	516	515	0.554	0.554	2.589	2.583	689	690
70	1906	1899	11387	11309	630	688	547	546	0.658	0.706	2.146	2.144	705	705
72	2679	2673	12261	12178	983	1056	621	620	0.942	1.064	1.240	1.290	799	797
77	3061	3059	12776	12734	1200	1263	666	662	1.123	1.285	0.853	0.889	859	862
79	3455	3450	13301	13302	1500	1539	711	710	1.331	1.618	0.472	0.521	928	937
87	3669	3662	13604	13593	1640	1677	736	734	1.318	0.292	0.284	0.312	971	978
Allowable Error	187		683		93		36		[illegible]		0.239		47	

Reading No.	N_1, rpm		N_2, rpm		PS_3, psia		T_3, ° R		MVP, in.		C, in.		T_5, ° R	
	M	C	M	C	M	C	M	C	M	C	M	C	M	C
69	1592	1602	10889	10879	73.2	73.0	928	927	0.218	0.218	1.019	1.017	1240	1242
70	1906	1899	11387	11309	91.4	99.8	984	983	0.259	0.278	0.845	0.844	1269	1269
72	2679	2673	12261	12178	142.6	153.1	1117	1116	0.371	0.419	0.488	0.508	1438	1434
77	3061	3059	12776	12734	174.1	183.2	1198	1192	0.442	0.506	0.336	0.350	1547	1552
79	3455	3450	13301	13302	217.5	223.2	1279	1278	0.524	0.637	0.186	0.205	1671	1686
87	3669	3662	13604	13593	237.9	243.2	1325	1322	0.519	0.115	0.112	0.123	1748	1761
Allowable Error	187		683		13.5		65		0.229		0.094		84	